



**Ministry of Higher Education  
And Scientific Research  
University of Baghdad  
Institute of Laser for Postgraduate Studies**



**The Effect of Working Parameters of Nanosecond and  
Microsecond Fiber Lasers on the Coloring of SS 304 and  
Al 3003**

**A Thesis Submitted to the Institute of Laser for Postgraduate Studies,  
University of Baghdad in Partial Fulfilment of the Requirements for the  
Degree of Master of Science in Laser / Mechanical Engineering**

**By**

**Ayat Khalaf Rahma**

**B.Sc. Manufacturing processes Engineering – 2008**

**Supervised by**

**Asst. Prof. Dr. Ziad Aeyad Taha**

**2021 A.C.**

**1443 A.H.**

بِسْمِ اللَّهِ الرَّحْمَنِ الرَّحِيمِ

رَبِّ أَوْزِعْنِي أَنْ أَشْكُرَ نِعْمَتَكَ الَّتِي أَنْعَمْتَ عَلَيَّ وَعَلَى  
وَالِدِيَّ وَأَنْ أَعْمَلَ صَالِحًا تَرْضَاهُ وَأَصْلِحْ لِي  
فِي ذُرِّيَّتِي ۖ إِنِّي تُبْتُ إِلَيْكَ وَإِنِّي مِنَ  
الْمُسْلِمِينَ ﴿١٥﴾

صَدَقَ اللَّهُ الْعَظِيمَ

سورة الأحقاف الآية ﴿١٥﴾

## **Certification**

I certify that this thesis was prepared under my supervision at the  
Institute of Laser for Postgraduate Studies, University of Baghdad, as a  
partial fulfillment of requirements for the  
**Degree of "Master of Science in Laser / Mechanical Engineering**

Signature:

Name :**Asst. Prof .Dr. Ziad Aeyad Taha**

Title: Asst. Professor

Address: Institute of Laser for Postgraduate studies,  
University of Baghdad.

Date: 1/ 8 / 2021

(Supervisor))

In view of the available recommendation, I forward this thesis for debate  
by Examining Committee.

Signature:

Name: **Asst. Prof. Dr. Hanan Jaafar Taher**

Title: Head of the Scientific Committee.

Address: Institute of Laser for Postgraduate studies,  
University of Baghdad.

Date: 1 / 8 / 2021

## Examination Committee Certification

We certify that we have read this thesis " **The Effect of Working Parameters of Nanosecond and Microsecond Fiber Lasers on the Coloring of SS 304 and Al 3003** " and as Examination Committee, we examined the student in its content and in our opinion, it is adequate with standards as a thesis for a degree of Master in Science in Laser / mechanical Engineering.

**Signature:**

**Name:** Dr. Zainab Fadhil Mahdi.

**Title:** Assistant Professor.

**Address:** Institute of Laser for Postgraduate Studies / University of Baghdad.

**Date:** / / 2021

(Chairman)

**Signature:**

**Name:** Dr. Ahmed Al-Hamaoy

**Title:** Assistant Professor.

**Address:** College of Engineering /  
Al- Nahrain University

**Date:** / / 2021

(Member)

**Signature:**

**Name:** Dr. Furat I Hussein

**Title:** Assistant Professor.

**Address:** Mechatronics Engineering  
Department / Al-khwarizmi College  
of Engineering / University of  
Baghdad

**Date:** / / 2021

(Member)

**Signature:**

**Name:** Dr. Ziad Aeyad Taha.

**Title:** Assistant Professor.

**Address:** Institute of Laser for Postgraduate Studies /  
University of Baghdad.

**Date:** / / 2021

(Supervisor)

Approval by the Deanship of Institute of Laser for Postgraduate Studies, University of Baghdad.

**Signature:**

**Name:** Prof. Dr. Hussein Ali Jawad

**Title:** Dean.

**Address:** Institute of Laser for Postgraduate Studies/ University of Baghdad.

**Date:** / / 2021

## ***Dedication***

***This work is dedicated to my parents and my husband, they are the reason for my success and the shine of my life, who gave me support and force at every step of the road. I would also like to dedicate this work to my sons, my daughter, my brothers, my sisters and my friends.***

***Ayat***

## *Acknowledgement*

First and foremost, I am grateful to my creator "**ALLAH**" for giving me the strength, enablement, knowledge and understanding required to complete this work.

I would like to express my deep gratitude and appreciation to my supervisor **Asst. Prof. Dr. Ziad Aeyad Taha**, for suggesting this work, valuable instructions, continuous advice and guidance throughout this research.

I would like to give special thanks to Deanship of Institute of Laser for Postgraduate Studies **Prof. Dr. Hussein Ali Jawad**.

I would like to introduce a great thank to Head of the Engineering and Industrial Applications Department **Asst. Prof. Dr. Tahreer Safa'a Mansour**

My thanks to **Asst. Prof. Dr. Mahammad K. Dhahir** for his support, grateful remarks and care during the period of my project work.

Special thanks to **Asst. Prof. Dr. Hanan Jaafar Taher, Asst. Prof. Dr. Zainab Fadhil Mahdi**. for their kindness and assistance.

I am very grateful to **Mr. Atheer Rasheed** and **Mr. Saif Aqeel** for their assistance and support throughout the period of this work.

At last, I offer my regards and blessings to all of those who supported me in one way or another during the completion of this research.

Deep thanks go to all friends at Institute of Laser for Postgraduate Studies especially my classmates.

*Ayat*

## Abstract

Ferrous and non-ferrous metals surface color marking induced during laser treatment offers many interesting applications in different fields such as products recognition, esthetics and arts. Its main advantage in comparison with the traditional marking processes that is no generation of toxic products is presented.

Because of the lack of studies on the use of microsecond laser to color marking we presented the study by utilizing two types of Ytterbium fiber laser emitted wavelength 1064 nm. The first one is a microsecond fiber laser of a pulse width of 10 $\mu$ s and the second one is a nanosecond fiber laser with a pulse width of 81ns, to color two targets stainless steel 304 and aluminum 3003.

The colors generation results from surface oxidation during the laser beam heating of the material surface under normal atmospheric conditions, with different scanning speeds, power and hatch. The stainless-steel surface produces different color with the changes of power 4 W and 8 W, scanning speed from 50 to 650 mm/s, pulse repetition rate 80 kHz and hatch 0.001 mm and 0.01mm due to the changes in the thermal interaction of laser with the metal surface and due the absorption effect.

Microsecond laser results in color of dark brown at speed 125mm/s, brown at 275mm/s, gray at 450mm/s and yellow at 650 mm/s.

Nanosecond laser results in colors of (light gray at 50 mm/s, dark green at 275mm/s, naval blue at 475 mm/s and faded yellow at 600 mm/s.

Nanosecond pulse lasers produced less roughness than microsecond pulse lasers and more protect against corrosion due to the oxide layer

contain Nickel. Aluminum appears different behavior result in just white color at 200mm/s, P 6W, hatch 0.005 mm and gray color produced at 25 mm/s, hatch 0.001 mm and microsecond pulse width fiber laser have higher corrosion resistance.

For an objective assessment of color changings, many instruments were used, such as an optical microscope, for modification of surface state.

Field Emission Scanning Electron Microscope FESEM and EDS to studying Surface morphology and elementary composition, XRD analysis to identification of surface phases, roughness surface tester, wavelength measurement and hand colorimeter for reflection spectrum and identify color and corrosion polarization measurements for examining the color stability against the environmental conditions.

## List of Contents

N0	Subject	Page
-	Abstract	I
-	List of Contents	III
-	List of Tables	VII
-	List of Figures	VIII
-	List of Abbreviations	XII
	List of Symbols	XIV
<b>Chapter One: Introduction and Basic Concepts</b>		
1.1	Introduction	1
1.2	Laser matter interaction	2
1.2.1	Heating	2
1.2.2	Melting	3
1.2.3	Vaporization	3
1.2.4	Plasma Formation	4
1.3	Laser Material Processing	4
1.3.1	Laser Marking Process	4
1.3.2	Methods of Laser Marking	9
1.3.3	Beam Delivery System	10
1.4	Laser Types Used in Marking	11
1.5	Mechanisms of Color Generation	12

<b>N0</b>	<b>Subject</b>	<b>Page</b>
<b>1.5.1</b>	<b>Mechanisms of Laser Coloring Through Layer Oxidation</b>	<b>13</b>
<b>1.5.2</b>	<b>CIE La*b* and Color Difference</b>	<b>15</b>
<b>1.6</b>	<b>Advantages of Laser Color Marking</b>	<b>16</b>
<b>1.7</b>	<b>Disadvantages of Laser Color Marking</b>	<b>17</b>
<b>1.8</b>	<b>Stainless Steel Types, Grades and Uses</b>	<b>17</b>
<b>1.8.1</b>	<b>Types of Stainless-Steel Alloy</b>	<b>20</b>
<b>1.8.2</b>	<b>Applications of austenitic stainless steel</b>	<b>21</b>
<b>1.9</b>	<b>Aluminum and aluminum alloys</b>	<b>21</b>
<b>1.9.1</b>	<b>Properties of Aluminum and its Alloys</b>	<b>21</b>
<b>1.9.2</b>	<b>Aluminum alloys classification</b>	<b>22</b>
<b>1.9.3</b>	<b>Wrought alloys 3 xxx</b>	<b>24</b>
<b>1.10</b>	<b>Applications 3003Al of The Alloy</b>	<b>25</b>
<b>1.11</b>	<b>Oxide Dispersion Strengthened Steels and Aluminum</b>	<b>25</b>
<b>1.12</b>	<b>Literature review</b>	<b>27</b>
<b>1.13</b>	<b>The aim of the work</b>	<b>32</b>
<b>Chapter Two: Materials and Methods</b>		
<b>2.1</b>	<b>Introduction</b>	<b>33</b>
<b>2.2</b>	<b>Materials</b>	<b>33</b>
<b>2.2.1</b>	<b>Workpiece preparation</b>	<b>33</b>
<b>2.3</b>	<b>Laser devices</b>	<b>35</b>

<b>N0</b>	<b>Subject</b>	<b>Page</b>
<b>2.4</b>	<b>Experimental procedures</b>	<b>36</b>
<b>2.5</b>	<b>Specimens testing</b>	<b>38</b>
<b>2.5.1</b>	<b>Microscopic inspection</b>	<b>38</b>
<b>2.5.2</b>	<b>Field Emission Scanning Electron Microscope (FESEM)</b>	<b>38</b>
<b>2.5.3</b>	<b>X-ray diffraction (XRD)</b>	<b>39</b>
<b>2.5.4</b>	<b>Double Beam Spectrophotometer</b>	<b>40</b>
<b>2.5.5</b>	<b>Colorimeter test</b>	<b>40</b>
<b>2.5.6</b>	<b>Roughness test</b>	<b>40</b>
<b>2.5.7</b>	<b>Corrosion test</b>	<b>41</b>
<b>Chapter Three: Results and Discussion</b>		
<b>3.1</b>	<b>Introduction</b>	<b>43</b>
<b>3.2</b>	<b>Experimental results</b>	<b>43</b>
<b>3.2.1</b>	<b>Laser power effect on SS 304</b>	<b>43</b>
<b>3.2.2</b>	<b>Effect of hatch on SS 304</b>	<b>44</b>
<b>3.2.3</b>	<b>Effect of frequency on SS 304</b>	<b>45</b>
<b>3.2.4</b>	<b>Effect of the scanning speed on SS 304</b>	<b>46</b>
<b>3.2.5</b>	<b>Surface morphology analysis</b>	<b>46</b>
<b>3.2.6</b>	<b>Final Experimental Results of Stainless Steel 304</b>	<b>47</b>
<b>3.2.6.1</b>	<b>Wavelength s' Measurements</b>	<b>53</b>
<b>3.2.6.2</b>	<b>Colorimeter Result</b>	<b>56</b>

<b>N0</b>	<b>Subject</b>	<b>Page</b>
<b>3.2.6.3</b>	<b>Roughness Results</b>	<b>58</b>
<b>3.2.6.4</b>	<b>Corrosion Result</b>	<b>66</b>
<b>3.3</b>	<b>Result of Al 3003</b>	<b>67</b>
<b>3.3.1</b>	<b>Effect of hatch (line spacing) on Al 3003</b>	<b>67</b>
<b>3.3.2</b>	<b>Effect of frequency on Al3003</b>	<b>68</b>
<b>3.3.3</b>	<b>Effect of power on Al 3003</b>	<b>69</b>
<b>3.3.4</b>	<b>Effect of scanning speed on Al3003</b>	<b>69</b>
<b>3.3.5</b>	<b>Surface morphology analysis</b>	<b>71</b>
<b>3.3.6</b>	<b>Final results of Al 3003</b>	<b>74</b>
<b>3.3.7</b>	<b>Final results of Al 3003</b>	<b>75</b>
<b>3.3.8</b>	<b>Corrosion Results of Al 3003</b>	<b>77</b>
<b>3.4</b>	<b>Conclusions</b>	<b>78</b>
<b>3.5</b>	<b>Future projects suggested</b>	<b>79</b>
	<b>References</b>	<b>80</b>

## List of Tables

No	Title	Page
(1-1)	<b>A Comparison of Different Marking Technologies</b>	<b>8</b>
(1-2)	<b>Typical compositions and properties of stainless steel</b>	<b>19</b>
(1-3)	<b>Designation system for aluminum alloys</b>	<b>23</b>
(2-1)	<b>Chemical composition of stainless steel 304</b>	<b>33</b>
(2-2)	<b>Physical and optical properties of AISI 304 stainless steel</b>	<b>34</b>
(2-3)	<b>Chemical composition of Al3003</b>	<b>34</b>
(2-4)	<b>Physical and optical properties of Al 3003</b>	<b>34</b>
(2-5)	<b>parameters of Laser devices</b>	<b>36</b>
(2-6)	<b>parameters of Laser for experimental of SS304</b>	<b>37</b>
(2-7)	<b>parameters of Laser for experimental of Al 3003</b>	<b>38</b>
(3-1)	<b>The chemical composition of SSt.304 surface according to EDS analysis of substrate and treated samples P=8 W, Frequency = 80 kHz, H=0.01mm</b>	<b>51</b>
(3-2)	<b>Different color results with different laser parameters for all experiments</b>	<b>55</b>
(3-3)	<b>Spectrophotometer results for L*, a*- and b*-values of CIELAB color space for the twenty-five samples, at power = 8 W pulse duration 10 <math>\mu</math>s frequency 80 kHz, line spacing 0.01mm and scanning speed from 50 to 650 mm/s</b>	<b>58</b>
(3-4)	<b>Spectrophotometer results for L*, a* and b*values of CIELAB color space for the twenty-five samples, at power 8W pulse duration 81 ns, line spacing 0.01mm, frequency 80 kHz and scanning speed from 50 to 650 mm/s</b>	<b>60</b>
(3-5)	<b>Spectrophotometer results for L*, a* and b*values of CIELAB color space for the twenty-five samples, at power 4W, line spacing 0.001 mm, frequency 80 kHz and scanning speed from 50 to 650 mm/s, pulse width 10<math>\mu</math>s</b>	<b>61</b>

No	Title	Page
(3-6)	<b>Spectrophotometer results for L*, a* and b* values of CIELAB color space for the twenty-five samples, at power 4W, line spacing 0.001 mm, frequency 80 kHz and scanning speed from 50 to 650 mm/s, Pulse width 81ns</b>	<b>63</b>
(3-7)	<b>The chemical composition according to EDS results for substrate and samples treated with different parameters</b>	<b>74</b>

### List of Figures

No	Title	Page
(1-1)	<b>General classification of the laser material processing techniques</b>	<b>5</b>
(1-2)	<b>The processes in terms of laser power density as a function of contact time for the processing of various laser materials</b>	<b>6</b>
(1-3)	<b>Laser marking technologies</b>	<b>9</b>
(1-4)	<b>Setups for laser color marking experiments (a) galvanometer scanning and (b) translation phases, M1, M2 and M3 are mirrors reflections</b>	<b>10</b>
(1-5)	<b>The interference effect of the oxide film(<math>n_0</math> and <math>n_1</math>) are the refraction indices of air and oxide, respectively</b>	<b>14</b>
(1-6)	<b>The CIELAB color space is depicted in this diagram</b>	<b>15</b>
(1-7)	<b>Ellingham diagram for metallurgic alloy important oxides</b>	<b>26</b>
(2-1)	<b>Microsecond fiber laser</b>	<b>35</b>
(2-2)	<b>Nanosecond fiber laser</b>	<b>35</b>
(2-3)	<b>The schematic diagram of laser scanning on stainless steel 304</b>	<b>37</b>
(2-4)	<b>The schematic diagram of laser scanning on Al 3003</b>	<b>37</b>
(2-5)	<b>FESEM ZEISS MODEL <math>\Sigma</math>IGMA/VP</b>	<b>39</b>
(2-6)	<b>X-ray diffractometer</b>	<b>39</b>

No	Title	Page
(2-7)	<b>Complete system setup for corrosion polarization measurements</b>	<b>42</b>
(3-1)	<b>Optical microscope image with different of hatch ,scanning speed 100mm/, PRR 80kHz for SS 304</b>	<b>43</b>
(3-2)	<b>Coloring parameters: hatch 0.05mm, P 8W ,PRR 80 kHz scanning speed from(100mm/s) incremented 25 for Ss 304</b>	<b>44</b>
(3- 3)	<b>Microscopic image (A)line spacing 0.01mm , (B) line spacing 0.001mm, scanning speed 100 mm/s, PRR 80 kHz</b>	<b>44</b>
(3-4)	<b>Color results at different range of frequency and power 4W, hatch 0.001mm and scanning speed from 175 mm/s to 625mm/s incremented 25.</b>	<b>45</b>
(3-5)	<b>Microscopic images magnification 10 X of the colored samples with laser parameters at power 4 W, frequency 80 kHz, hatch 0.001mm and 10<math>\mu</math>s pulse width</b>	<b>46</b>
(3-6)	<b>Morphology which distinguish between treated p 8 W , scanning speed 350 mm/s, PRR 80 kHz and (HAZ) of SS 304</b>	<b>47</b>
(3-7)	<b>(A) SEM micrograph showing the cracks on a colored surface of stainless steel, power 4 W, scanning speed 325 mm/s, frequency 80 kHz, pulse duration 10<math>\mu</math>s, hatch 0.001mm, (B) cracks width</b>	<b>48</b>
(3-8)	<b>FESEM images of different sample surface (A) brown, (B) yellow, (C) dark green, (D) dark brown. Parameters illustrated in Table (3-2)</b>	<b>48</b>
(3-9 )	<b>EDS analysis of the sample surface (A)untreated stainless steel 304, (B) laser treated sample at speed 650 mm/s, P 8 W, h 0.01mm</b>	<b>49</b>
(3-10)	<b>XRD graph of sample scanning 275 mm/s microsecond pulse width result brown color</b>	<b>50</b>
(3-11)	<b>XRD graph of sample scanning (275mm/s) 81nanosecond pulse width, h (0.01mm) result dark green color</b>	<b>52</b>
(3-12)	<b>Stainless steel 304 color plate A (power 8 W, hatch 0.01 mm, pulse width 10 <math>\mu</math>s), B (power 4 W, hatch 0.001 mm, pulse width 10 <math>\mu</math>s), C (power 8 W, hatch 0.01 mm, pulse width 81 ns), D (power 4 W, hatch 0.001 mm, 81 ns) all scanning speed from 50 to 650 mm/s incremented 25 and fixed frequency at 80 kHz</b>	<b>53</b>

No	Title	Page
(3-13)	Spectrum reflection untreated stainless steel 304	54
(3-14)	Colored samples at nanosecond pulse width with different speed scanning at power 8 W	56
(3-15)	Colored sample at microsecond fiber laser with different speed scanning at power 8W	57
(3-16)	Comparison roughness results between microsecond and nanosecond pulse width at power 8 W, hatch0.01mm, PRR 80 kHz with scanning speed from 50 to 650 mm/s	57
(3-17)	Comparison roughness results between microsecond and nanosecond pulse width at power 4W, hatch0.001mm, PRR 80 kHz and scanning speed from 50 to 650 mm/s	65
(3-18)	Comparison of the corrosion result between base stainless steel 304, microsecond and nanosecond pulse width at power 4 W hatch 0.001mm with scanning speed 325mm/s and frequency 80 kHz	65
(3-19)	Optical microscope image with different of hatch for Al 3003	66
(3-20)	Effect of low frequency 40 kHz on color result when scanning speed was from 650 to 850 mm/s	67
(3-21)	Al 3003 treated by laser colorizing parameters	68
(3-22)	P 3W, PRR 80 kHz, h 0.005 mm scanning speed (25-125) mm/s	75
(3-23)	Al 3003 plate at scanning speed (25 to 125) mm/s step 25, power 8W	69
(3-24)	Al 3003plate treated by power 6 W, scanning speed 25 mm/s, PRR 80 kHz, hatch 0.005mm, (A) 10 $\mu$ s pulsed width and (B) 81 ns pulsed width	69
(3-25)	Al plate treated by 10 microsecond pulsed width and scanning speed from (400 -850) mm/s.	70
(3-26)	SEM image of Al sample at parameters scanning speed 150 mm/s, power 6W, hatch 0.005 mm, PRR 80 kHz (A)10 $\mu$ s pulse width (B)81 ns pulse width	71
(3-27)	FESEM image Cross section of Al sample at parameters scanning speed 150 mm/s, power 6 W, hatch 0.005 mm frequency 80 kHz (A)10 $\mu$ s pulse width (B)81 ns pulse width	72

No	Title	Page
(3-28)	<b>EDS analysis of Al surface: (A) laser untreated Al (B) laser treated sample at speed 150 mm/s, P 6 W, hatch 0.005mm and pulse width 10 <math>\mu</math>s</b>	<b>73</b>
(3-29)	<b>Al 3003 plate treated by power 6 W, Scanning speed from 25 to 375 mm/s, PRR 80 kHz, hatch 0.005mm, (A) 10 <math>\mu</math>s pulsed width, (B) 81 ns pulsed width, (C) 10 <math>\mu</math>s pulsed width with hatch 0.001mm and (D) 81 ns pulsed width with hatch 0.001mm</b>	<b>75</b>
(3-30)	<b>Comparison roughness of Al 3003 results between microsecond and nanosecond pulse width at power 6 W, hatch 0.001mm and scanning speed (25-375) mm/s</b>	<b>76</b>
(3-31)	<b>Comparison roughness of Al 3003 results between microsecond and nanosecond pulse width at power 6 W, hatch 0.005mm and scanning speed (25-375) mm/s</b>	<b>76</b>
(3-32)	<b>Comparison corrosion result between base Al 3003, microsecond and nanosecond pulse width at power 6 W hatching 0.005mm with scanning speed 150mm/s and frequency 80 kHz</b>	<b>77</b>

## List of abbreviations

<b>Abbreviations</b>	<b>Meaning</b>
<b>2-D</b>	<b>Two Dimensions</b>
<b>3- D</b>	<b>Three Dimensions</b>
<b>AISI</b>	<b>American Iron And Steel Institute</b>
<b>Al</b>	<b>Aluminum</b>
<b>Au</b>	<b>Gold</b>
<b>B</b>	<b>Boiling Point</b>
<b>C</b>	<b>Carbon</b>
<b>CIE</b>	<b>International commission on illumination color system</b>
<b>CO<sub>2</sub></b>	<b>Carbon Dioxide</b>
<b>Cr</b>	<b>Chromium</b>
<b>Cr<sub>2</sub>O<sub>3</sub></b>	<b>Chromium(XII) Oxide</b>
<b>Cu</b>	<b>Copper</b>
<b>Cu- Br</b>	<b>copper bromide vapor laser</b>
<b>DSS</b>	<b>Duplex stainless steels</b>
<b>EDS</b>	<b>Energy Dispersive Spectroscopy</b>
<b>EFL</b>	<b>Effective Focal Length</b>
<b>FCC</b>	<b>Face-Centered Cubic</b>
<b>FESEM</b>	<b>Field Emission Scanning Electron Microscope</b>
<b>H</b>	<b>Hight</b>
<b>Hz</b>	<b>Hertz</b>
<b>ISO</b>	<b>International Organization For Standardization</b>
<b>J</b>	<b>Joule</b>

<b>Abbreviations</b>	<b>Meaning</b>
<b>k</b>	<b>Kilo</b>
<b>K</b>	<b>Kelvin</b>
<b>L</b>	<b>Low</b>
<b>LIPSS</b>	<b>Laser Induced Periodic Surface Structure</b>
<b>M</b>	<b>Melting Point</b>
<b>Mg</b>	<b>Magnesium</b>
<b>Mn</b>	<b>Manganese</b>
<b>Mo</b>	<b>Molybdenum</b>
<b>MOPA</b>	<b>Master Oscillator Power Amplifier</b>
<b>Nd:YAG</b>	<b>Neodymium Doped Yttrium-Aluminum- Garnet</b>
<b>Ni</b>	<b>Nickel</b>
<b>NiO</b>	<b>Nickel Oxide</b>
<b>O<sub>2</sub></b>	<b>Oxygen</b>
<b>ODS</b>	<b>Oxide Dispersion Strengthen</b>
<b>R</b>	<b>Reflectance</b>
<b>SEM</b>	<b>Scanning Electron Microscope</b>
<b>Si</b>	<b>Silicon</b>
<b>SPR</b>	<b>Surface Plasma Resonance</b>
<b>Ti</b>	<b>Titanium</b>
<b>TiO</b>	<b>Titanium oxide</b>
<b>TiO<sub>2</sub></b>	<b>Titanium Dioxide</b>
<b>UV</b>	<b>Ultraviolet</b>
<b>XRD</b>	<b>X-Ray Diffraction</b>

## List of symbols

<b>Symbols</b>	<b>Meaning</b>	<b>Units</b>
$\omega$	Spot size	$\mu\text{m}$
$\tau$	Pulse duration	$\mu\text{s}, \text{ns}$
$\lambda$	Wavelength	nm
$\theta_i$	The incidence angle	degree
$\delta$	Optical path difference	nm
$R_a$	Average roughness	$\mu\text{m}$
PRR	Pulse repetition rate	Hz
$P_{\text{avg}}$	Average power	watt
P	Power	watt
$n_1$	Refractive Index of The Oxide Film	-
$n_0$	Refractive Index of The Air	-
M	Melting point	Celsius
$L^*$	Lightness value (0 to 100)	-
$k$	An integer	-
IE	Protection efficacy	-
I corr	The corrosion current density	$\mu\text{A}/\text{cm}^2$
h	The oxide film thickness.	nm
H	Hatch	mm
$F_{\text{acc}}$	The accumulated heat	$\text{J}/\text{cm}^2$

<b>Symbols</b>	<b>Meaning</b>	<b>Units</b>
<b>f</b>	<b>Focal length</b>	<b>mm</b>
<b>E</b>	<b>Laser pulse energy</b>	<b>Joule</b>
<b>b*</b>	<b>Blue/yellow value (-128 to 127)</b>	<b>-</b>
<b>B</b>	<b>Boiling point</b>	<b>Celsius</b>
<b>a*</b>	<b>Red/green value (-128 to 127)</b>	<b>-</b>
$\Sigma$	<b>Sigma (summation)</b>	<b>-</b>
$\Delta L^*$	<b>L sample - l standard</b>	<b>-</b>
$\Delta G$	<b>Cibss energy</b>	<b>Joule</b>
$\Delta b^*$	<b>B sample - b standard</b>	<b>-</b>
$\Delta a^*$	<b>A sample - a standard</b>	<b>-</b>
<b>+a</b>	<b>Direction depicts a shift toward red</b>	<b>-</b>
<b>%</b>	<b>Percent sign</b>	<b>-</b>
<b>T<sub>s</sub></b>	<b>Final surface temperature</b>	<b>Kelvin</b>

# **Chapter One**

## **Introduction and Basic Concepts**

---

**1.1 Introduction**

Laser surface treatment has been commonly used to improve the functional properties for metallic materials, such as their optical properties[1]. Laser marking is a thermal process that includes scanning or projecting intense laser energy onto a target material to create permanent contrasting marks [2].

Lasers could mark almost any material type, that is to be used for imprinting complex logos, information production, bar-code, 2D matrix code, data-code, part-number, graphics and aesthetic laser marks [3].

Metal surface color marking was made possible by, emulsion coating, printing, or electrolytic oxidization procedure, poor scratch features and wear resisting, the process difficulty and the long-term color fade, usually, the drawbacks of the printing process anodization include the inability to label selectively or in several colors' simultaneously[4].

Color marking by lasers has been known as a technique for years ago, nevertheless it has not been widely used in industrial production as it is being considered as hard, time-consume and mostly not repeatable [4,5].

These methods are based on interaction between the laser beam and the material surface[6]. The properties of the laser beam and a material used, identify what kind of process will occurs. The material absorbs one part of laser radiation when the second part reflects and the third part passes through the material[7].

In laser metal interaction the laser fluence is the most important parameter, which is given by combination of laser parameters such as pulse repetition rate, energy, hatch and scanning speed of the laser and the material parameters temperature, absorptivity, reflectivity, geometry of the surface and state. The absorbed laser radiation causes different

processes on the material surface, that can lead to ablation, bleach in, thermal oxidation, foaming, etc.[7].

## 1.2. Laser Matter Interaction

The processes of laser matter interaction can be divided into three major categories, heating, melting and vaporization, as well as plasma formation. Laser cleaning process is a special case of machining of laser matter interaction [8,9].

### 1.2.1. Heating

When the material is irradiated by an appropriate laser beam parameter, its surface temperature begins to increase due to the surface absorption after certain time. An approximate estimate of the surface temperature ( $T_s$ ) of a work piece illuminated by spatially uniform energy source which is turned at time ( $t$ ) is obtained from the equation (1.1) [10].

$$T_s = T_o + \frac{2 F_o (1 - R) \left( \frac{kt}{\pi} \right)^{1/2}}{K} \text{----- [1-1]}$$

Where,

$T_s$ : Final surface temperature ( $^{\circ}\text{K}$ )

$T_o$ : Initial temperature ( $^{\circ}\text{K}$ )

$F_o$ : Incident flux ( $\text{Wm}^{-2}$ )

$R$ : Surface reflectivity (dimensionless)

$k$ : Thermal diffusivity ( $\text{m}^2\text{s}^{-1}$ )

$t$ : Irradiation time (s)

$K$ : Thermal conductivity ( $\text{Wm}^{-1} \text{ } ^{\circ}\text{K}^{-1}$ )

Equation (1-1) is valid up to the time that the surface begins to melt.

### 1.2.2. Melting

If the laser beam heats a surface for a long time, then surface temperature may reach the melting temperature ( $T_m$ ) and the surface melting begins. This occurs at a time ( $t_m$ ) given by the equation (1-2) [10].

$$t_m = \frac{\pi K}{4kF_o^2} \left( \frac{T_m - T_o}{1 - R} \right)^2 \text{----- [1-2]}$$

Where,

$t_m$ : Time to reach melting (s)

$T_m$ : Melting temperature ( $^{\circ}\text{K}$ )

Effective melting by laser beam depends on propagation of a fusion front through the sample during the time of interaction, at the same time avoiding vaporization of the surface. In most cases the melting occurred in areas with a large number of small craters [11].

### 1.2.3. Vaporization

After melting of the surface, the vaporization begins, Because of the great speed with which vaporization begins; there is no time for much material to melt. Thus, at high laser irradiance ( $> 10^6 \text{ W/cm}^2$ ), the dominant physical process is vaporization and the role of melting tends to be less significant. The time ( $t_B$ ) to reach the vaporization temperature is given by the equation (1-3) [12].

$$t_B = \frac{\pi}{4} \frac{K \rho C}{F^2} (T_B - T_o)^2 \text{----- [1-3]}$$

Where,

$t_B$ : Time to reach the vaporization temperature (s)

$\rho$ : Density ( $\text{Kg m}^{-3}$ )

C: Heat capacity ( $\text{J. Kg}^{-1} \cdot ^\circ\text{K}^{-1}$ )

$T_B$ : Boiling temperature ( $^\circ\text{K}$ )

F: Absorbed irradiance ( $\text{W. m}^{-2}$ )

The time to reach the vaporization temperature is often small fraction of the laser pulse duration. In this case, an equilibrium condition may be reached, so that the vaporizing surface retreats at a steady rate, this rate is given by the equation (1-4) [12].

$$v_B = F / \rho [L + C (T_B - T_o)] \text{-----} [1-4]$$

Where,

L: The specific latent heat ( $\text{J. Kg}^{-1}$ )

$v_B$ : Vaporizing surface rate ( $\text{m. s}^{-1}$ )

#### 1.2.4. Plasma Formation

When the laser irradiant is greater than  $1 \text{ GW/cm}^2$ , then in most materials the vaporized material is heated and ionized by the laser beam forming hot opaque plasma. The plasma will grow back towards the laser and a laser supported absorption wave is produced. The plasma absorbs the light and shields the surface [10]. The plasma will continue until the end of the laser pulse, also plasma can play an effective role in absorbing laser radiation and reheating the target surface [8].

### 1.3 Laser Material Processing

Military, scientifically, medical and commercial applications of lasers were developed since the laser invention, in the 1960. Coherence, high mono chromaticity and ability of reaching the extreme high power, are all features that allows for specialized uses. In general, laser

applications for material processing can be divided into two broad categories [16].

- (a) Applications requiring a small amount of intensity and resulting in no major phase or state transition.
- (b) Applications requiring substantial amount of intensity to induce the state transformations. Figure (1-1) [14].

Laser material processing can be broadly divided into four major categories, namely, forming (manufacturing of near net-shape or finished products), joining (welding, brazing, etc.), machining (cutting, cleaning, etc.) and surface engineering (processing confined only to the near-surface region) [16].

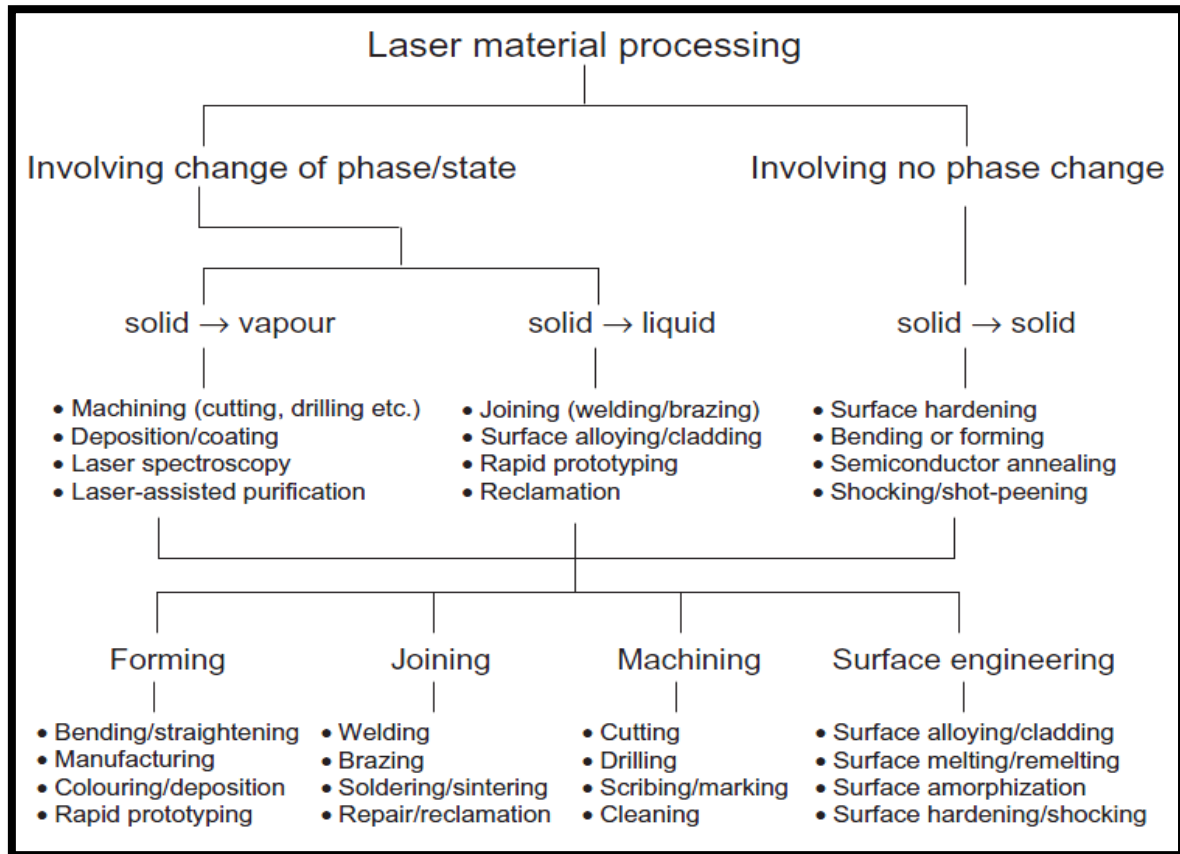
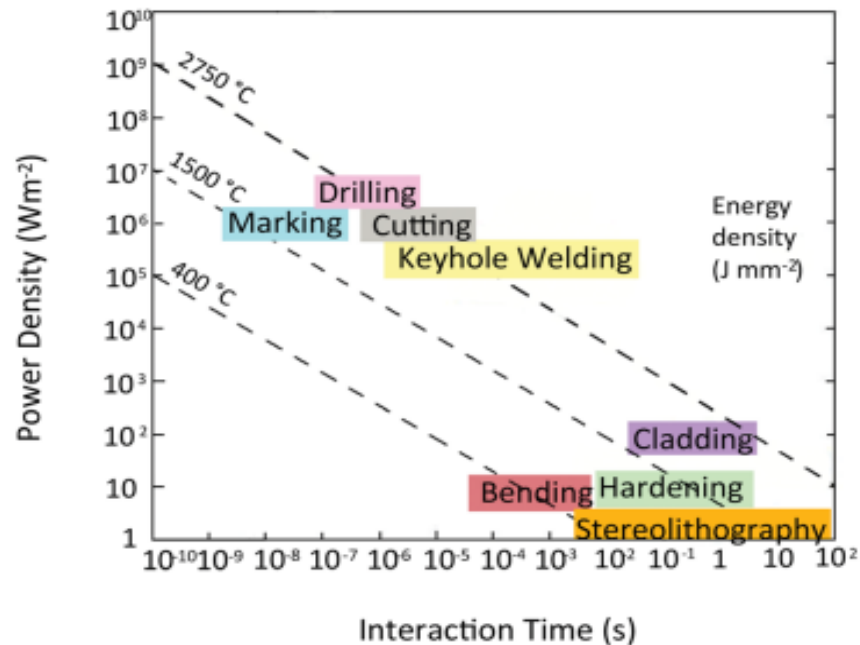


**Figure (1-1): General classification of the laser material processing techniques[16].**

The processes in terms of laser power density as a function of interaction time for the processing of various laser materials. As Figure (1-2) [17].



**Figure(1-2): The processes in terms of laser power density as a function of contact time for the processing of various laser materials [18].**

The laser power density and interaction time, are carefully determined, that the material exhibit the desired heat changing and phase transformation. It was proved that the stereolithography, hardening and bending could be dependent on surface heating without the surface being melt, which requires low power density [17].

On the contrary, surface melting, cladding, glazing, welding and cutting, involving material melting, requires elevated power densities. Same as in cutting, drilling operations that remove material via vaporization, which need the delivery of high power densities within a very short laser interaction time and pulse duration[16].

---

### 1.3.1 Laser Marking Process

Laser marking is primarily in the form of alphanumeric and 2D Data-Matrix codes applied to the product's surface, which contain details about the product's manufacturing date and serial number [19-21]

Different types of lasers and optical delivering systems for transportations, focus locked and beam deviation, are used by laser marking systems for metals marking, ceramic, leathers, glasses, plastics, wood and other different materials types [22].

The laser marking is accomplished by creation of visual surface contrasting which could be produced in two different ways: either a specular reflection changing or a color changing [23].

Several different processes were available, that could be used to change the color or the specular reflection of materials. Nevertheless, the laser marking process could have the same principle for different materials kinds. Metals can be colored by oxidization in the same way as they can be colored by other methods (Inkjet , Electrochemical etching, Dot peening) [24].

It is important to evaluate and decide the most effective marking form ,as illustrated in Table (1-1)[25].

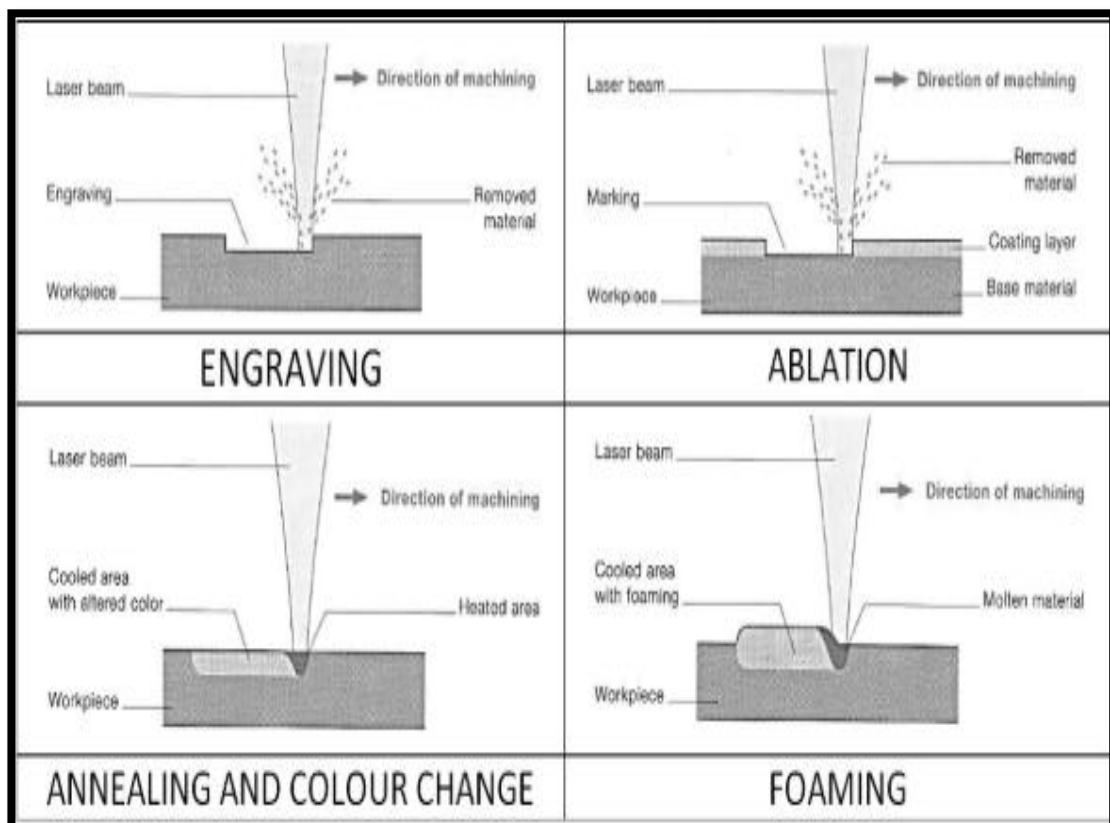
Table (1-1): A Comparison of Different Marking Technologies [25,26].

Parameters	Laser marking	Inkjet	Electrochemical etching	Dot peening
Labelable materials	High	Average	Low	High
Capital purchase	Average	Low	Low	High
Adaptability	High	High	High	Low
Frictional (chemical stresses)	No	No	No	Yes
Type of marking method	Non- contact	Contact	Contact	Non- contact
Flexibility (distance between part and mark device)	Average	Average	Low	High
Marking technologies	Steel, Al, Fe, Ti, Mg, Cu, Glass, Ceramic, Plastic	Steel, Al, Fe, Ti, Mg, Cu, Glass, Ceramic, Plastic	Steel, Al, Fe, Ti, Mg, Cu	Steel, Al, Fe, Cu, Plastic

### 1.3.2 Methods of Laser Marking

Laser marking was used in various methods of marking as shown and explained below in Figure (1-3) [27].

1. Engraving, in which portions of the parent material are removed by a laser beam. The mark appears as depressions.
2. Ablation is the process of removing coating layers with a laser. The mark can see through to the underlying base material.
3. Annealing and color change processing, which involves heating the workpiece with a laser to change the color while keeping the surface smooth [27].
4. Foaming is a chemical reaction that occurs inside the plastic material that results in the formation of gas bubbles that produce raised, textured markings[28].



**Figure(1-3): Laser marking technologies [28].**

### 1.3.3 Beam Delivery System

Laser color marking requires relative motion between the laser beam and the sample. There are two common methods for achieving relative motion: The first approaches use two galvanometer-driven scanning mirrors to scan over samples. The second type is moving a sample under a fixed laser beam using a computer-controlled 2D or 3D translational stage [29].

It allows for a large processing tool for high-moving-speed processing, while the first type allows for a reliable, repeatable and fine resolution for low-speed processing, as shown in Figure (1-4)[30].

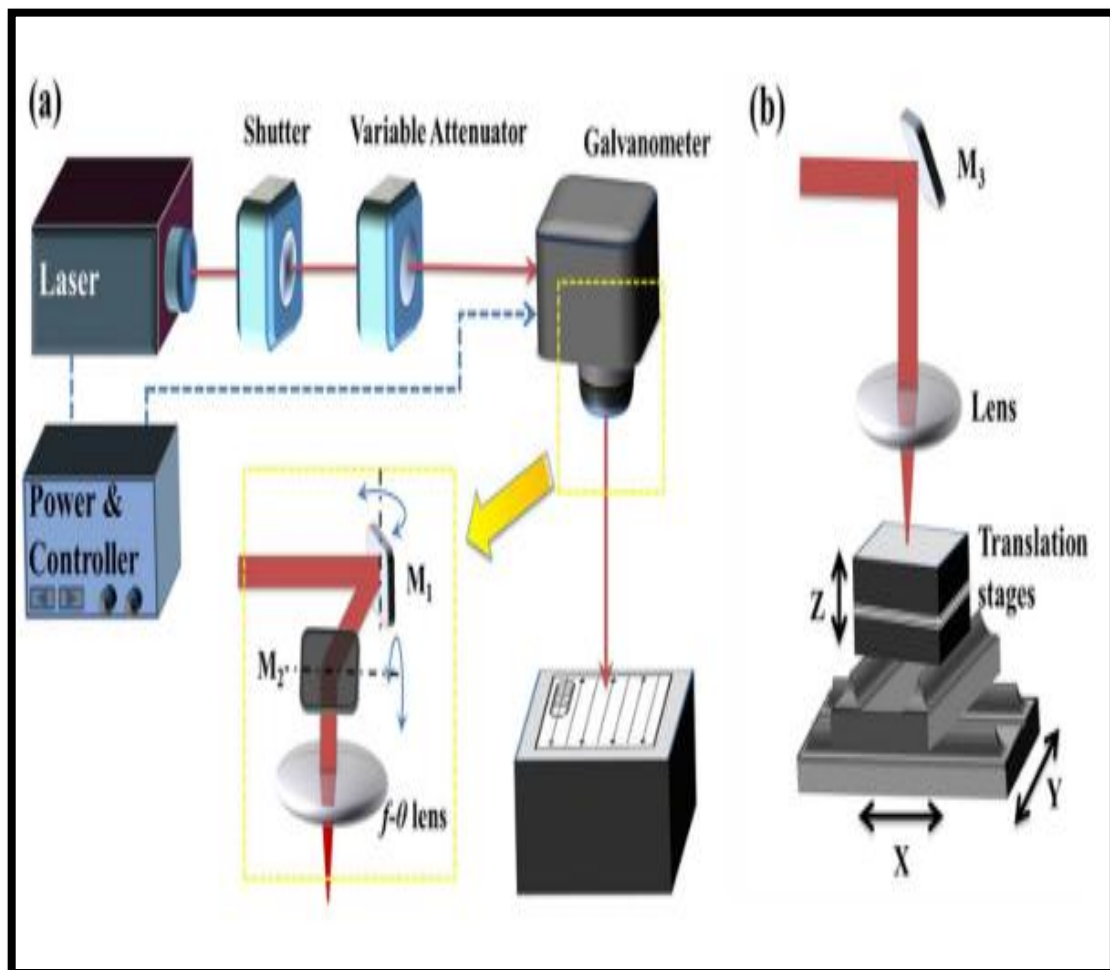


**Figure (1-4): Setups for laser color marking experiments (a) galvanometer scanning and (b) translation phases,  $M_1$ ,  $M_2$  and  $M_3$  are mirrors reflections[29].**

---

## 1.4 Laser Types Used in Marking

Depending on the materials and the required marking rate, various types of laser marking can be used.

**1- Carbon Dioxide or CO<sub>2</sub> laser:** - They are suitable for a large variety of materials, relatively soft, including wood and plastic. The CO<sub>2</sub> laser emits 10.6  $\mu\text{m}$  of infrared radiation and can be generated with power outputs of between a few watts and a few kilowatts, generally (but not always) [6,31,32]

**2- Neodymium yttrium aluminum garnet (Nd: YAG) laser:** - This is the most widely used in laser machining applications. The output of the Nd: YAG laser can be continuous, pulsed, or Q-switched. The absorption properties of the crystal dictate the wavelength of the light used for pumping.

In addition, the Nd: YAG laser can be worked in frequency-doubled mode, which generates an output in the visible green spectrum at 532 nm. In addition to frequency-doubled operation, the laser is available in frequency tripled 355 nm and frequency quadrupled 266 nm modes[3]. The Nd: YAG laser produces a superior result on metals and alloys [6,33].

**3- Fiber Laser:-** Optical fiber lasers in which an appropriately doped optical fiber forms the gain medium is revolutionizing the field of lasers[13]. Fiber lasers have a number of unique advantages over other laser systems. High pump intensities can be accomplished even with limited pump powers since the laser beam is restricted to a very small cross-sectional region within the center of the fiber, resulting in lower pump power thresholds[34].

Because both pump and the laser beam propagate inside the fiber, they converge very well, which increases the laser's efficiency to

the point where efficiencies of up to 80% are possible. Since the pump laser beam is guided by the fiber, very long cavities can be used without worrying about the pump laser beam diverging. Because of their high surface area to volume ratio, fiber lasers have no thermal issues and heat dissipation is even easier[31].

The output beam has very high quality and relatively inexpensive as it emerges as the fundamental mode of the fiber [35]. The laser's components are made up of spliced fibers, there are no mechanical problems as there are with bulk lasers that have different mirrors. There are many important fiber lasers, including erbium-doped fiber lasers (1550 nm wavelength) and ytterbium-doped fiber lasers (1060 nm wavelength) [31].

The Master Oscillator Power Amplifier (MOPA) and Q-switched were the two most general fiber laser sources utilized in industrial metal marking applications [36].

## 1.5 Mechanisms of Color Generation

Three major mechanisms based on pulse width and material properties have been demonstrated for laser coloring on mineral surfaces.

1. **Surface Oxidation:** - Pulsed Laser such as microsecond and nanosecond as a Nd: YAG or fiber laser [37,38] acts as a heating source, creating a transparent or semi-transparent oxide film on the metal surface. The interference effect of the thin film creates the observed color at any point[39].
2. **Laser Induced Periodic Surface Structure (LIPSS) :-** The ultrashort pulse laser, for example picosecond or femtosecond laser produced color by grating diffraction [40,41] and different morphology formation[42], like as Nano-structures in the form of Nano-protrusions and Nano voids[43].

The color of the surface changes depending on the viewing angle[29] but ultrashort pulse laser is extremely costly and is not conducive to the promotion of laser coloring technology. So many researches have been conducted to better understand the short pulse laser color[39].

**3-Surface Plasma Resonance(SPR) :-** The metallic nanoparticles and nanostructures a plasma resonance effect caused by metal nanoparticles and nanostructures is the main cause of the color formation which lead to high absorption at some wavelengths[40]. The color of the surface is not viewing angle-dependent [29,45].

### **1.5.1 Mechanisms of Laser Coloring Through Layer Oxidation**

The mechanism begins as follows: -

1. After absorbing laser energy, electrons on the material surface changed from a low-energy state to a high-energy state and the surface temperature of the irradiated region increased. Oxygen in the air interacts with the mineral at high temperatures[46].
2. The first oxide begins to form on the surface after the formation of ionic bonds between oxygen-free electrons and mineral ions.
3. In the laser-irradiated region, the metal oxide grows laterally and forms a continuous thin film [19].
4. The lateral growth is followed by a perpendicular growth due to the cation/anion diffusion at the metal/oxide interface[40].

When a transparent or semitransparent oxide film forms on the substrate surface as a result of laser heating. It can be reflected from the top and bottom surfaces of the oxide film when illuminated with white

light. The difference in optical paths between the two reflected beams can be expressed by the following equation: -

$$\delta = 2h \sqrt{n_1^2 - \sin^2 \theta_i} \text{ ----- (1-5)}$$

Whereas: -

$h$  = the oxide film thickness (nm).

$n_1$  = refractive index of the oxide film.

$\theta_i$  = the angle of incidence (degree).

When the optical path difference  $\delta = k \lambda$  ( $k$  is an integer) for a wavelength  $\lambda$ , the specific color is enhanced due to the constructive interference. The above equation indicates that the enhanced color is dependent on the refractive index of the oxide layer, the thickness, viewing angle and order of interference ( $k$ ).

The oxide film interference and surface color changing with viewing angle, which confirms this laser color marking method Figure (1-5). But according to some studies, the intrinsic colors of metal oxides play a larger role in the creation of surface color [29].

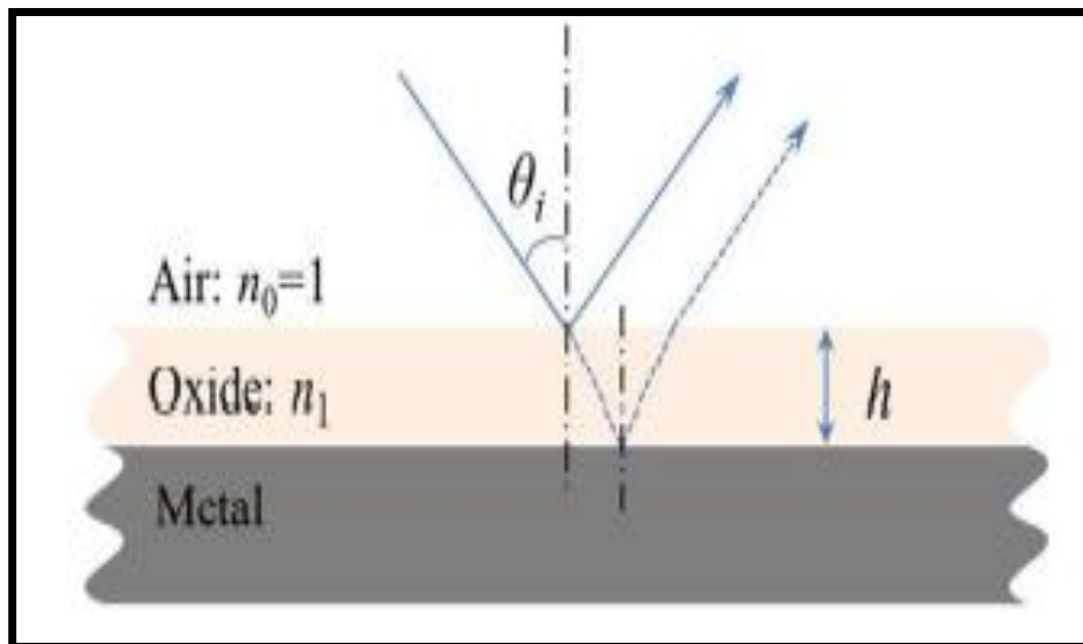


**Figure (1-5): The interference effect of the oxide film ( $n_0$  and  $n_1$ ) are the refraction indices of air and oxide, respectively [29].**

## 1.5.2 CIE $L^*a^*b^*$ and Color Difference

Color is a visual sensation that observed when light refracts or reflects off the surface of objects [47]. CIE is Commission International de l'Éclairage [48] or International Commission on illumination that is capable of expressing in all color nature thus the CIE-Lab model provides color options[49].

$L^*$ : Lightness value (0 to 100),  $L = 0$  (black or total absorption) at the bottom.

$a^*$ : Red/Green Value (-128 to 127), +a direction depicts a shift toward red.

$b^*$ : Blue/Yellow Value (-128 to 127), +b movement represents a shift toward yellow, at the center of this plane is neutral or gray [49] as shown in Figure (1 -6 ) the color-plotting diagrams for CIE  $L^*a^*b^*$ .

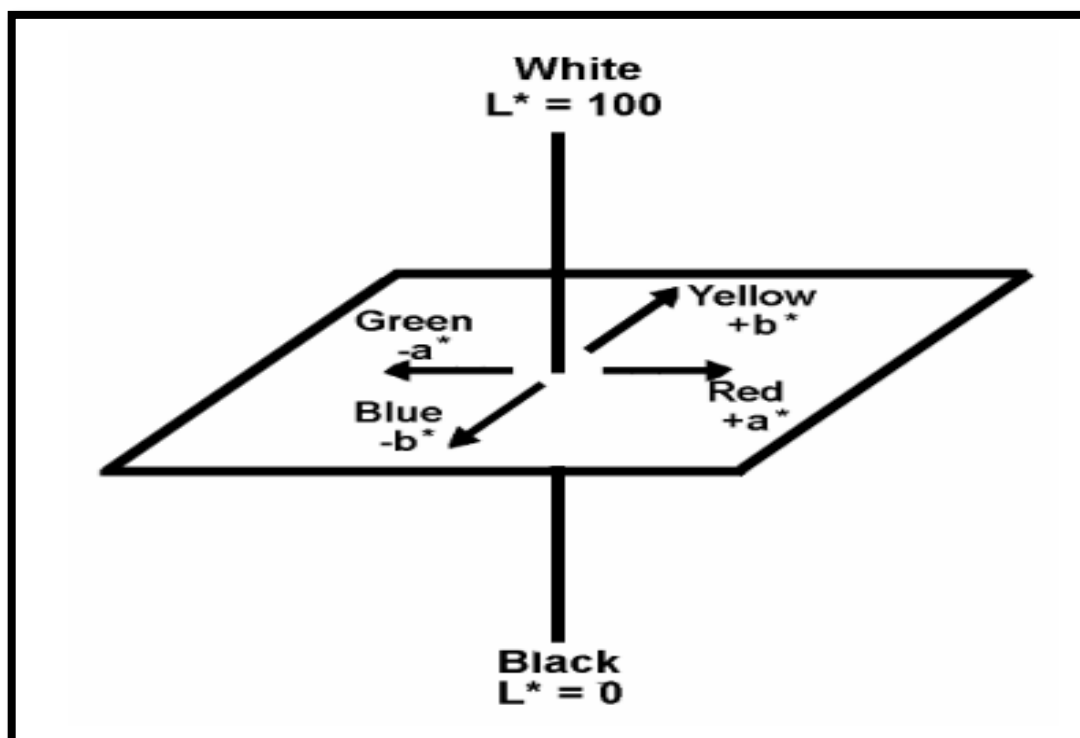


**Figure (1-6 ):** The CIELAB color space is depicted in this diagram [51].

Color shift can be calculated as the modulus of the distance vector between the original color values and the real color coordinates. This is referred to as total color variation. Total color difference ( $\Delta E$ ) expresses the color difference from the standard plate calculated as equation below [51, 52].

$$\Delta E = \sqrt{\Delta a^{*2} + \Delta b^{*2} + \Delta L^{*2}} \quad \text{----- (1-6)}$$

$\Delta a^*$  = a sample - a standard.

$\Delta b^*$  = b sample - b standard.

$\Delta L^*$  = L sample - L standard [53].

Standard: - mean the work piece before coloring (control).

Sample: - means the work piece after coloring.

$0 < \Delta E < 1$  - observer does not notice the difference,

$1 < \Delta E < 2$  - only experienced observer can notice the difference,

$2 < \Delta E < 3.5$  - The disparity is also noticeable by an inexperienced observer,

$3.5 < \Delta E < 5$  - clear difference in color is noticed,

$5 < \Delta E$  - observer notices two different colors [49].

## 1.6 Advantages of Laser Color Marking

The laser color marking has many advantages: -

1. The advantages of the new technology include increased precision, versatility and the ability to record a large amount of data per unit area (bar and matrix codes) [54].
2. As compared to traditional technologies such as ink printing, electrolytic oxidation and emulsion blackening or coloring on the metal surface, it has a number of advantages, including contactless

treatment, scratch resistance, no fading and digital technology that allows the marking patterns to be changed or edited easily[55].

3. This technique is very effective, non-contact, fast and it can be used on a variety of metallic and nonmetallic materials and it does not require any additional consumables or toxic solutions, reducing pollution[56].
4. A laser source has the advantage of allowing for very local changes in the physical-chemical properties of the sample surface without affecting the bulk material properties. This advantage enables the development of a diverse range of colors on small surfaces [19]
5. It's straight forward to automate and incorporate (direct writing of patterns can established using computer-controlled movement of the beam or sample) [32].
6. Excellent usability, even on uneven surfaces, with high efficiency and low running costs[32].

### **1.7 Disadvantages of Laser Color Marking**

The laser color marking has many disadvantages: -

1. Investing costs a lot of money[17].
2. A skilled operator is needed [17].
3. Not all materials respond to each laser in the same way: the parameters differ depending on the laser equipment (laser wavelength, lens, etc.) and most likely, the material composition[57].

### **1.8 Stainless Steel Types, Grades and Uses**

Stainless steels are so common in our everyday lives, it's hard to list all of their uses. The background development of these alloys, as well as

---

their relationship with other ferrous alloy systems, must be considered in order to fully comprehend their application [57].

It was discovered decades ago that steel with a minimum of 12 percent chromium can be rendered “stainless” by imparting corrosion and oxidation resistance. As a result, stainless steels are ferrous alloys with a minimum of 12% Cr content [58].

In relatively benign conditions, an adherent, self-healing chromium oxide may form on or at the steel surface at this Cr level, protecting the steel. Stainless steels, in addition to being corrosion-resistant, do not discolor in natural atmospheric conditions. Stainless steels have been used in construction since long time[57].

The numerous uses that rely on stainless steels illustrate their value to our economy. Cooking utensils, furniture and building construction are examples of simple applications, while parts for spacecraft, boilers in the chemical industry and cooling channels in nuclear reactors are examples of high-end applications [58].

This was the start of a family of stainless-steel alloys that were divided into subcategories (grades) including:

1. Austenitic stainless steel
2. Ferritic stainless steel Ferritic
3. Duplex stainless steels (DSS)
4. Martensitic stainless steel
5. Precipitation hardening stainless steel [59].

Stainless steel also contains a variety of other alloying components and their presence improves particular properties. Mo It, for example, increases the steel's resistance to localized uniform and pitting corrosion, as well as its strength.

In precipitation-hardening stainless steels, Cu is used to shape the strengthening precipitates, Ni increases the steel's hardness, mechanical strength and ductility, at high and low temperatures, Si increases oxidation resistance in strongly oxidizing solutions. Mn enhances steels' hot ductility while also increasing nitrogen solubility within the material, Table (1-2)

Table (1-2): Typical compositions and properties of stainless steel [59].

Steel	% C	% Cr	% Ni	Others	Tensile Strength (psi)	Yield Strength (psi)	%Elongation	condition
<b>Austenitic</b>								
<b>201</b>	0.15	17	5	6.5 % Mn	95,000	45,000	40	Annealed
<b>304</b>	0.08	19	10		75,000	30,000	30	Annealed
					185,000	140,000	9	Cold-worked
<b>304 L</b>	0.03	19	10		75,000	30,000	30	Annealed
<b>316</b>	0.08	17	12	2.5% Mo	75,000	30,000	30	Annealed
<b>321</b>	0.08	18	10	0.4% Ti	85,000	35,000	55	Annealed
<b>347</b>	0.08	18	11	0.8% Nb	90,000	35,000	50	Annealed
<b>Ferritic</b>								
<b>430</b>	0.12	17			65,000	30,000	22	Annealed
<b>442</b>	0.12	20			75,000	40,000	20	Annealed
<b>Martensitic</b>								
<b>416</b>	0.15	13		0.6% Mo	180,000	140,000	18	Quenched and tempered

Steel	% C	% Cr	% Ni	Others	Tensile Strength (psi)	Yield Strength (psi)	%Elongation	condition
431	0.20	16	2		200,000	150,000	16	Quenched and tempered
440C	0.10	17		0.7% Mo	285,000	275,000	2	Quenched and tempered
<b>Precipitation hardening</b>								
17-4	0.07	17	4	0.4% Nb	190,000	170,000	10	Age-hardened
17-7	0.09	17	7	1.0% Al	240,000	230,000	6	Age-hardened

### 1.8.1 Austenitic Stainless Steel

Austenitic stainless steels are a diverse steel class in terms of alloys and applications. Cr, which increases corrosion resistance and Ni, which stabilizes austenite, are main components in addition to iron and have good formability and can be molded and machined easily[61].

This is because of their FCC crystallographic structure. The steels are ductile and corrosion resistant, but they are fragile and have low mechanical strength. Grade 304 is the standard "18 Cr/8 Ni". It is the most versatile and most widely used stainless steel. Grade 304's balanced austenitic structure allows it to be deeply drawn. Since grade 304L, the low carbon variant of 304, does not require post-weld annealing, it is widely used in heavy gauge components (over about 6mm) [61].

Grade 304H is used at elevated temperatures due to its higher carbon content. Additionally, the austenitic structure provides these grades with exceptional durability, even at cryogenic [61,62].

---

## 1.8.2 Applications of Austenitic Stainless Steel

Common applications include[61]: -

1. Woven or welded screens for mining and water filtration.
2. Heat exchanger.
3. Threaded fasteners.
4. Food processing equipment, particularly, milk processing.
5. Kitchen benches, sinks, troughs, equipment and appliances.
6. Paneling, railings and trim for architectural purposes[61].
7. Containers for storing and transporting chemicals.

## 1.9 Aluminum and Aluminum Alloys

Aluminum (Al) is the third most abundant metal in the earth's crust and in its natural form is combined with oxygen and other elements[63,64]. It has a face-centered cubic (FCC) structure, is extremely ductile at room temperature and is relatively simple to machine [65]. Compared to other engineering metals, aluminum has a low melting temperature about 660 °C [66,67]

### 1.9.1 Properties of Aluminum and its Alloys

Aluminum is not ferromagnetic, a property of importance in the electrical and electronics industries. It is non-pyrophoric, which is important in applications requiring the handling or exposure of flammable or explosive materials. Aluminum is also non-toxic. It has an attractive appearance in its natural finish, which can be soft and lustrous or bright and shiny. It can be virtually free of any color or texture[65].

Polished aluminum's reflectance over a wide range of wave lengths makes it ideal for a variety of decorative and practical application [66].

Aluminum has a density of only  $2.7 \text{ g/cm}^3$ , approximately one-third as much as steel ( $7.83 \text{ g/cm}^3$ ). This lightweight, combined with the high strength of some aluminum alloys (which exceeds that of structural steel), enables the design and construction of heavy. Aluminum is resistant to the form of progressive oxidation that corrodes steel[65].

Aluminum's exposed surface reacts with oxygen to form an inert aluminum oxide layer that is just a few of sub nanometer thick and prevents further oxidation. And, unlike iron, it does not rust, the aluminum oxide film does not flake off to expose a fresh surface to further oxidation. If the protective layer of aluminum is scratched, it will instantly reseal itself [67].

The thin oxide layer itself clings tightly to the metal and is colorless and transparent—invisible to the naked eye. The discoloration and flaking of iron and steel rust do not occur on aluminum[66].

### **1.9.2 Aluminum Alloys Classification**

Aluminum alloys are classified into two broad categories based on their manufacturing method:

- 1- wrought alloys
- 2- casting alloys.

Wrought alloys, which are formed by plastic deformation, have substantially different compositions and microstructures than casting alloys, owing to the manufacturing process's requirements.

Under each main category, alloys can be classified into two subcategories:

- 1- heat-treatable alloys.
- 2- non-heat-treatable alloys.

Aluminum alloys are classified according to the numbering scheme illustrated in Table(1-3) [60].

Table (1-3): Designation system for aluminum alloys [60]

<b>Wrought alloys</b>		
1xxx <sup>a</sup>	Commercially pure Al (>99% Al)	Not age hardenable
2xxx	Al-Cu and Al-Cu-Li	Age hardenable
3xxx	Al-Mn	Not age hardenable
4xxx	Al-Si and Al-Mg-Si	Age hardenable if magnesium is present
5xxx	Al-Mg	Not age hardenable
6xxx	Al-Mg-Si	Age hardenable
7xxx	Al-Mg-Zn	Age hardenable
8xxx	Al-Li, Sn, Zr, or B	Age hardenable
9xxx	Not currently used	
<b>Casting alloys</b>		
1xx.x. <sup>b</sup>	Commercially pure Al	Not age hardenable
2xx.x.	Al-Cu	Age hardenable
3xx.x.	Al-Si and Al-Mg-Si	Some are age hardenable

4xx.x.	Al-Si	Not age hardenable/'
5xx.x.	Al-Mg	Not age hardenable
7xx.x.	Al-Mg-Zn	Age hardenable
8xx.x.	Al-Sn	Age hardenable
9xx.x.	Not currently used	

(a) The first digit shows the main alloying element, the second digit shows modification and the last two digits shows the decimal % of the Al concentration (e.g., 1060: will be 99.6% Al alloy). (b) Last digit indicates product form, 1 or 2 is ingot (depends upon purity) and 0 is fore casting[60]

### 1.9.3 Wrought alloys 3 xxx

Manganese is the primary alloying element in this category of alloys, which are usually non-heat treatable. Due to the fact that manganese can be applied to aluminum in an effective amount of up to around 1.5 percent, it is used as a main component in just a few cases[68].

However, one of these is the well-known 3003, which is commonly used as a general-purpose alloy for moderate-strength applications that require good workability [68].

---

## 1.10 Applications 3003Al of The Alloy

Formability and weld ability are excellent, making it suitable for a wide variety of applications, including the following:

1. Fuel tanks, chemical equipment, containers, freezer liners.
2. Cooking utensil[66].
3. Pressure vessels, builder's hardware[69].
4. Storage tanks, agricultural applications, appliance parts and trim.
5. Architectural applications, electronics[66].
6. Fin stock, fan equipment, name plates.
7. Vehicles for recreation, vans and trailers. Used in the drawing and spinning processes[66,69].

## 1.11 Oxide Dispersion Strengthened Steels and Aluminum

The insertion of oxide particles into the steel matrix is one way to enhance service applications of steels, especially at high temperatures [70,71]. The oxide particles are very stable at high temperatures close to the steel's melting point and can effectively improve the steel's high temperature resistance[72,73].

Selective oxidation means which alloying elements (Cr, Ti, Al, C etc.) of an alloy or composite, have a higher affinity for oxygen than other alloying elements (Ni, Fe, Co, Cu etc.) and consequently, oxidize earlier and more rapidly. The selective oxidation occurrence is based on the higher negative free energy,  $\Delta G$ , in forming metal oxides[72].

For example, Cr has a stronger tendency to form an oxide than Ni or Co. This means that in an oxide layer, there is more  $\text{Cr}_2\text{O}_3$  than NiO, of an alloy being oxidized. Kinetic factors additionally control the oxidation process. The affinity of a metal for oxygen can be seen from the

Ellingham diagram, Figure (1-7) [74]. The higher the negative  $\Delta G$ , the higher the tendency of a metal to form an oxide in an alloy. However, the affinity of the element for oxygen does not predict the rate of oxidation.

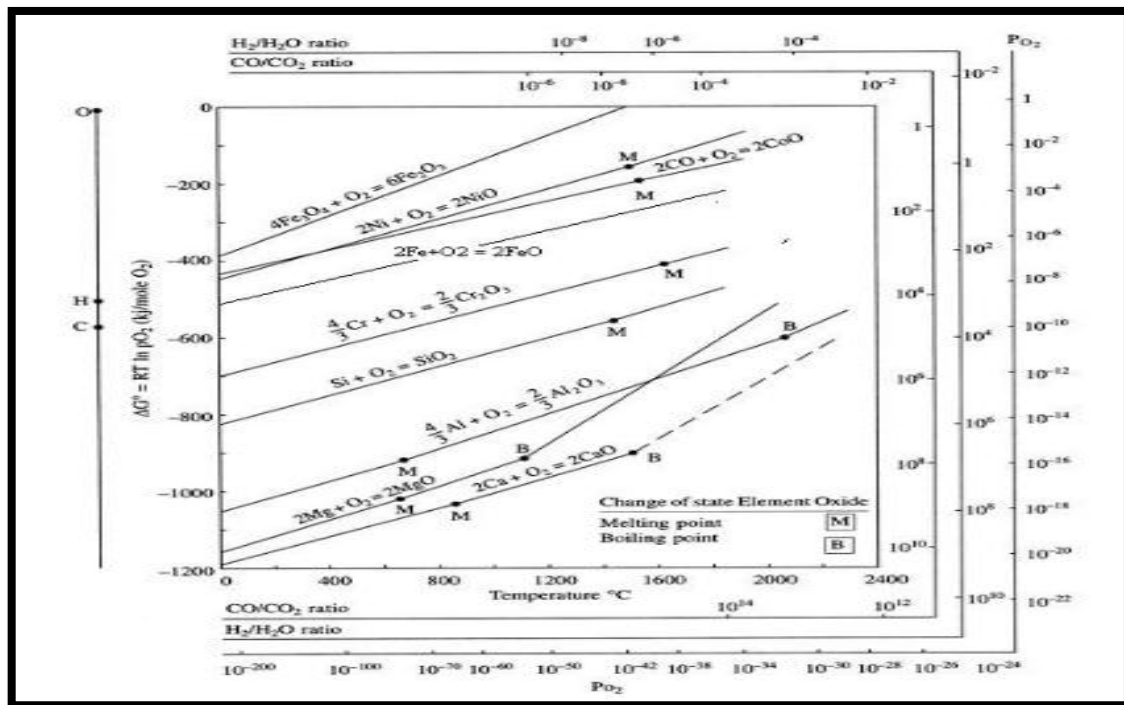


**Figure (1-7): Ellingham diagram for metallurgic alloy important oxides [75].**

It is clear to see that Mn and O elements can form the  $Mn_2O_3$  and  $MnO_2$  at a corresponding stoichiometric ratio nearly, from the Ellingham reaction diagram for metal oxidation [76].

The standard Gibbs energies of formation of  $MnO_2$  are lower than that of  $Fe_3O_4$ ,  $Fe_2O$ ,  $Fe_2O_3$ ,  $FeO$  and  $Cr_2O_3$ . So, Mn can react preferentially with oxygen to form oxide on the stainless steel's surface. It can be inferred that in the laser-irradiated phase, various morphologies of manganese oxides ( $MnO_2$  and  $Mn_2O_3$ ) with different sizes can be manufactured [76].

The oxide inclusions can act as a catalyst for annihilating radiation-induced structural defects, such as vacancies and self-interstitial atoms. Super boilers, steam plants and structural components for a nuclear reactor's first wall and blanket, as well as structural materials in the fusion and fission industries, all use oxide dispersion strengthened steels (ODS) [71].

The oxide layer of aluminum is porous layer depends on the temperature during its formation, according to Ellingham diagram the line for Al (oxidation of aluminum  $\text{Al}_2\text{O}_3$ ) is found to be below that for Fe (formation of  $\text{Fe}_2\text{O}_3$ ) lead to the greater is the stability of its oxide [77].

## 1.12 Literature Review

Laser-induced colorization, which is generally known as laser color marking[78]. Oxidation of metals provides ample opportunities for creating color images with high resolution on oxidized metals[79].

There are currently a significant number of experiments relating to laser oxidation of metal surfaces for coloration. The possibility of coloring the metal surface by forming thin oxide interference films by Nd: YAG,  $\text{CO}_2$ , fiber and excimer lasers.

Perez Del Pino et al. (2002) treated Titanium surface in air using a pulsed Nd: YAG (1064nm) laser beam scanned at a high repetition rate. Depending on the laser cumulative fluence, different colored samples were collected. A bi-layer structure formed, with a thin shallow layer covering a thicker layer.

Numerous oxide phases such as  $\text{TiO}$ ,  $\text{TiO}_2$ ,  $\text{Ti}_2\text{O}_3$  and  $\text{Ti}_2\text{O}$  were present. Although the results show that color is attributable to the

coating's composition, the influence of light interference phenomena inside the thin surface layer, which is primarily made up of  $\text{TiO}_2$ , should not be discounted[80].

Lavisse et al. (2007) looked at the impact of Nd: YAG laser fluences ranging from 4 to 60 J/cm<sup>2</sup> on the color, roughness and morphology of a marked titanium surface. The color of the layers changed from colorless to yellow for low laser fluences and from purple to blue for higher laser fluences [81].

It was discovered, the laser pass caused scars and cracks at low fluences, but the surface layer was smooth and the sample surface was very rough at higher fluences [81].

Lin et al. (2008) investigated the effects of  $\text{CO}_2$  laser power and feed speed ratio on the depth and color difference of engraved Moso bamboo that were investigated [82].

They found that these two parameters helped laser engraving achieve various effects and applied this technique to the field of decoration and gift industry[82].

Vorobyev et al. (2008) produced a gold color on an aluminum surface by femtosecond laser pulses where SEM images reveal that the surface of the gold aluminum is predominantly covered by nanostructures in the form of Nano-protrusions and Nano-voids[44].

Zhang et al. (2009) Studied the oxidation of the AISI 304 steel in order to obtain various colors on its surface using the third harmonic of the radiation UV laser induced coloration and photo thermal oxidation of stainless steel are investigated because the color's created by laser surface and Oxide layer thickness increased as a result of Fe diffusion to the surface after each laser pass [83].

Lehmuskero et al. (2010) obtained colors on stainless steel AISI 304L surfaces by heating them with a fiber laser, modelled them as an effective sum of small color pixels and presented a qualitative relationship between energy, color and the thickness of the oxide layer [84].

Leone et al. (2010) conducted laser color marking tests on AISI 304 steel, using a Q-switched diode pumped Nd: YAG laser. Surface roughness and oxidation increased as a function of frequency, resulting in an improvement in contrast[85].

Chang et al. (2012) studied the coloration of stainless-steel (304,316,430) utilizing fiber laser oxidation. It has been a systematic investigation of the effects of pre-surface condition prior to processing, line distance, laser power, engraving speed and laser pulse frequencies on stainless work pieces[38].

The color of the processed work pieces. It was changed due to changes in the oxidation layer thickness caused by the processing parameters (except the engraving angle)[38].

Adams et al. (2013) used infrared laser irradiation (1064 nm) with nanosecond pulses to deposit metal oxide coatings on the surface of polished stainless steel 304L austenite for use as color markings and unique markers[87].

The oxide layer formed consistent with  $\text{MnCr}_2\text{O}_4$  and  $\text{Fe}_3\text{O}_4$  at accumulated fluences greater than 600–800 J/cm<sup>2</sup>, evaporation and particle ejection hampered oxide development, resulting in a reduction in coating thickness[87].

Faucon et al. (2014) used Nd: YAG laser for four types of materials (stainless steel 316L, aluminum, titanium and copper). They found the interaction of laser pulses and surface material may produce ripples, which are subwavelength surface structures[42].

---

As energy is deposited, ripples increase in size, forming cone-shaped structures called spikes. These structures are interesting because they allow for the modification of the treated surface's properties such as coloration, light absorption, or wettability [42].

Amara et al. (2015) used fiber laser to color marking of many types of steel with different chemical composition under different laser beam operating parameters. Different colors have been obtained except sample that was not presence of chromium which remain colorless [19].

Fraser et al. (2016) studied (6061 and 5052) alloys of Al where the first process consists of a whitening of the background of the piece and the second is the realization of dark marks on the top of this white background. Using a 100 W average power with different values of scanning speed and hatch Q-switched laser for two different focal length, 160 mm and 420 mm. The results show higher contrast and much lower marking time with the 420 mm FL[36].

Li et al (2016) used microsecond fiber laser with a wavelength of 1064 nm to miniaturization of 2D Data Matrix Codes on Aluminum alloy (5A06) formed by raster mode laser direct part marking is demonstrated. The reading quality of miniature Data Matrix code is greatly improved using ultrasonic cleaning in water by avoiding the interference of color speckles surrounding modules [88].

Maltais et al (2016) investigated the physics of laser marking on aluminum by using a fiber laser with a wavelength of 1064 nm and a pulse length of 100 ns to investigate the whitening and blackening of aluminum (6061) surfaces by laser[37].

At elevated temperatures, good contrast can be achieved with a fast enough marking speed. Additionally, due to the white space between lines, a large line spacing results in low contrast[37].

Y. Lu *et al* (2017) investigated various colors were formed on the mechanically polished 304 steel surfaces via the low-cost and fast nanosecond pulse laser coloration route. A typical radiation time is around 1 minute to color each square with an area of  $5 \times 5 \text{ mm}^2$ . Three colorized samples were prepared, displaying straw-yellow, cornflower-blue and fuchsia colors[89].

X. Ma, *et al* (2019) used nanosecond pulsed laser (532 nm) to irradiate stainless steel, resulting in various colors. The effect of laser scanning speed and hatch distance on the resulting surface coloring of stainless steel was investigated [35].

R. Linggamm *et al.* (2021) used the pulse laser nanosecond (1064nm) to irradiate the stainless steel 304L, resulting in the formation of various color's permeating on the sample surface. The surface characterization and surface roughness were analyzed by using the 3D optical microscope. The effect of laser processing parameters such as hatching distance, pulse width and defocusing distance on the evolution of surface colors were investigated[90].

The results show that a thin oxide film was essentially formed that resulted in the formation of four different colors. Each color exhibited a different surface texture and surface roughness, implying the effect of parameters significantly affects the surface characteristics[90].

The grey color formed registered the highest roughness (Rz) of about 3.5 microns followed by a decreasing roughness trend for blue, purple and green respectively[90].

Lazov *et al* (2021) analyzed through numerical experiments the influence of the laser beam speed on the marking process of aluminum samples in the cases of a Cu-Br laser and a fiber laser and two power densities[91].

---

They made compaction between the effects of laser radiation on aluminum samples in the visible narrow range ( $\lambda = 511, 578$  nm) and near-infrared range ( $\lambda = 1064$  nm) that shows which a lower power density is required to achieve the same depth of the evaporated zone with a Cu -Br laser the energy efficiency of the Cu- Br laser is better than that of the fiber laser (by about 25%). This is due to the fact that the absorption is a function of the of laser radiation wavelength [91] .

### **1.13 The Aim of The Work**

The aim of the work is to investigate the laser coloring process of ferrous metal (stainless steel 304) and Non-ferrous metal (Aluminum 3003) by two different lengths of pulse duration nano and microsecond fiber laser and study the effect of the process parameters on the coloring obtained.

# **Chapter Two**

## **Materials and Methods**

## 2.1 Introduction

This chapter explains the materials which are utilized in the thesis, a description of the experimental setup and techniques of examination of prepared samples.

## 2.2 Materials

Two groups of samples were used in this research, the first one is stainless steel, grade (304), The material standard specification according to the American Iron and Steel Institute (AISI) and the second one is Aluminum (3003). The material standard according to the International Organization for Standardization (ISO) Equivalents of Alloys in B 209M, that was manufactured by K-mac. Company.

### 2.2.1 Workpiece preparation

The preparation steps that followed for both samples are square plate 50mm in length and the thickness for stainless steel 304 was 0.8 mm and 0.5 mm for Al 3003. The samples were cleaned with alcohol before the laser colorizing to avoid dirt or fingerprints. The chemical composition, physical and optical properties of stainless steel as shown in Table (2-1), Table (2-2) respectively, also the chemical composition, physical and optical properties for Al 3003 are shown in Tables (2-3), (2-4) respectively.

Table (2- 1): Chemical composition of stainless steel 304

	<b>C%</b>	<b>Si%</b>	<b>Mn%</b>	<b>P%</b>	<b>S%</b>	<b>Cr%</b>	<b>Mo%</b>	<b>Ni%</b>	<b>Co%</b>	<b>Cu%</b>	<b>Fe%</b>
<b>workpiece</b>	<b>0.0401</b>	<b>0.484</b>	<b>1.60</b>	<b>0.0399</b>	<b>0.0005</b>	<b>18.92</b>	<b>0.281</b>	<b>8.45</b>	<b>0.144</b>	<b>0.541</b>	<b>Bal</b>
<b>SS 304 standard</b>	<b>0.08 max</b>	<b>1.0 max</b>	<b>2.0</b>	<b>0.045</b>	<b>0.03</b>	<b>18-20</b>	<b>-</b>	<b>8-10</b>	<b>-</b>	<b>-</b>	<b>Bal</b>

Table ( 2-2): Physical and optical properties of AISI 304 stainless steel [20]

Property	Value	Unit
Reflectance R ( $\lambda = 1.06 \mu\text{m}$ )	0.75	-
Thermal conductivity	37.00	W/m.K
Melting point	1800	°C
Boiling point	3145	°C

Table (2-3): Chemical composition of Al3003.

	Si%	Fe%	Cu%	Mn%	Mg%	Cr%	Ti%	Pb%	Al
workpiece	0.236	0.579	0.0694	1.09	0.0372	0.0072	0.0313	0.0036	Bal
Al 3003 standard	0.60 max	0.70 max	0.05- 0.2	1-1.5	0.05	0.05 max	0.05 max	0.05	Bal

Table(2-4): Physical and optical properties of Al 3003[14,92].

Properties	Value	Unit
Reflectance R ( $\lambda = 1.06 \mu\text{m}$ )	0.94	-
Thermal Conductivity	154	W/m.K
Melting point	655	°C
Boiling point	2467	°C

### 2.3 Laser devices

Two lasers that were used are industrial ytterbium fiber lasers made in China. As shown in Figures (2-1) , (2-2) . Table (2-5) depicts the parameters of it , software used for lasers is named E-Z CAD.



**Figure (2-1): Microsecond fiber laser.**

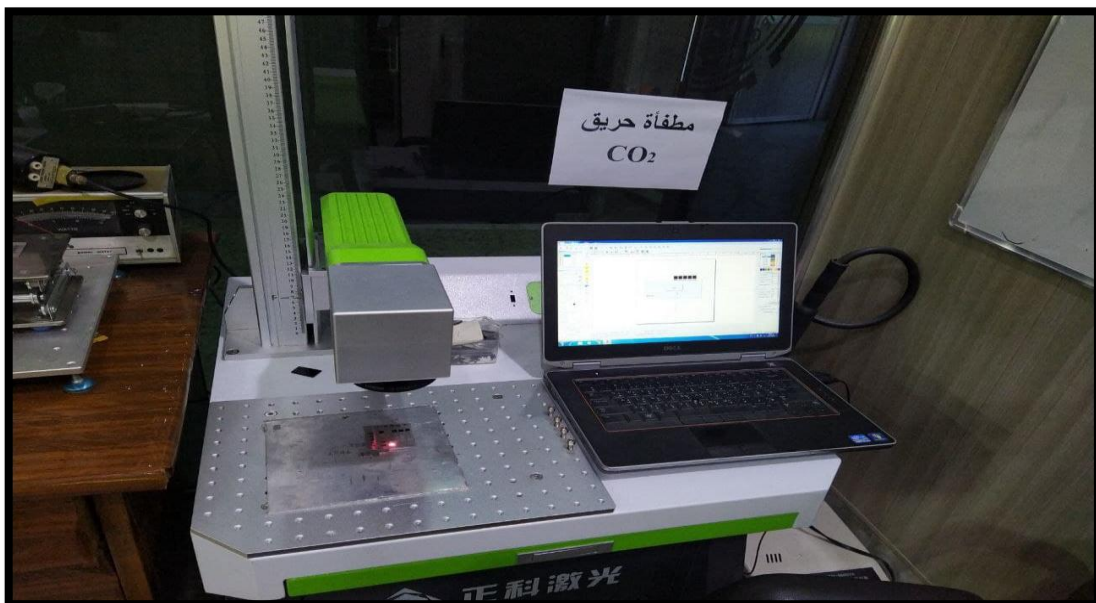


**Figure (2-2): Nanosecond fiber laser.**

Table (2-5 ) parameters of Laser devices

Parameters	Microsecond fiber laser	Nanosecond fiber laser
Wavelength	1064 nm	1064nm
Average power	10 w	100 w
Frequency	20 – 80 kHz	20-200 kHz
Pulse width	10 $\mu$ s	81 ns
Spot size	50 $\mu$ m	50 $\mu$ m
Focal length	163 mm	119 mm
Scanning speed	2- 8000 mm/s	2 – 10000 mm/s

## 2.4 Experimental procedures

The parameters that were fixed during the experiments are shown in table (2-6) , the laser beam was guided by a galvanometric scanner to raster scanning a square of 5 cm in length, with the scanning style illustrated in Figure (2-3,a). Thus, the laser beam completed line scans from right to left and the galvanometer scan mirror will adjust the scanning direction for each square 5 mm in length as Figure (2-3,b)

Table (2-6) parameters of Laser for experimental of SS304

Parameters	Value
Laser power	(2 ,4, 8, 10) W
Hatching	(0.1,0.05,0.01, 0.001)mm
Pulse width	10 $\mu$ s , 81 ns
Frequency	40,60,80 kHz
Scanning speed	50-650 mm/s

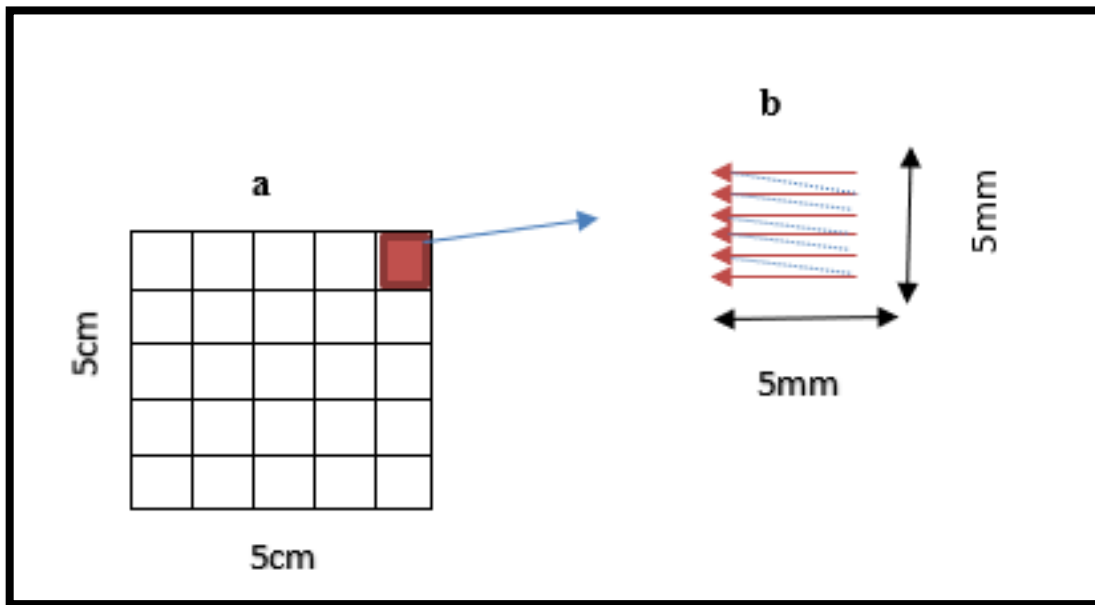


**Figure (2-3): The schematic diagram of laser scanning on stainless steel 304.**

The scanning style illustrated in Figure (2-4-a) and the galvanometer scan mirror will adjust the scanning direction for each square 5mm in length as illustrated in Figure (2-4, b) and parameters used in table (2-7).

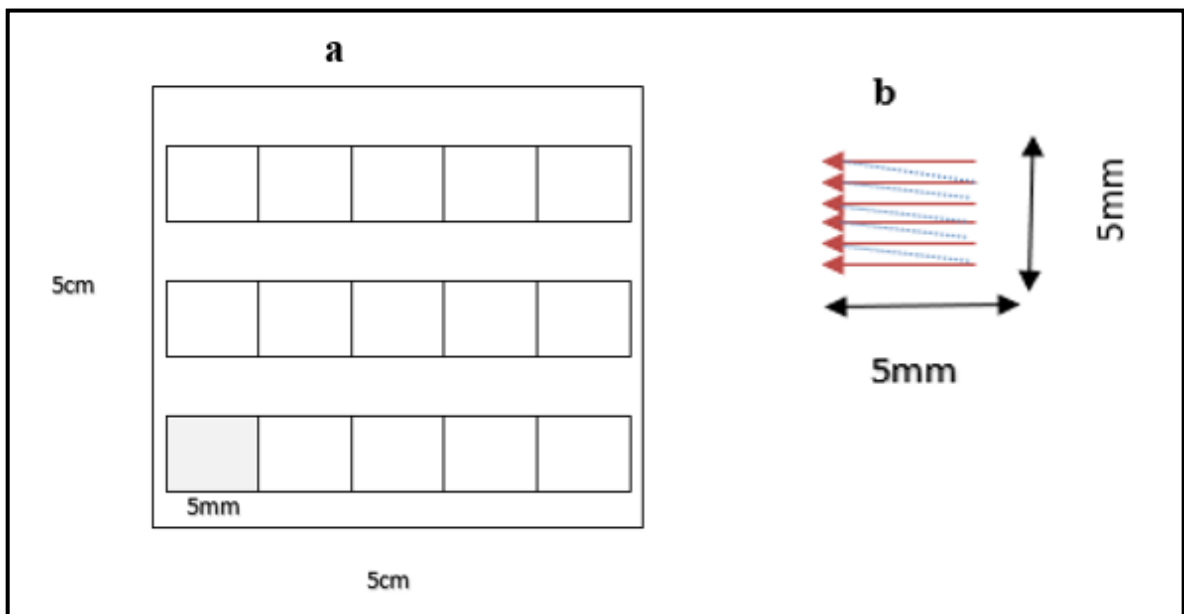


**Figure (2-4): The schematic diagram of laser scanning on Al 3003.**

Table (2-7) parameters of Laser for experimental of Al 3003.

Parameters	Value
Laser power	(1- 10) W
Hatching	(0.05,0.01,0.005, 0.001)mm
Pulse width	10 $\mu$ s , 81 ns
Frequency	(20,40 ,80) kHz
Scanning speed	25-850 mm/s

## 2.5 Specimens testing

### 2.5.1 Microscopic inspection

laser coloring results were inspected by stereo microscope (ME,2665, Euronext, Holland). The microscope lens that was used has 10X magnification power to investigate the samples.

### 2.5.2 Field Emission Scanning Electron Microscope (FESEM)

FESEM was the main method used to analyses the surface characteristics before and after coloring to identify Surface morphology High-energy beams of electrons were used and interact with the conductive surface on the specimen sample. The SEM (with EDS) used was (ZEISS MODEL  $\Sigma$ IGMA/VP) in Figure (2-5).



**Figure (2-5): FESEM ZEISS MODEL  $\Sigma$ IGMA/VP.**

### 2.5.3 X-ray Diffraction (XRD)

X-ray diffraction (XRD) is a reliable technique that can give us the crystal structure, chemical composition [93]. Type (SHIMADZU Lab X6000 -Japan) . As shown Figure (2-6).

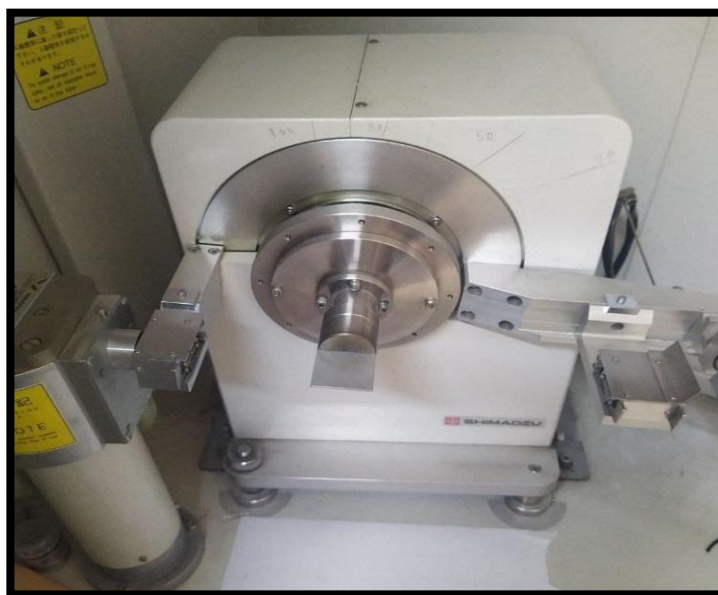


**Figure (2-6): X-ray diffractometer**

---

### 2.5.4 Double Beam Spectrophotometer

The reflectivity of the surface oxide film was detected by Double Beam Spectrophotometer device type UV 3600 Plus, Shimadzu Japan equipped with multi-function large sample room and integrating sphere. The wavelength range is (200–2600) nm and the resolution can be up to 0.1 nm. In the experiment, in order to objectively evaluate the color change.

### 2.5.5 Colorimeter Test

A colorimeter includes of a light source, fixed-geometry viewing optics, three photo-cells coordinated to an internationally established Standard observer and an onboard processor or cable connection to a processor/display unit. In operation, the sensor lens of the colorimeter typically is placed directly over the area of the specimen to be measured, an operator activates the light source that is reflected from the specimen and passed through the three photocells, which determine the red, green and blue components and transmit the data to the microcomputer. The microcomputer calculates the  $L^*$ ,  $a^*$ ,  $b^*$  tristimulus values and captures the data, which are displayed.

### 2.5.6 Roughness Test

A roughness measuring device type SRT-6210 (China made) was used to measure the average roughness ( $R_a$ ) for the samples before and after the laser coloring process. This device can measure the roughness of the required area by automatic scanning with a fine needle and present it on a digital screen, consequently it takes the average value for all scanned areas.

---

### 2.5.7 Corrosion Test

Corrosion cell is made of Pyrex with (1L) capacity consists of two vessels, internal and external. Figure (2-9) shows the corrosion cell and the three electrodes. Three electrodes and a thermostat are placed in the internal vessel [94].

The three electrodes can explain as follows:

1. Reference Electrodes is used to determine the working electrode potential according to the potential of the reference electrode. The potential of the reference electrode is well known and accurate and it combined with two tubes; the inner tube contains AgCl, Ag, KCl, the outer tube filled with the prepared seawater solution (3.5% NaCl). The reference electrode is replaced at the distance (2) mm from working electrode.
2. The Auxiliary Electrode consists of high purity platinum metal; its length is (10 cm).
3. The Working Electrode is the studying and testing subject that potential will be measured; this electrode is formed from (20) cm length metallic wire and connected to the mounted specimen.
4. Chiller device was used to adjust the temperature of water which flows through the external vessel constant at (25, 35, 45 and 55) °C.

[94]

The sample inserted in the holder in which the diameter of the exposed surface of the seawater solution is (1cm<sup>2</sup>). Figure (2-7) shows the complete system setup for polarization measurement.

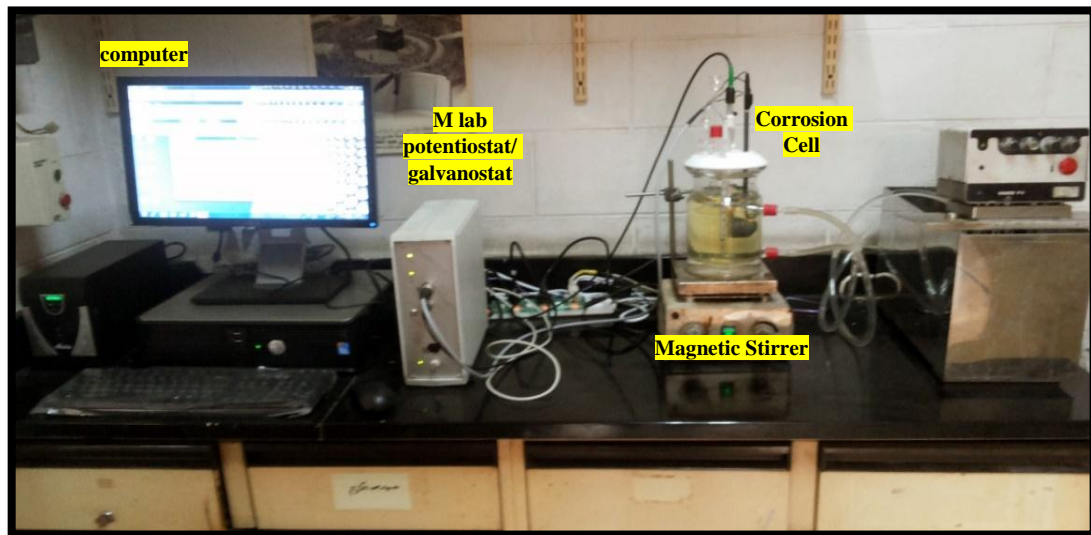


**Figure (2-7): Complete system setup for corrosion polarization measurements [94].**

# **Chapter Three**

## **Results and Discussion**

### 3.1 Introduction

This chapter presents and discusses the results of the experimental work of two different types of lasers, nanosecond and microsecond fiber lasers, which were used to color two targets, stainless steel 304 and aluminum 3003.

### 3.2 Experimental results

The effect of variable laser parameters such as power, frequency, scanning speed, hatch (line spacing), were examined for both stainless steel 304, Aluminum 3003

#### 3.2.1 Laser power effect on SS 304

Different values of power were used. The power of 2 W has an insufficient influence on the substance where the non-shift color of SS 304, then when the power is increased to 4 W the grooves became wider but a rise in depth occurs when power of 6 W was used which leads to many particles of molten material being ejected from the surface area.

At high power is used 8 W the surface morphology become like the ripple. As illustrated in Figure (3-1)

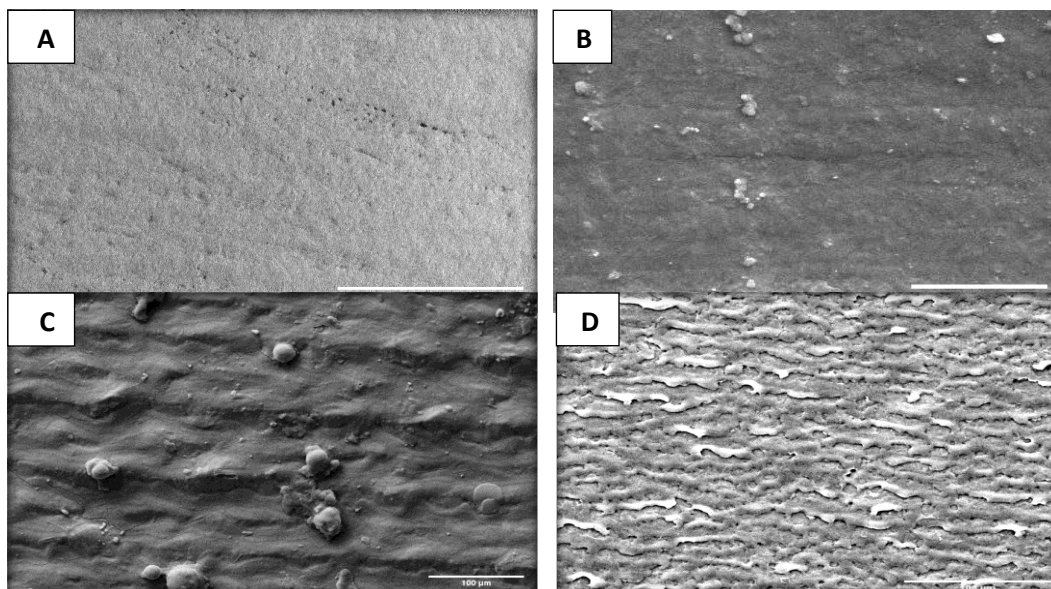


**Figure (3-1): FESEM images of the surface structures created with various average laser powers (A to D) 2,4,6 and 8 W respectively, scanning speed 100 mm/s, frequency (80) kHz, hatch 0.01 mm.**

### 3.2.2 Effect of hatch on SS 304

Using different hatch space as Figure (3-2) showed that homogenous colored was found when hatch value equal to 0.001mm with low power 4 W and when hatch value was 0.01mm with high power 8W.

Increasing the hatch from 0.05 to 0.1 mm leads to the increases of total reflectance, so the color will approximately be white as shown in Figure (3-3). Shorter hatch distance had a greater influence on the surface morphology that the molten materials will be within limited area leading to more chance to be more smooth and less rough before re - solidification.

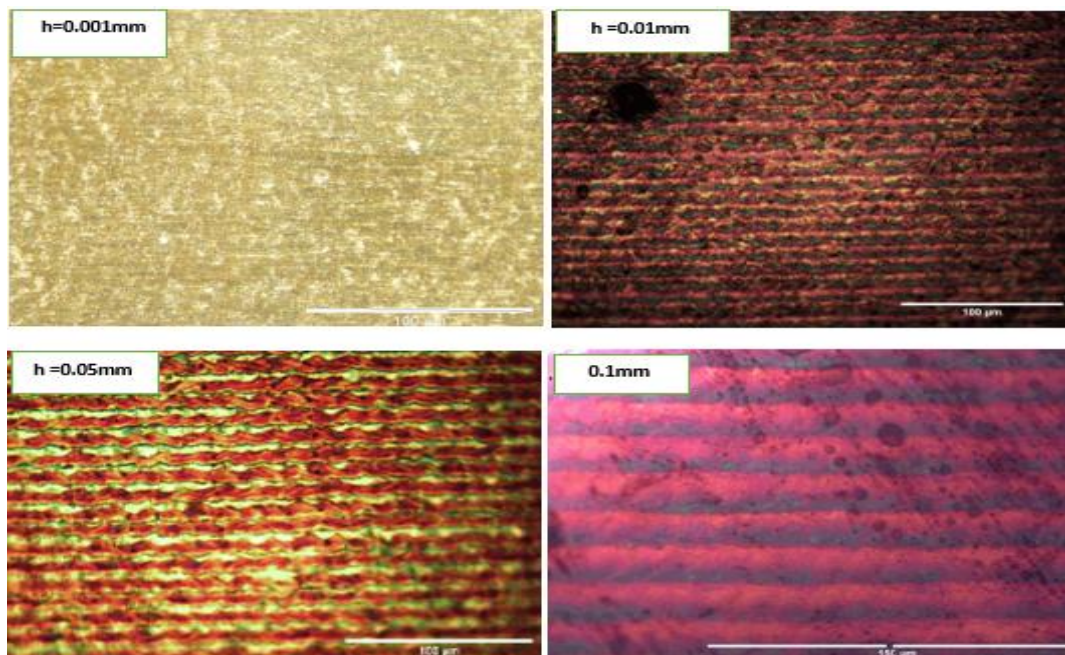


**Figure (3-2): Optical microscope image with different of hatch ,scanning speed 100mm/, PRR 80kHz for SS 304.**



**Figure (3-3): Coloring parameters: hatch 0.05mm, P 8W ,PRR 80 kHz scanning speed from(100mm/s) incremented 25 for Ss 304.**

If the hatch is wider, the direction of the scan lines becomes visible. A narrow band of the base material can be seen between the colored lines, but these are not visible to the human eye. As illustrated in Figure (3-4).

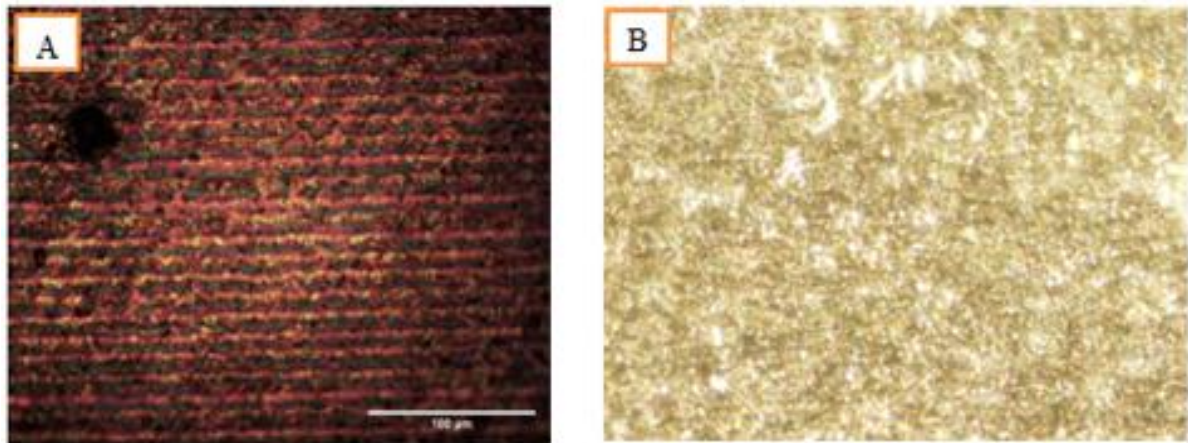


**Figure (3-4): Microscopic image (A) line spacing 0.01mm , (B) line spacing 0.001mm, scanning speed 100 mm/s, PRR 80 kHz.**

### 3.2.3 Effect of frequency on SS 304

It was found that the lowest repetition rates that began to ablate material from the surface due to increase energy per pulse according to the equation[95]:

$$E = P_{\text{avg}} / \text{PRR} \text{ -----(3- 1)}$$

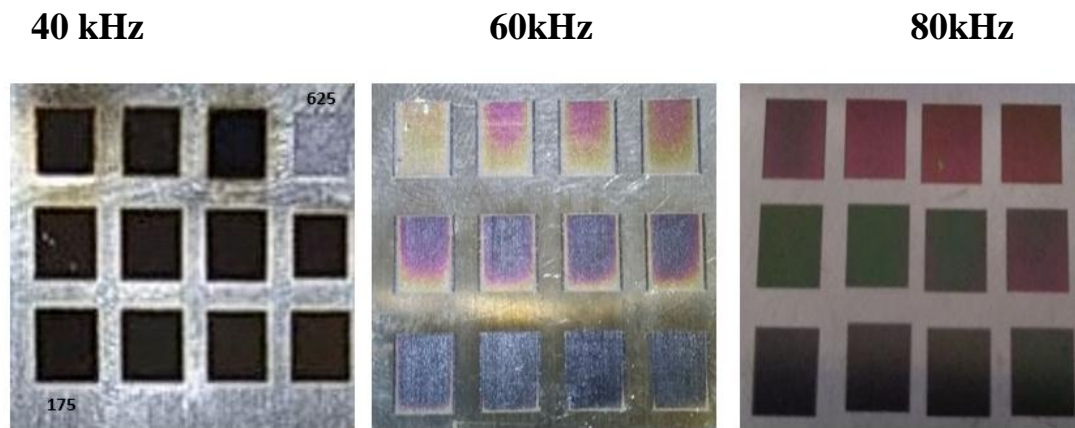
Where: -

E = energy J.

$P_{\text{avg}}$  = average power W.

PRR= pulse repetition rate Hz.

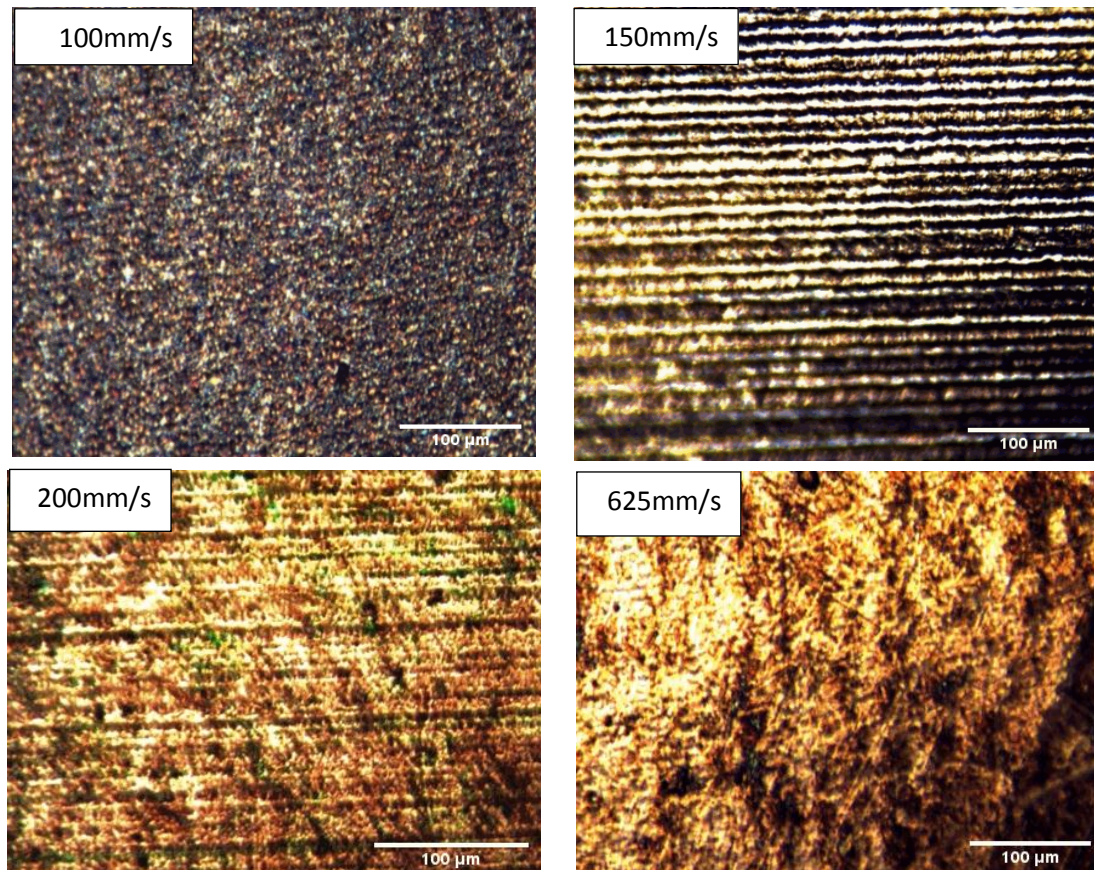
While increasing repetition rate resulted in more bright colors with distinct tones. As shown Figure (3-5).



**Figure (3-5): Color results at different range of frequency and power 4W, hatch 0.001mm and scanning speed from 175 mm/s to 625mm/s incremented 25.**

### **3.2.4 Effect of the scanning speed on SS 304**

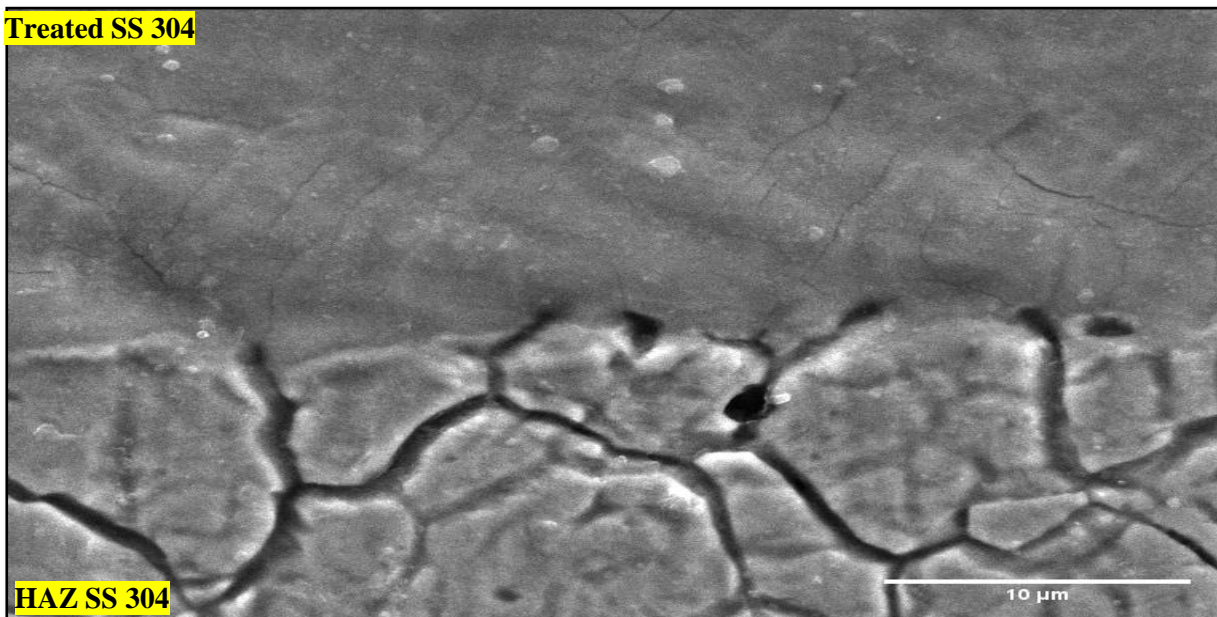
The surface morphology changed as the scanning speed increased. When the speed was 100 mm/s the structure showed irregular and random orientation while with high speed 150 mm/s the structure was similar to grating groove but the grooves became wider at 200 mm/s. Finally, the structure showed few dark spots because a faster scanning speed 625 mm/s has reduced laser -material interaction time which led to less diffusion of elements within the heated layer as shown in Figure (3-6).



**Figure (3-6):** Microscopic images magnification 10 X of the colored samples with laser parameters at power 4 W, frequency 80 kHz, hatch 0.001mm and 10µs pulse width.

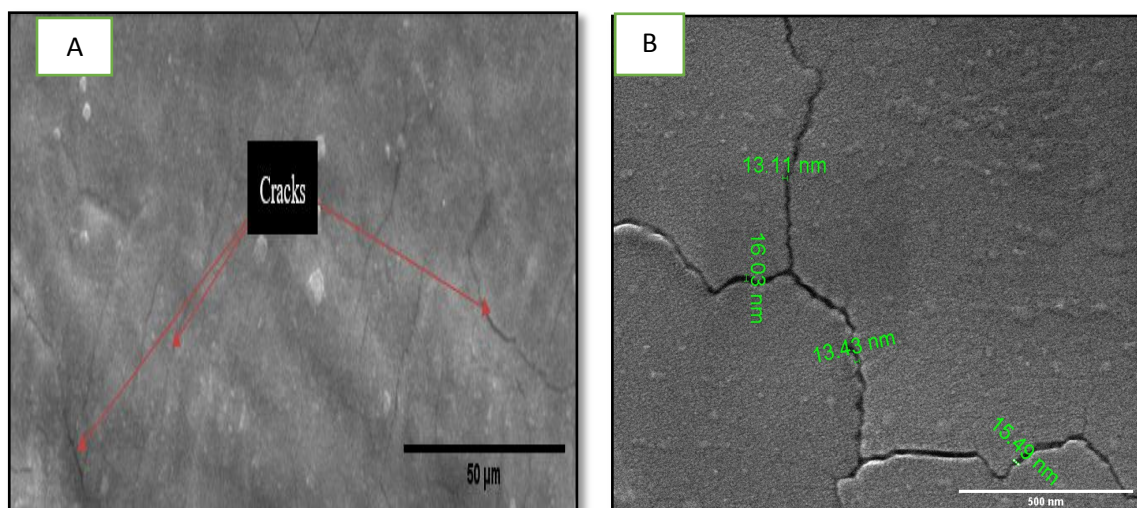
### 3.2.5 Surface morphology analysis

To investigate structures with more detail treated and Heat Affect Zone (HAZ) samples of stainless steel 304 were observed using Field Emission Scanning Electron Microscope (FESEM) as in Figure (3 - 7).



**Figure (3-7): Morphology which distinguish between treated p 8 W , scanning speed 350 mm/s, PRR 80 kHz and (HAZ) of SS 304.**

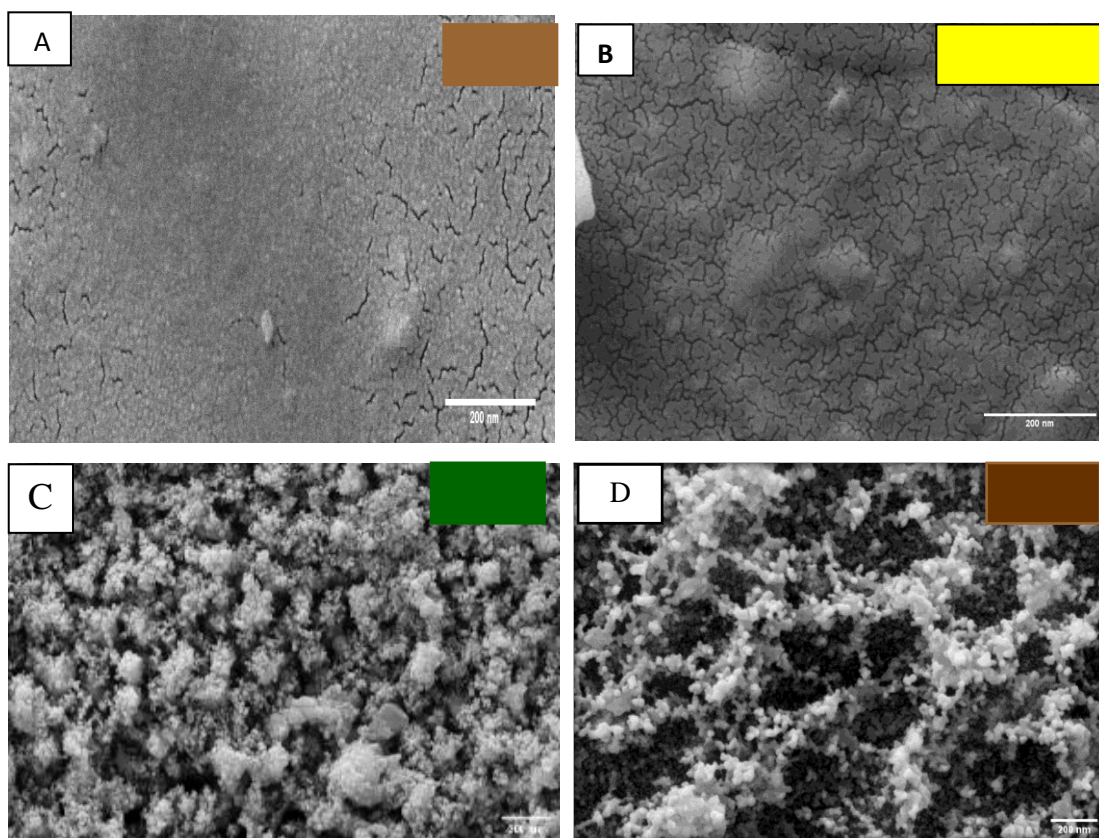
Micrograph of a green color sample, which shows the observed typical surface and cracks. However, these cracks do not affect the appearance of color on the sample surface[40].The crack width average is approximately 14 nm as shown Figure (3-8)



**Figure (3-8): (A) SEM micrograph showing the cracks on a colored surface of stainless steel, power 4 W, scanning speed 325 mm/s, frequency 80 kHz, pulse duration 10μs, hatch 0.001mm, (B) cracks width.**

Oxide layer morphology shows different structure morphologies. When using microsecond laser pulse width of 10  $\mu$ s the resulting microstructure looks like soil thirsty for water (mud structure) in Figure (3-9). Show appendices A,B.

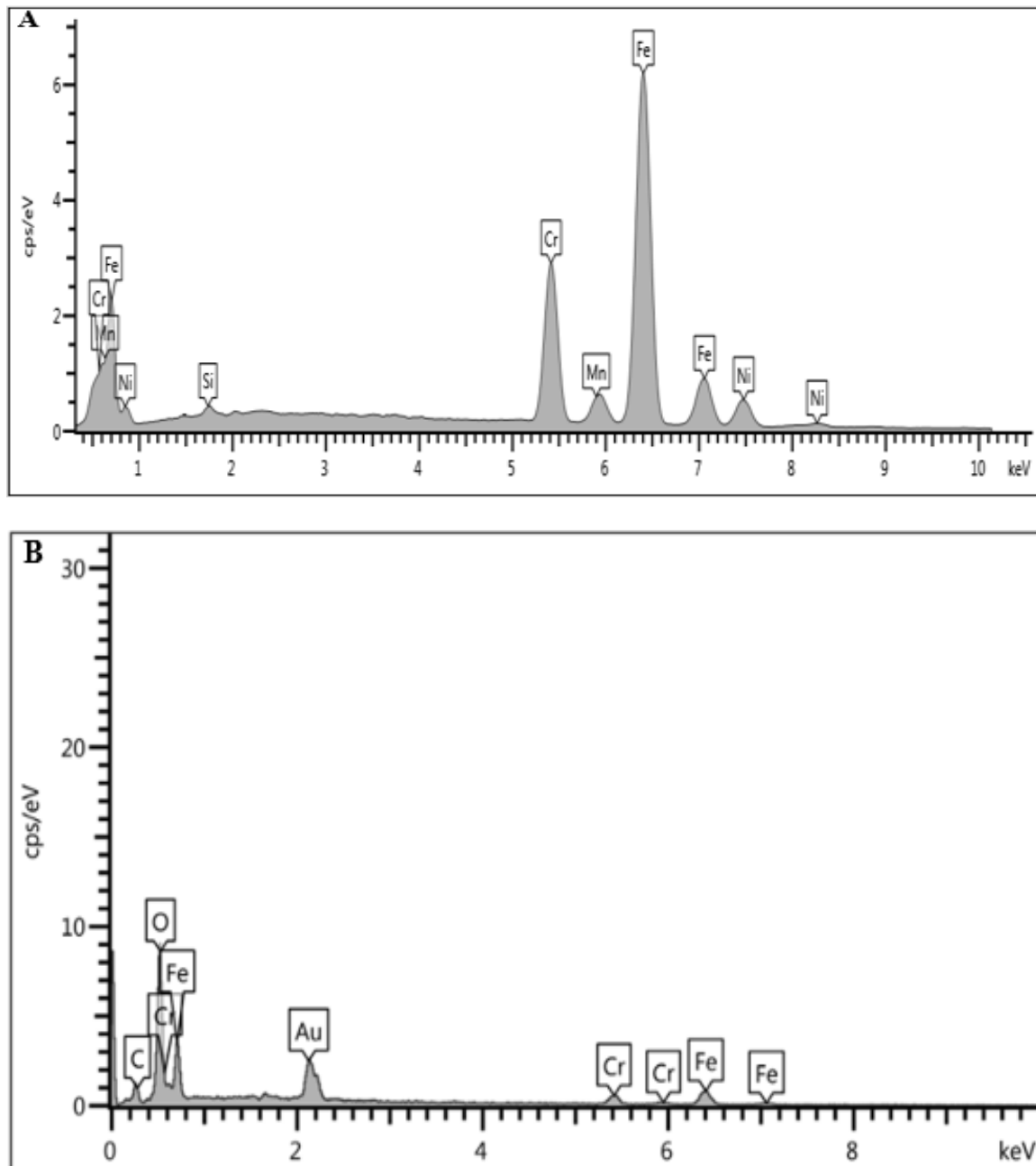
When using nanosecond laser pulse width 81ns nanostructure pores because like a coral reef shape and when decrease the speed it becomes more dense structure as shown Figure (3-9 C and D). Show appendices C,D.



**Figure (3-9): FESEM images of different sample surface (A) brown, (B) yellow, (C) dark green, (D) dark brown. Parameters illustrated in Table (3-2).**

A thin oxide layer was formed on the sample surface after laser irradiation. EDS was used to investigate the element content of the

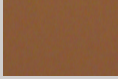
stainless steel before and after laser irradiation in order to determine the changes of the surface elements. in Figure (3- 10) the surface elements of untreated sample are Fe, Cr, Ni, Mn, Si, after laser irradiation, oxygen elements appeared on the sample surface.



**Figure (3-10): EDS analysis of the sample surface (A) untreated stainless steel 304, (B) laser treated sample at speed 650 mm/s, P 8 W, h 0.01mm.**

The content of C, Si, Mn and Ni on the surface of the colored sample basically, changed compared with the untreated stainless steel 304. According to Table (3-2),

Table (3-1): The chemical composition of SSt.304 surface according to EDS analysis of substrate and treated samples P=8 W, Frequency = 80 kHz, H=0.01mm.

Sample speed mm/s			Element (Wt.%)							Pulse width
			Fe	Cr	Ni	O	Si	Mn	C	
<b>Substrate</b>			<b>70.55</b>	<b>18.79</b>	<b>8.25</b>	<b>-</b>	<b>0.54</b>	<b>1.87</b>		
<b>A</b>		<b>275</b>	<b>50.7</b>	<b>23</b>	<b>-</b>	<b>22.3</b>	<b>-</b>	<b>-</b>	<b>4</b>	<b>10μs</b>
<b>B</b>		<b>650</b>	<b>28</b>	<b>31</b>	<b>-</b>	<b>20</b>	<b>1.9</b>	<b>13.5</b>	<b>5.6</b>	
<b>C</b>		<b>125</b>	<b>44</b>	<b>23.8</b>	<b>5</b>	<b>23.5</b>	<b>0.7</b>	<b>-</b>	<b>3</b>	<b>81ns</b>
<b>D</b>		<b>275</b>	<b>28</b>	<b>21</b>	<b>2.1</b>	<b>21.9</b>	<b>7</b>	<b>14</b>	<b>6</b>	

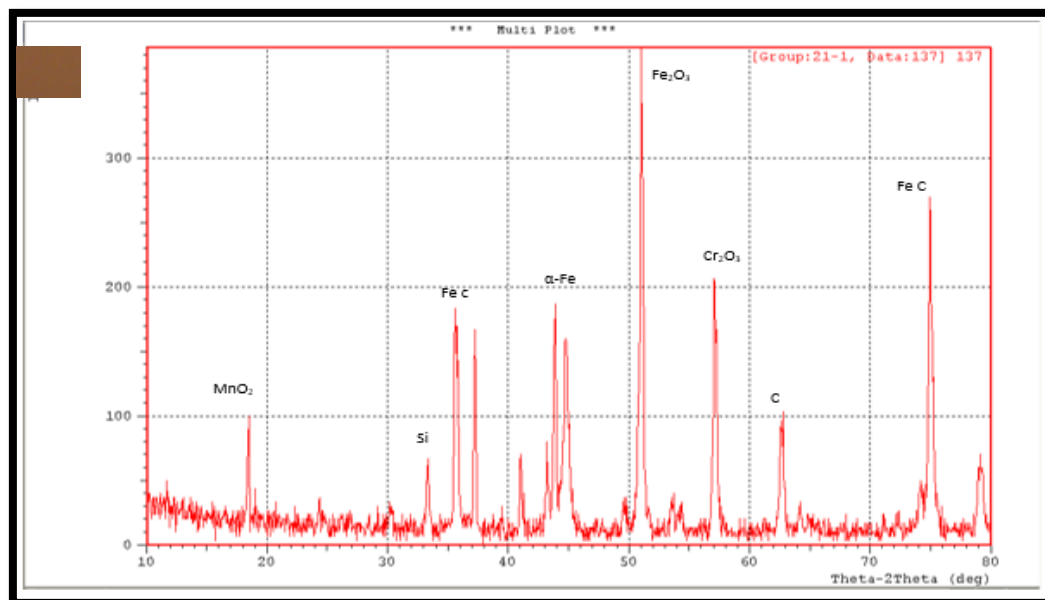
The content of oxygen elements increased to different values. In particular, the content of oxygen elements on the surface of microsecond samples were formed to be (22.3 %, 20 %), respectively and (23.5% ,21.9 %) in the case of nanosecond fiber laser.

The oxygen content on the samples surface increases with the decrease of scanning speed. It indicates that the oxide content on the surface of the sample is increased due to the longer interaction time between laser and the sample, the thermal absorption effect of the material is enhanced and the reaction with surrounding atmosphere is

more complete. The Cr content on the sample surface increased but Fe and Ni content of each colored sample was lower than that of untreated samples. When using microsecond fiber laser Ni element was not found.

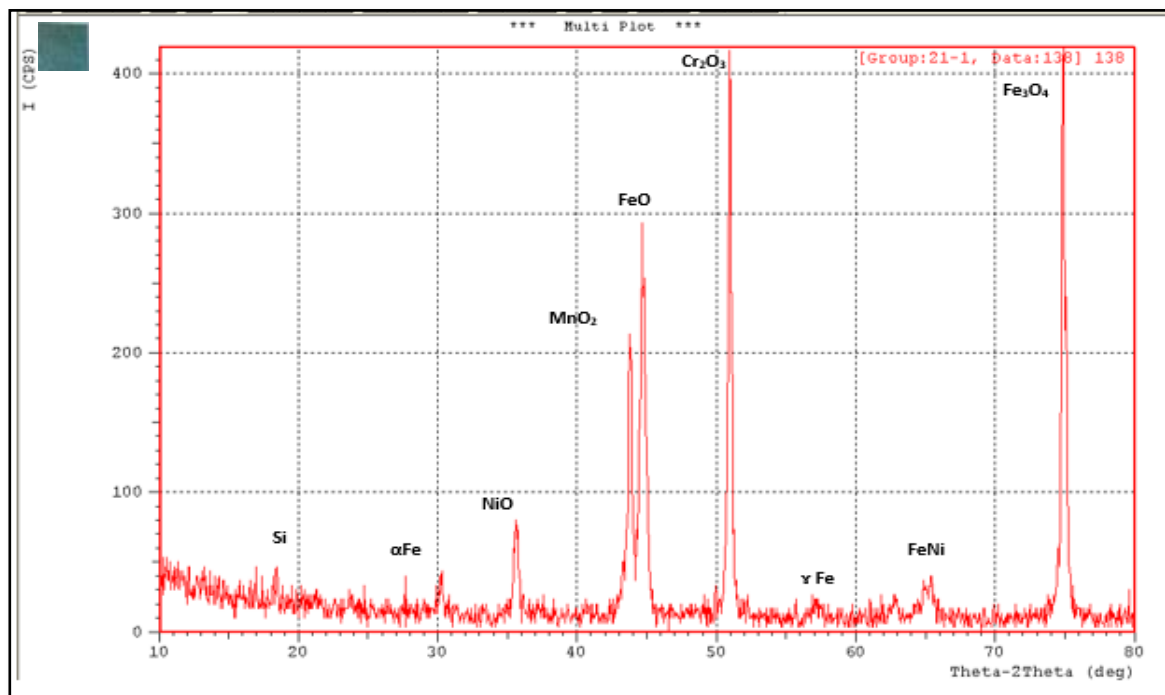
The XRD analysis were performed on several selected areas to determine the variations between colored areas prepared by different laser types in greater details. When using a microsecond laser with a pulse width of 10  $\mu$ s, a power of 8 W, a speed of 275 mm/s and hatch of 0.01mm, the color was brown and when using a nanosecond pulse laser with a pulse width of 81 ns and scanning speed 275 mm/s the outcome was dark green color. The surface elements of the untreated sample are Fe, Cr, Ni, Mn, Si and C.

Fe<sub>2</sub>O<sub>3</sub> formation as a high peak following laser irradiation when two thetas are 51 degrees, FeC formation as two peaks when two thetas are 75,36 degrees and Peak heights for Cr<sub>2</sub>O<sub>3</sub> and  $\alpha$ -Fe converge when two thetas are 57 and 45 degrees, respectively. Si appear when two theta is 33 degrees. Finally, peak heights for MnO<sub>2</sub> and C converge when two thetas are 18,64 degrees respectively. Figure (3-11).



**Figure (3- 11): XRD graph of sample scanning 275 mm/s microsecond pulse width result brown color.**

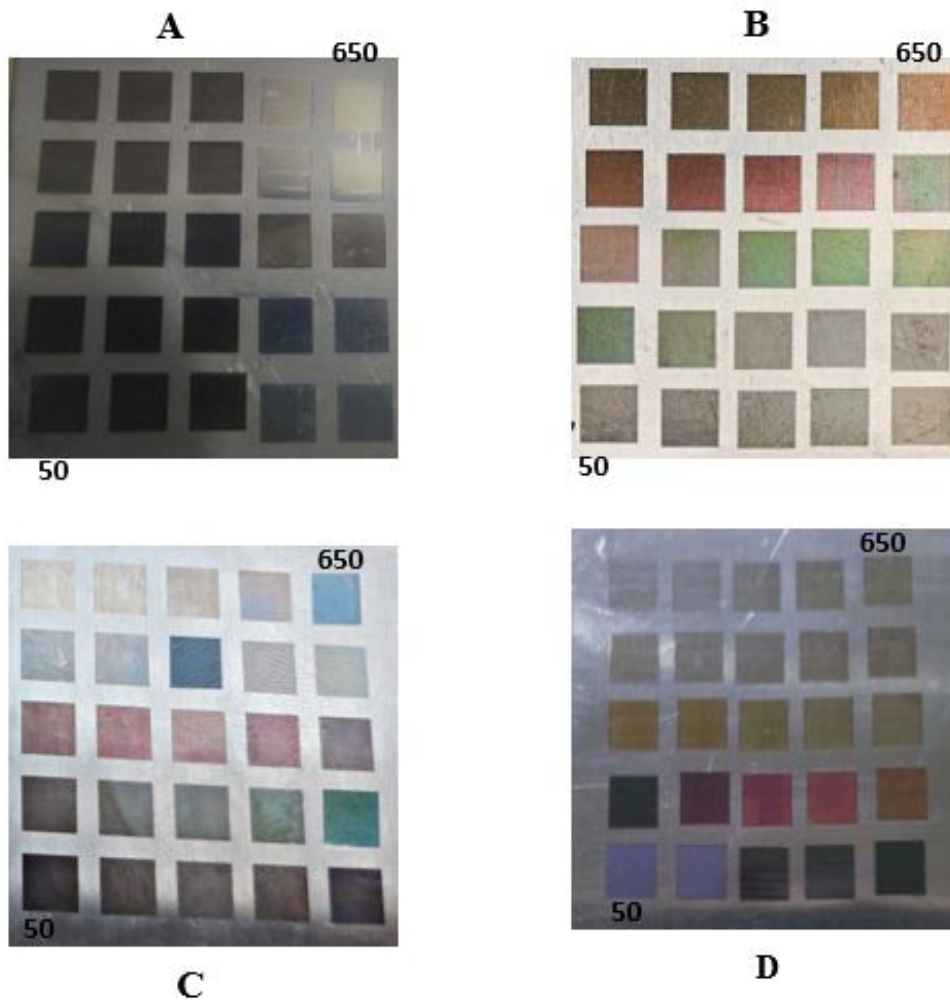
For nanosecond pulsed width the height of the peak is the same for each of  $\text{Cr}_2\text{O}_3$   $\text{Fe}_3\text{O}_4$  when two thetas are 51 and 75 degrees respectively, NiO formation at two theta is 35-degree, Fe Ni when angle is 65, matching the angle 44.5 degree for formation peak of  $\text{MnO}_2$  and FeO small amount of  $\alpha\text{Fe}$  and  $\gamma\text{Fe}$  when two theta 28 and 58 degree respectively. Finally, Si in 18 degrees. Figure (3- 12).



**Figure (3-12): XRD graph of sample scanning (275mm/s) 81nanosecond pulse width, h (0.01mm) result dark green color.**

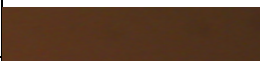
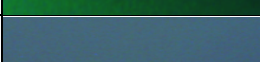
### 3.2.6 Final Experimental Results of Stainless Steel 304

To study the coloring effect of lasers (microsecond and nanosecond) different laser parameters were used for stainless steel 304. A series of experiments were carried out to investigate the correlation of color quality with laser parameters (power, pulse repetition rate, line spacing and speed). As illustrated in Figure (3-13) and Table (3- 2).



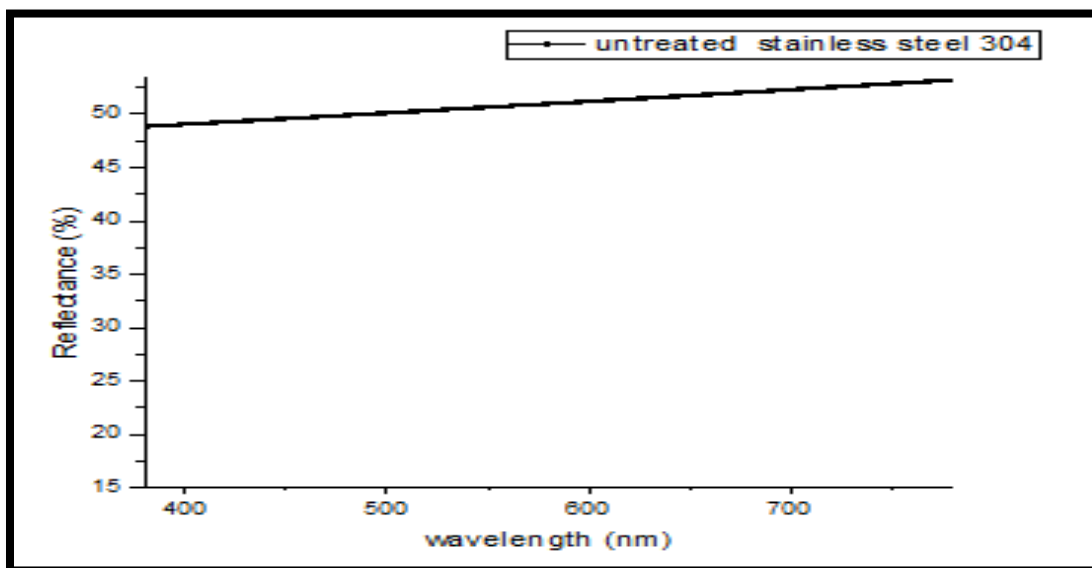
**Figure (3-13):** Stainless steel 304 color plate A (power 8 W, hatch 0.01 mm, pulse width 10  $\mu$ s), B (power 4 W, hatch 0.001 mm, pulse width 10  $\mu$ s), C (power 8 W, hatch 0.01 mm, pulse width 81 ns), D (power 4 W, hatch 0.001 mm, 81 ns) all scanning speed from 50 to 650 mm/s incremented 25 and fixed frequency at 80 kHz

Table (3-2): Different color results with different laser parameters for all experiments.

Power (W)	speed (mm/s)	pulsed width		Hatch (mm)	colored result	
		$\mu$ s	ns			
8	125	10		0.01		dark brown
8	275	10		0.01		brown
8	450	10		0.01		gray
8	600	10		0.01		light brown
8	650	10		0.01		yellow
4	50	10		0.001		gray
4	325	10		0.001		green
4	400	10		0.001		pink
4	475	10		0.001		dark red
8	50		81	0.01		light gray
8	125		81	0.01		dark brown
8	600		81	0.01		faded yellow
8	250		81	0.01		light green
8	275		81	0.01		dark green
8	475		81	0.01		naval blue
8	225		81	0.01		khaki
8	400		81	0.01		maroon
8	500		81	0.01		beige
8	650		81	0.01		blue
4	50		81	0.001		dark blue
4	125		81	0.001		gray
4	150		81	0.001		olive
4	175		81	0.001		green
4	250		81	0.001		red
4	275		81	0.001		orange
4	300		81	0.001		gold
4	325		81	0.001		yellow
4	425		81	0.001		light yellow

### 3.2.6.1 Wavelength s' Measurements

Double beam spectrophotometer was used before laser treatment of stainless steel 304 as shown in Figure (3-14). Where the X- value represents the wavelength, in nano meter while Y- represented the reflectance (R) of the incident light by the sample in percentage.



**Figure (3- 14): Spectrum reflection untreated stainless steel 304.**

As it can be seen from Figure (3-15), the black curve represented dark green which is formed by the interference of wavelength from 450 nm to 780 nm, while the red curve represented the dark brown is formed by interference from 650 nm to 780 nm.

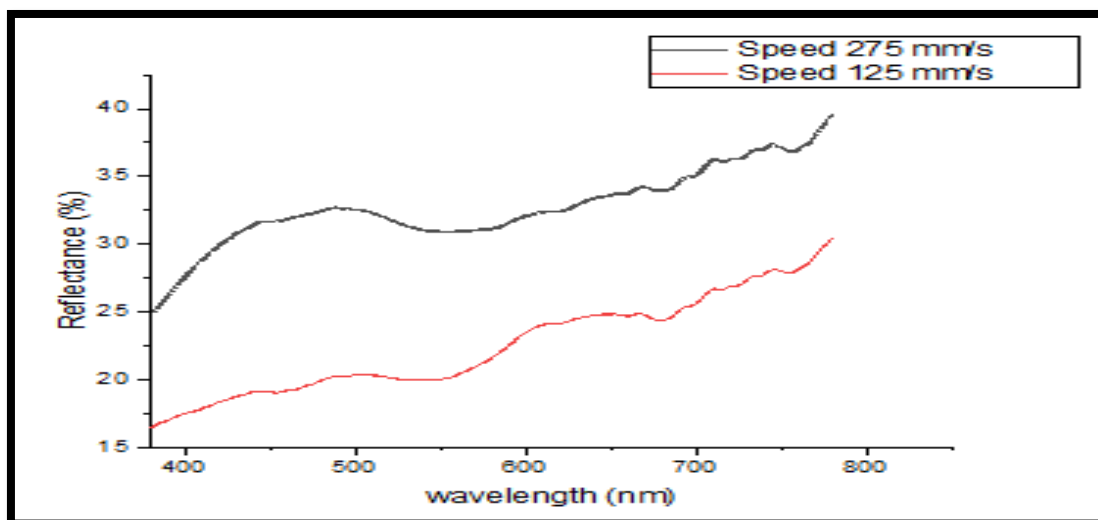


**Figure (3-15): Colored samples at nanosecond pulse width with different speed scanning at power 8 W.**

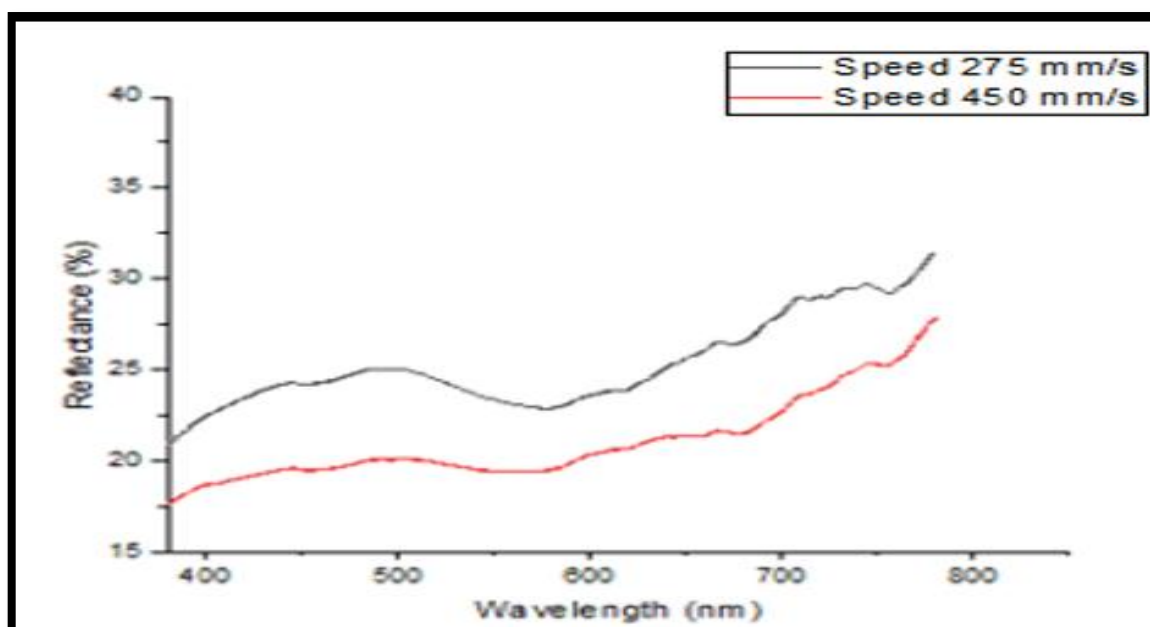


**Figure (3-16) Colored sample at microsecond fiber laser with different speed scanning at power 8W**

The microsecond pulse width the same behaviors when using nanosecond pulse width. Less reflection led to more absorption of light incident that indicated thick oxide layer.

It was found that the spectrum for each color means that it was not created by one wavelength but each color was an effect of a combination of different wavelengths, which interfered together to produce the presented color.

### 3.2.6.2 Colorimeter Result

Colors obtained from microsecond pulse and nanosecond pulse laser, CIE L\*a\*b\* color space was used and the difference between two measured color can be expressed by the CIE color difference formula where ( $\Delta E_{ab}^*$  (total color difference)). Calculated results shown in Tables (3- 3), (3-4), (3-5) and (3-6) respectively. In fact, the value of  $\Delta E_{ab}^*$ , provide that, all the colors obtained are recognized by human eyes with a high contrast in color and brightness and those colors are significantly different from original color of stainless steel 304 if the  $\Delta E_{ab}^*$  values exceed 5.

Table (3-3): Spectrophotometer results for L\*, a\*- and b\*-values of CIELAB color space for the twenty-five samples, at power = 8 W pulse duration 10  $\mu$ s frequency 80 kHz, line spacing 0.01mm and scanning speed from 50 to 650 mm/s.

speed mm/s	L*	a*	b*	$\Delta E_{ab}^*$
Stainless steel 304 untreated	87.82	4.56	4	-
50	44.96	3.78	3.64	42.8686086
75	45.48	5.37	4.64	42.3525832
100	34.97	5.45	7.75	52.9903491
125	52.36	3.71	3.52	35.4734337
150	47.22	4.24	3.93	40.6013214

speed mm/s	L*	a*	b*	$\Delta E_{ab}^*$
175	46.07	4.86	3.34	41.7562941
200	79.95	- 4.51	-20.75	27.6144943
225	53.67	5.12	3.28	34.1621794
250	54.62	4.93	2.91	33.2199488
275	55.33	4.05	-0.38	32.7878728
300	62.63	4.64	4.09	25.1902878
325	58.05	4.52	3.02	29.7861528
350	61.90	8.74	2.13	26.3213924
375	56.19	10.96	-0.88	32.6378814
400	64.86	4.63	0.22	23.2691835
425	56.09	0.59	-20.54	40.30837878
450	45.10	3.53	-24.55	51.39223482
475	30.19	12.5	40.1	68.46510425
500	60.20	0.54	42.3	47.39108355
525	61.70	0.75	40.32	44.8989187
550	50.70	0.66	-10.6	40.0782285
575	60.10	0.66	-11.7	32.09514605
600	25.69	13.54	42.52	73.65166461
625	65.83	0.85	41.2	43.37238984
650	70.70	0.66	50.6	49.79823692

Table (3-4): Spectrophotometer results for L\*, a\* and b\* values of CIELAB color space for the twenty-five samples, at power 8W pulse duration 81 ns, line spacing 0.01mm, frequency 80 kHz and scanning speed from 50 to 650 mm/s.

speed mm	L*	a*	b*	$\Delta E_{ab}$ *
untreated stainless steel	87.82	4.56	4	-
50	62.1	4.57	6.22	25.81563
75	63.25	5.97	4.39	24.61351
100	68.01	-10.28	0.407	25.011
125	56.61	4.89	4.23	31.21259
150	59.33	5.33	5.88	28.56234
175	61.88	1.6	5.72	26.16493
200	70.5	10.3	- 4.45	20.10802
225	59.68	3.68	6.3	28.24754
250	73.45	5.45	5.42	14.46739
275	51.74	6.71	4.91	36.15545
300	58.06	8.09	5.7	30.01680
325	50.04	10.35	6.5	38.30277
350	59.18	5.7	6.06	28.73661
375	59.39	1.72	2	28.64141
400	55.14	11.71	2.51	33.48619
425	54.7	7.7	7.39	33.44078

speed mm	L*	a*	b*	$\Delta E_{ab^*}$
450	52.97	1.1	0.54	35.25125
475	57.93	8.05	8.23	30.38889
500	64.43	10.52	7.47	24.38554
525	72.05	7.85	8.05	16.61082
550	58.93	11.27	12.92	30.97131
575	61	9.51	9.71	27.86429
600	75.37	10.16	11.79	15.71771
625	68.76	9.59	8.21	20.15709
650	65.74	8.81	8.09	22.85425

Table (3-5): Spectrophotometer results for L\*, a\* and b\* values of CIELAB color space for the twenty-five samples, at power 4W, line spacing 0.001 mm, frequency 80 kHz and scanning speed from 50 to 650 mm/s, pulse width 10 $\mu$ s.

speed mm/s	L*	a*	b*	$\Delta E_{ab^*}$
untreated stainless steel	87.82	4.56	4	-
50	59.17	4.08	1.23	28.78759802
75	54.87	3.6	-0.71	33.29877175
100	55.39	2.18	-1.06	32.9085536
125	64.59	2.99	-0.47	23.708199
150	74.73	4.34	3.43	13.10425122
175	69.85	-0.45	1.91	18.77202973

speed mm/s	L*	a*	b*	$\Delta E_{ab}^*$
200	78.67	3.32	1.7	9.515781628
225	77.95	4.02	2.12	10.06195309
250	69.1	4.89	-1.72	19.57717293
275	67.4	4.09	-2.16	21.33407837
300	70.38	-8.98	1.02	22.2792639
325	69.09	-8.64	1.02	23.10699678
350	79.69	3.58	50.4	47.11705954
375	67.54	-6.19	6.24	23.06205758
400	59.1	16.01	7.65	31.13299536
425	69.64	16.94	-7	24.59221015
450	96.24	22.14	-3.16	20.7657988
475	67.24	20.5	-9.41	29.28221474
500	68.2	5.41	-5.44	21.78945846
525	43.77	9.41	10.37	44.77166403
550	72.88	8.06	9.49	16.29704574
575	69.52	8.06	9.4	19.39845355
600	90	8.69	9.27	7.041462916
625	95	8	9	9.401382877
650	98	8	9	11.8518353

Table (3-6): Spectrophotometer results for L\*, a\* and b\* values of CIELAB color space for the twenty-five samples, at power 4W, line spacing 0.001 mm, frequency 80 kHz and scanning speed from 50 to 650 mm/s, Pulse width 81ns.

speed mm/s	L*	a*	b*	$\Delta E_{ab^*}$
untreated stainless steel	87.82	4.56	4	-
50	70.5	4.52	-23.2	32.24630211
75	74.07	3.98	-22.87	30.18933255
100	40.7	0.54	0.33	47.43336062
125	71.01	1.5	1.4	17.28293089
150	45.65	-20.10	11.5	49.42342056
175	70.8	-18.95	9.1	29.46880554
200	35.26	40.1	20.15	65.47112111
225	33.58	55.94	29.88	79.0674168
250	60.45	60.60	33.1	68.82157002
275	71.21	21.2	49.5	51.21554159
300	65.21	8.52	60.6	61.07744019
325	45.9	10.11	70.14	78.50215602
350	75.8	7.3	66.5	63.70430127
375	88.57	4.65	45.5	41.50687413
400	90.5	66.3	77.5	96.02739193
425	66.7	3.5	18.5	25.64035881

speed mm/s	L*	a*	b*	$\Delta E_{ab}$ *
450	77.7	-0.01	0.02	11.79574923
475	77.85	-0.02	0.02	11.67123387
500	91.37	-4.82	31.05	28.84942634
525	90.01	-4.1	31.02	28.45825188
550	90.01	-4.2	30.3	27.80690022
575	90	-4.5	30.2	27.80784062
600	90.1	-4.02	30.2	27.66323915
625	90.3	-4.2	33.9	31.25536754
650	92.5	-3.9	30.4	28.1146581

### 3.2.6.3 Roughness Results

The roughness average (Ra) is the surface parameter that was used to determine surface roughness in this study. (Ra) Surface roughness is critical in assessing and measuring a product's surface quality. in Figure (3-17) which showed that with increase of laser scanning speed led to less surface roughness and when decreasing both power and line spacing result in smooth surface due to regular melted and solidification areas which formed uniform oxide layer. As illustrated in Figure (3-18)

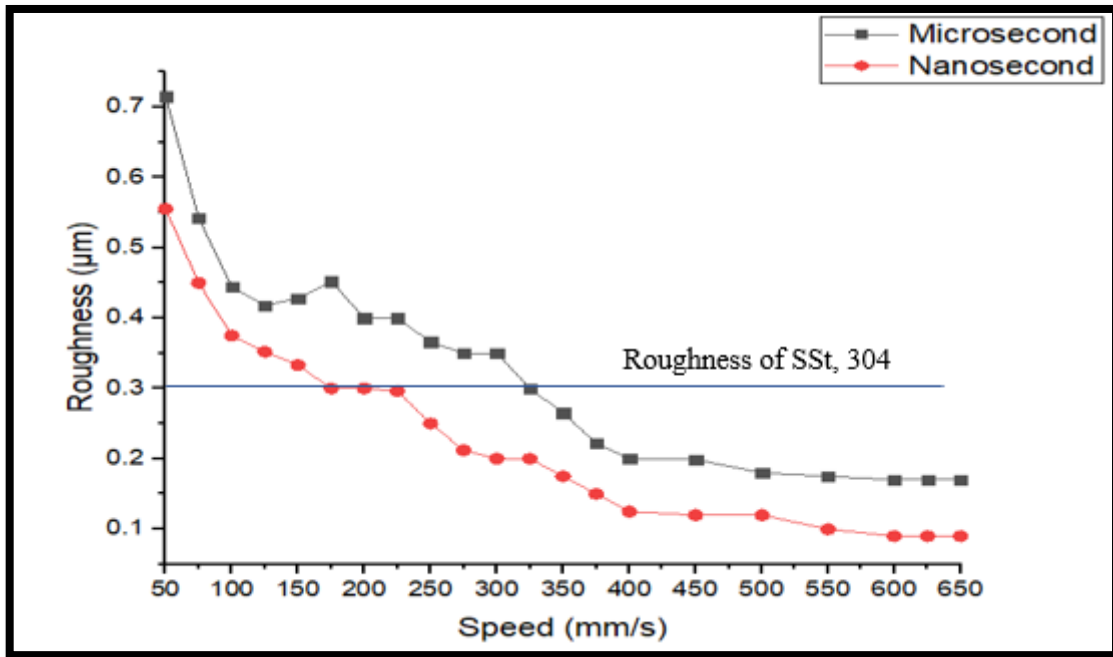


**Figure (3-17): Comparison roughness results between microsecond and nanosecond pulse width at power 8 W, hatch0.01mm, PRR 80 kHz with scanning speed from 50 to 650 mm/s.**

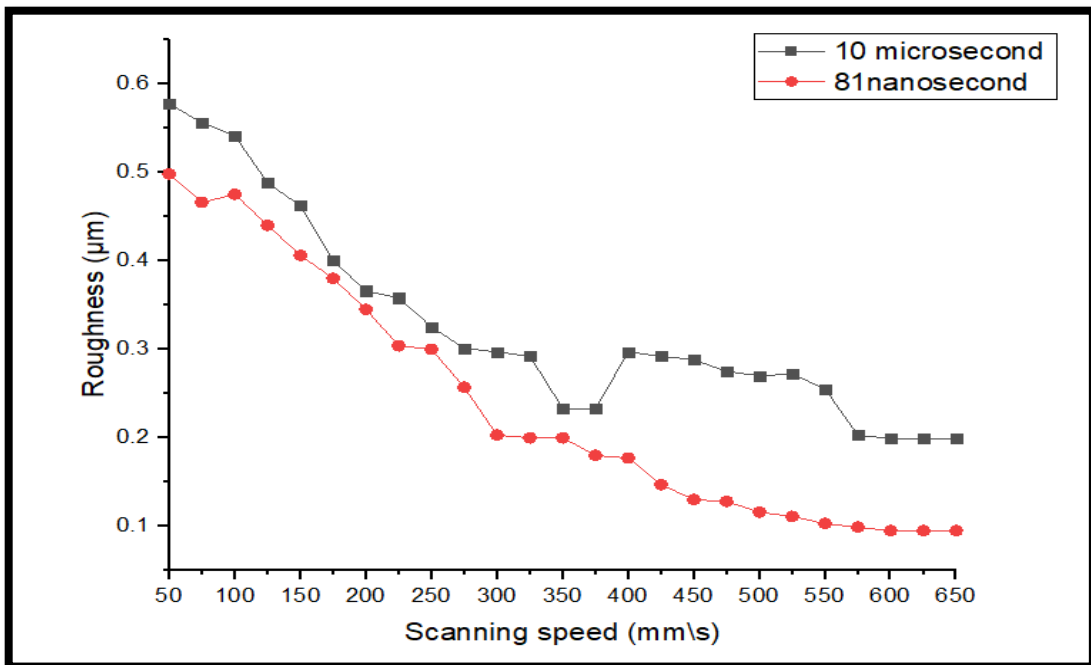


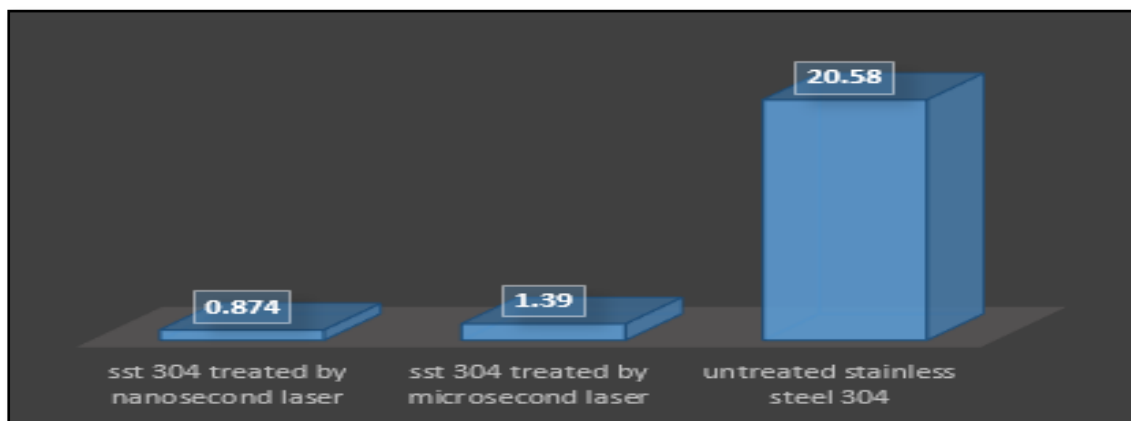
**Figure (3-18): Comparison roughness results between microsecond and nanosecond pulse width at power 4W, hatch0.001mm, PRR 80 kHz and scanning speed from 50 to 650 mm/s.**

### 3.2.6.4 Corrosion Result

The corrosion current density ( $I_{corr}$ ). Which was widely reduced from  $(20.58 \mu\text{A}/\text{cm}^2)$  for laser untreated stainless steel to  $(1.39 \mu\text{A}/\text{cm}^2)$  for microsecond laser treated stainless steel and for the nanosecond, laser treated one is  $(0.874 \mu\text{A}/\text{cm}^2)$ , from the value of  $I_{corr}$ . We can calculate the protection efficacy (IE) according to following equation

$$\text{Protection Efficacy (IE)} = \left( \frac{I_{corr} \text{ standard sample} - I_{corr} \text{ treated sample}}{I_{corr} \text{ standard sample}} \right) \quad (3-3)$$

where IE for microsecond, laser treated stainless steel was 93.24% while for the nanosecond laser treated stainless steel was 95.75%, where both laser types have parameters of P 4W, h 0.001mm and scanning speed 325 mm/s, at temperature range (298-328) K. The oxide layer protects the samples for both types of lasers treated samples with more protection for the nanosecond treated sample due to the more oxide layer that includes Nickel which enhance corrosion resistance. Figure (3-19).



**(3-19): Comparison of the corrosion result between base stainless steel 304, microsecond and nanosecond pulse width at power 4 W hatch 0.001mm with scanning speed 325mm/s and frequency 80 kHz.**

### 3.3 Result of Al 3003

#### 3.3.1 Effect of hatch (line spacing) on Al 3003

different line spacing (hatch) as shown in Figure (3-20). The homogenous color was resulted from applying hatch (0.001,0.005) mm, whereas the pale colors resulted when hatches were (0.01,0.05) mm respectively, due to reduction in the heat accumulated on metal surface which then led to incomplete oxide layer formed. The hatch lines could be easily recognized under light microscope hatch (0.07) mm.

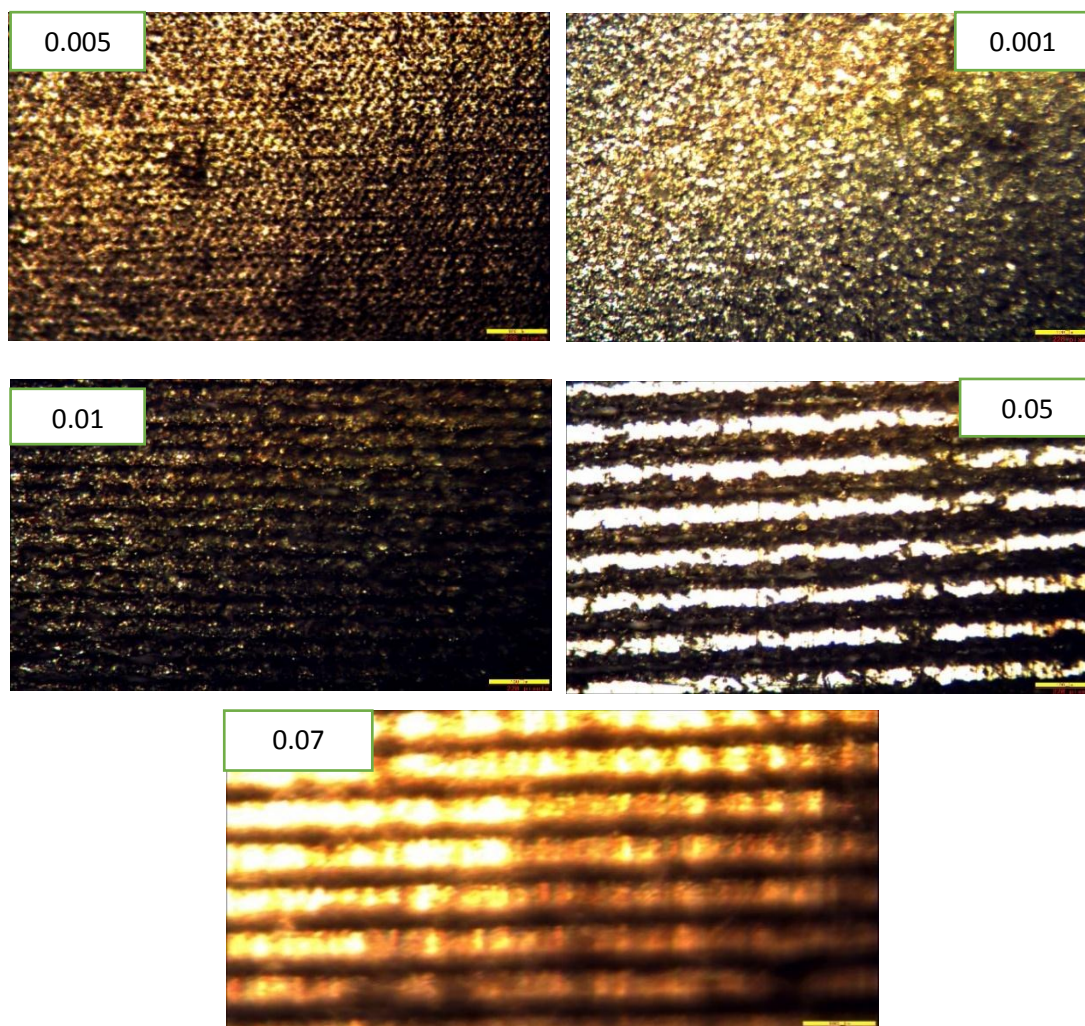


**Figure (3-20): Optical microscope image with different of hatch for Al 3003.**

Line spacing (hatch) is an important color parameter because it is inversely proportional to accumulated fluence ( $F_{acc}$ ) according to equation below[78].

$$F_{acc} = 2\sqrt{2} E / \pi \omega \circ L \quad (\text{J/cm}^2) \text{ -----(3-4)}$$

Where: -

E = laser pulse energy (J),

$\omega \circ$  = laser spot (cm),

L = line spacing (hatching)(cm)

i.e., with reduced hatch accumulated fluence increased which led to more melting and re- solidification that lead irregular surface and more dark color appearance. As shown in Figure (3-25, A and C)

### 3.3.2 Effect of frequency on Al3003

The pulse repetition rate, conducted (20,40,80) kHz. The energy inversely proportional with pulse repetition rate. Therefore, at frequency 20 kHz the Al ablated was with gray color oxide layer which then appeared dark gray at frequency 40 kHz and become white and more stable at 80 kHz (Figure 3-21).

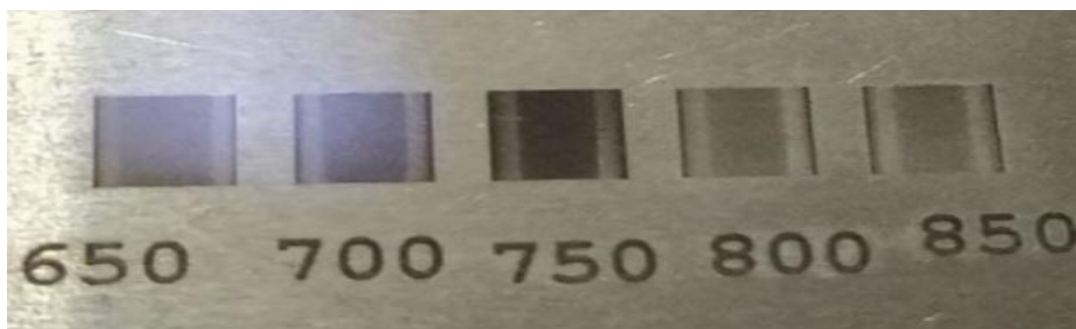


**Figure (3-21): Effect of low frequency 40 kHz on color result when scanning speed was from 650 to 850 mm/s.**

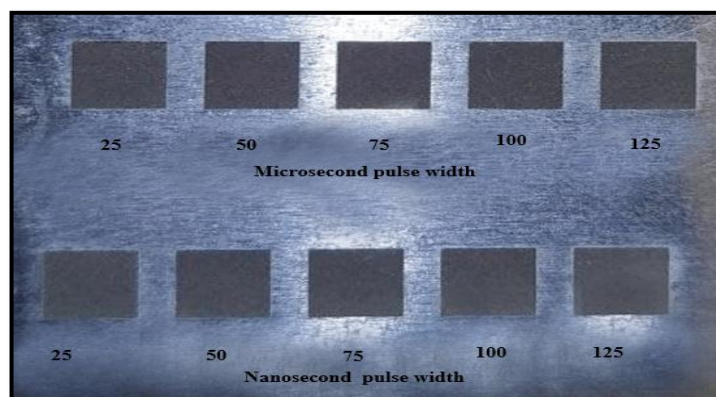
### 3.3.3 Effect of power on Al 3003

Which involved the use of low power (1,2,3,4) W, no color appears, only cleaning or shadowing as shown in the Figure (3 - 22).



**Figure (3-22): Al 3003 treated by laser colorizing parameters  
P 3W, PRR 80 kHz, h 0.005 mm scanning speed (25-125) mm/s.**

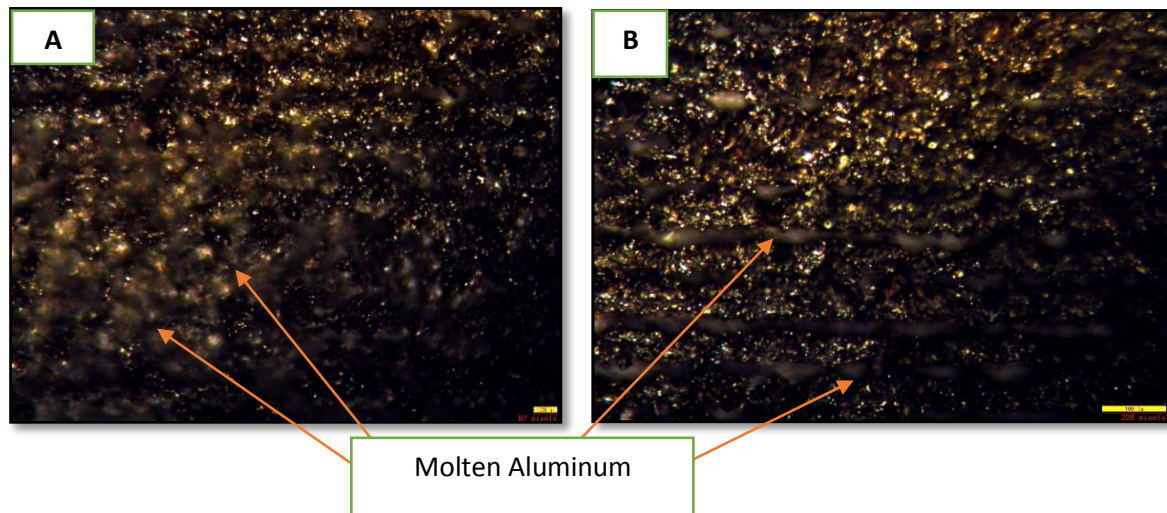
When the power become between (7 and 8)W, the color becomes dark grey, as illustrated in the Figure (3-23). And the Al 3003 plate begins to be engraved at 9 W and bending at 10 W due to the high heat accumulated. While power with 6W give accepted results.



**Figure (3-23): Al 3003 plate at scanning speed (25 to 125) mm/s steep  
25, power 8W.**

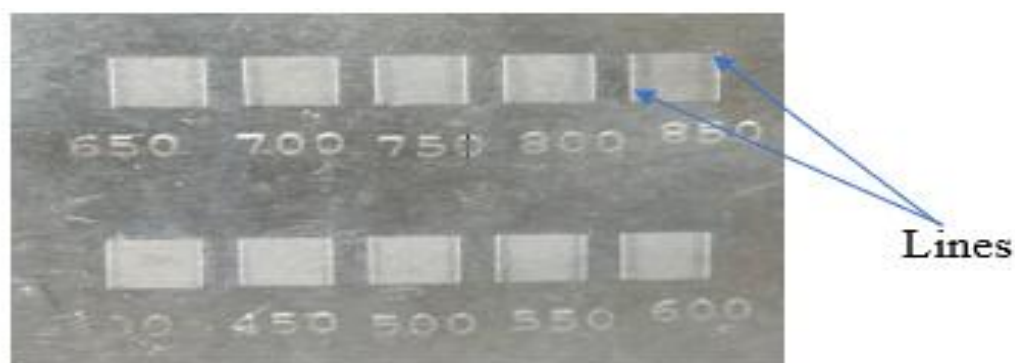
### 3.3.4 Effect of scanning speed on Al3003

At low scanning speed(25mm/s) the color became gray due to accumulation of aluminum melted and rapid re-solidification lead to irregular surface and rougher consequently. The light capture inside aluminum surface and appear gray color as illustrated in Figures (3-24).



**Figure (3-24): Al 3003 plate treated by power 6 W, scanning speed 25 mm/s, PRR 80 kHz, hatch 0.005mm, (A) 10  $\mu$ s pulsed width and (B) 81 ns pulsed width.**

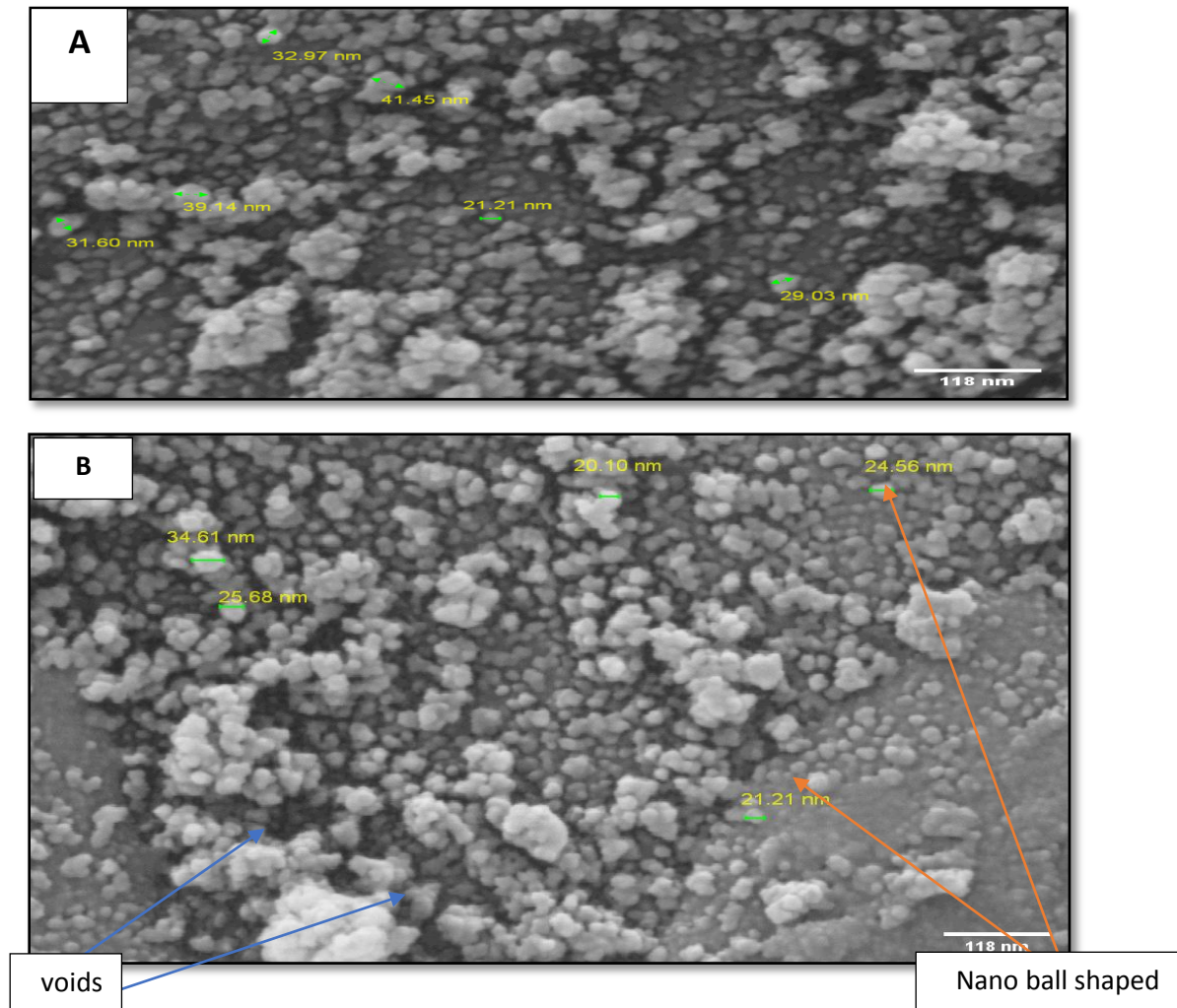
When the scanning speed was increased, the color become white due to less time interaction between metal surface and laser beam. However, as scanning speed increase from (400 to 850) mm/s, the color became unstable and two lines inside the marking square shift to faded grey due to less time interaction to form a normal oxide layer. As illustrated in Figure (3-25)



**Figure (3-25): Al plate treated by 10 microsecond pulsed width and scanning speed from (400 -850) mm/s.**

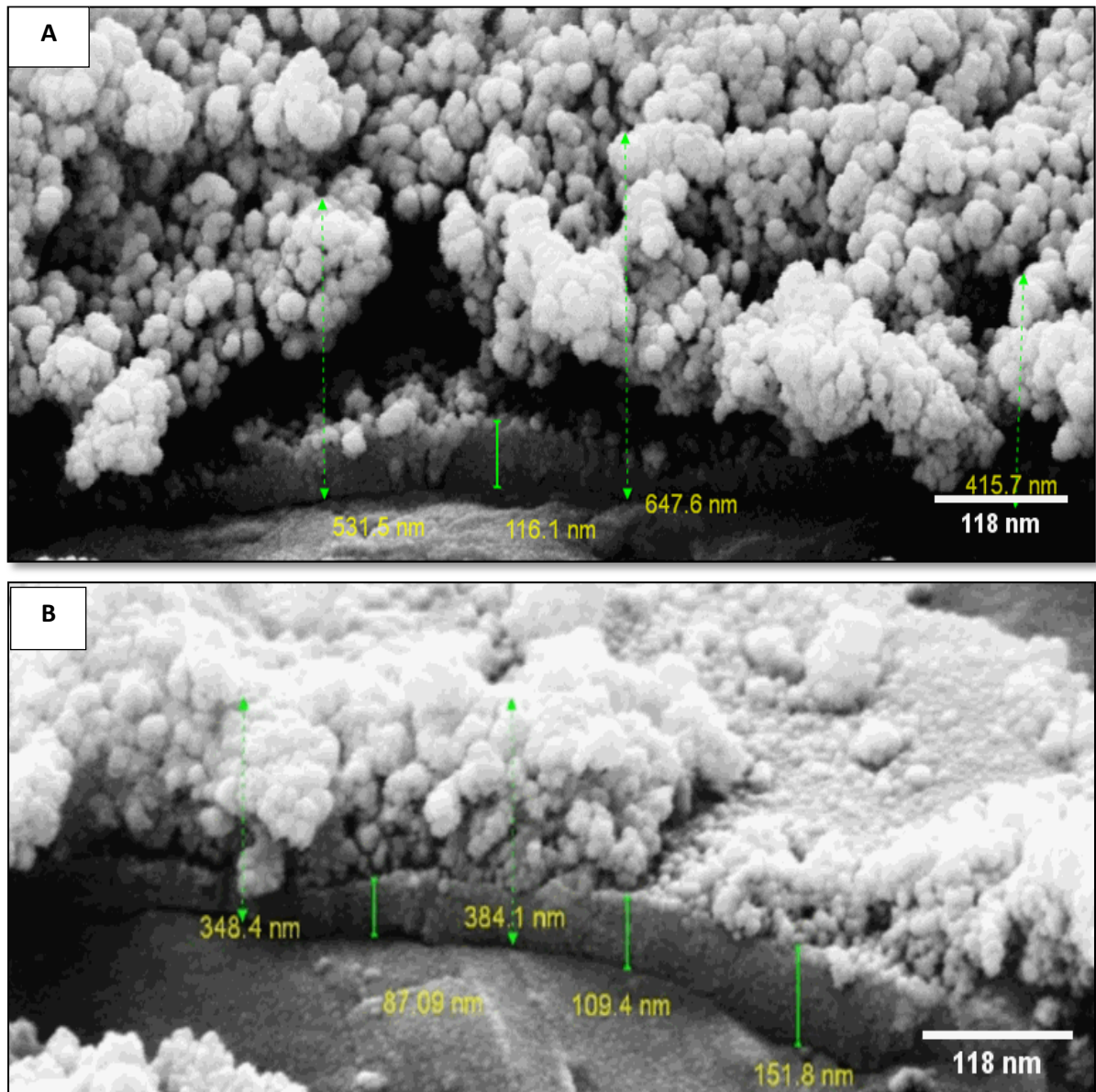
### 3.3.5 Surface morphology analysis

FESEM images revealed that, surfaces of treated aluminum were predominantly covered by nanostructures in form of nano ball shaped and nano voids. As Figure (3- 26).



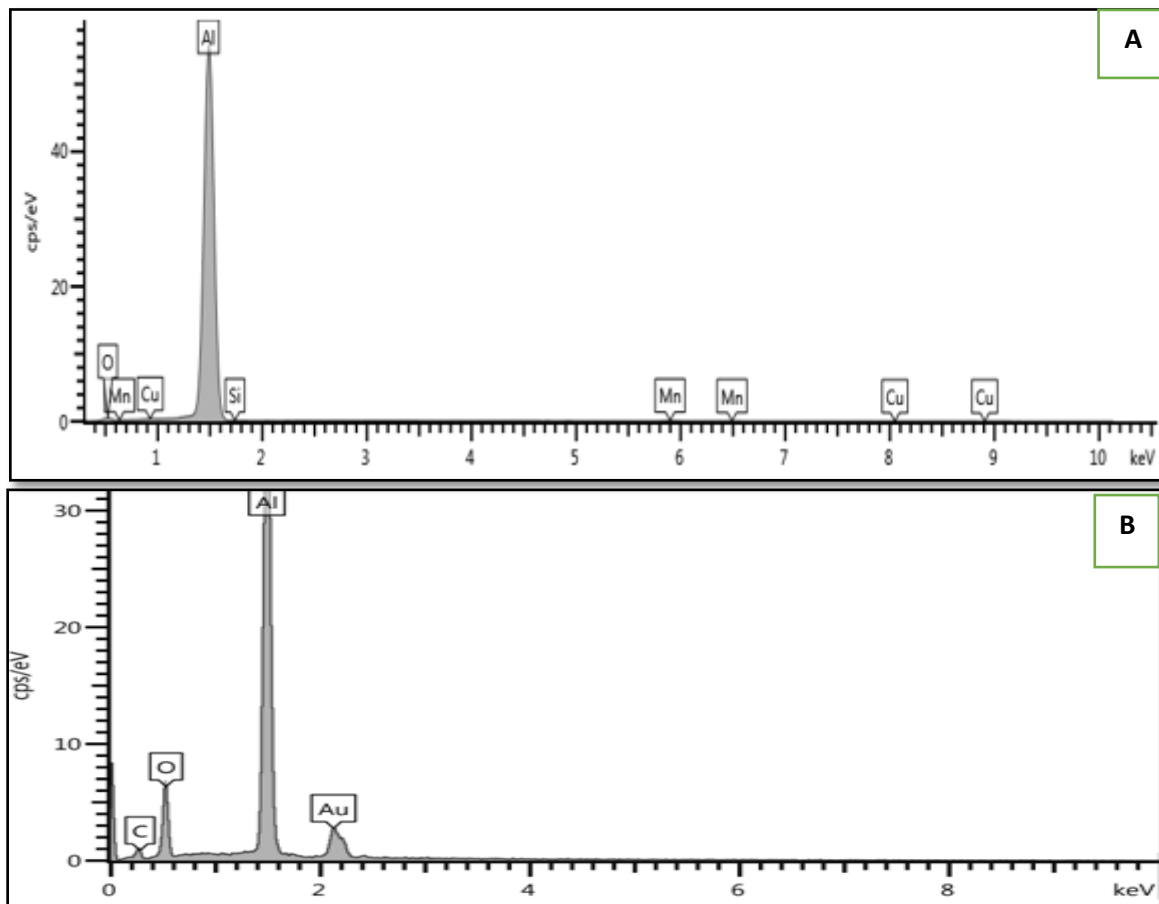
**Figure (3-26): SEM image of Al sample at parameters scanning speed 150 mm/s, power 6W, hatch 0.005 mm, PRR 80 kHz (A)10  $\mu$ s pulse width (B)81 ns pulse width.**

Figure (3-27) shows cross section of oxide layer consists of a very thin layer base and above it was nanoparticle aggregated. Average thickness of oxide layer was approximately 300 nm formation at microsecond laser and 200nm in case of nanosecond fiber laser.



**Figure (3-27): FESEM image Cross section of Al sample at parameters scanning speed 150 mm/s, power 6 W, hatch 0.005 mm frequency 80 kHz (A)10  $\mu$ s pulse width (B)81 ns pulse width.**

EDS results were illustrated in Figure (3-28) For Al.



**Figure (3-28): EDS analysis of Al surface: (A) laser untreated Al (B) laser treated sample at speed 150 mm/s, P 6 W, hatch 0.005mm and pulse width 10  $\mu$ s.**

According to Table (3-7) there was low amount of oxygen no Table on the surface of Al 3003 before laser treatment which increase approximately triple times when using microsecond laser and less when nanosecond laser used. The oxygen content changes with thickness of oxide layer, where height oxygen concentrations were an indication of thicker oxide layers and aluminum decrease approximately (10 %) from base Al 3003 laser treated, where there was no amount of Mn, Cu and Si

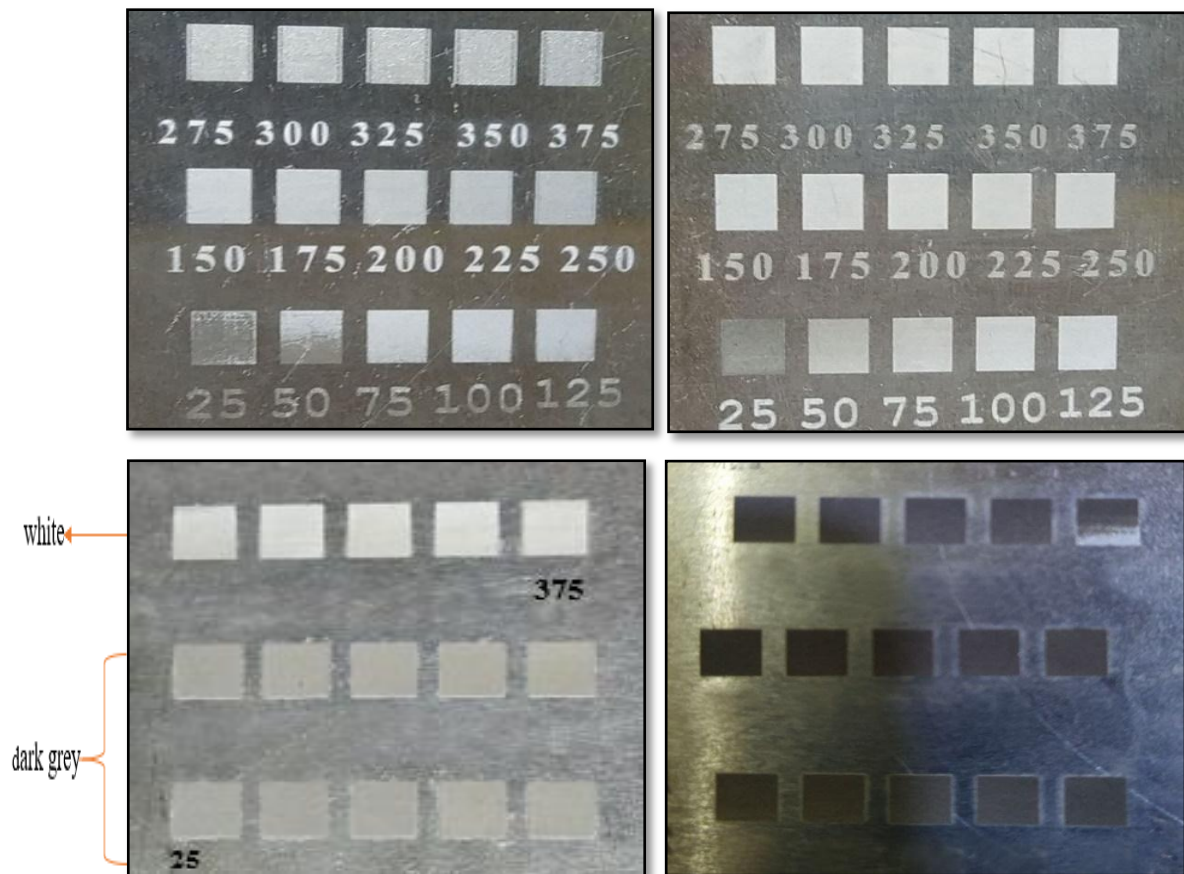
on surface due to high affinity of the aluminum to oxygen according to Ellingham diagram of formation of  $\text{Al}_2\text{O}_3$ . The carbon observed on the surface was adventitious carbon originated from sample base test.

Table (3-7): The chemical composition according to EDS results for substrate and samples treated with different parameters.

	Al	Si	Mn	Cu	O	C
<b>Al 3003 untreated</b>	<b>95.37</b>	<b>0.23</b>	<b>0.71</b>	<b>0.15</b>	<b>3.45</b>	
<b>p 6W, speed 150mm/s, pulse width 10 <math>\mu</math>s</b>	<b>83.5</b>	-	-	-	<b>12.6</b>	<b>4</b>
<b>p 6W, speed 150mm/s, pulse width 81 ns</b>	<b>84.8</b>	-	-	-	<b>11.5</b>	<b>3.8</b>

### 3.3.6 Final results of Al 3003

Aluminum and its alloys behavior differently from stainless 304 when treated by laser color marking, yielding no color results other than whitening or blackening. In this study, white and grey colors were obtained using different laser parameters. As shown in Figure (3-29)



**Figure (3-29): Al 3003 plate treated by power 6 W, Scanning speed from 25 to 375 mm/s, PRR 80 kHz, hatch 0.005mm, (A) 10  $\mu$ s pulsed width, (B) 81 ns pulsed width, (C) 10  $\mu$ s pulsed width with hatch 0.001mm and (D) 81 ns pulsed width with hatch 0.001mm.**

### 3.3.7 Roughness Results of Al 3003

Roughness has a significant impact on absorption incident light by aluminum surface that was laser colored. Because of many reflections in hills and valleys led to incident light interference with sideways-reflected beams, some stimulated absorption [3]. Therefore, the surface that owns more roughness resulted in more grey color occurred. Figures (3-30), (3-31) respectively show the roughness results for Al 3003.

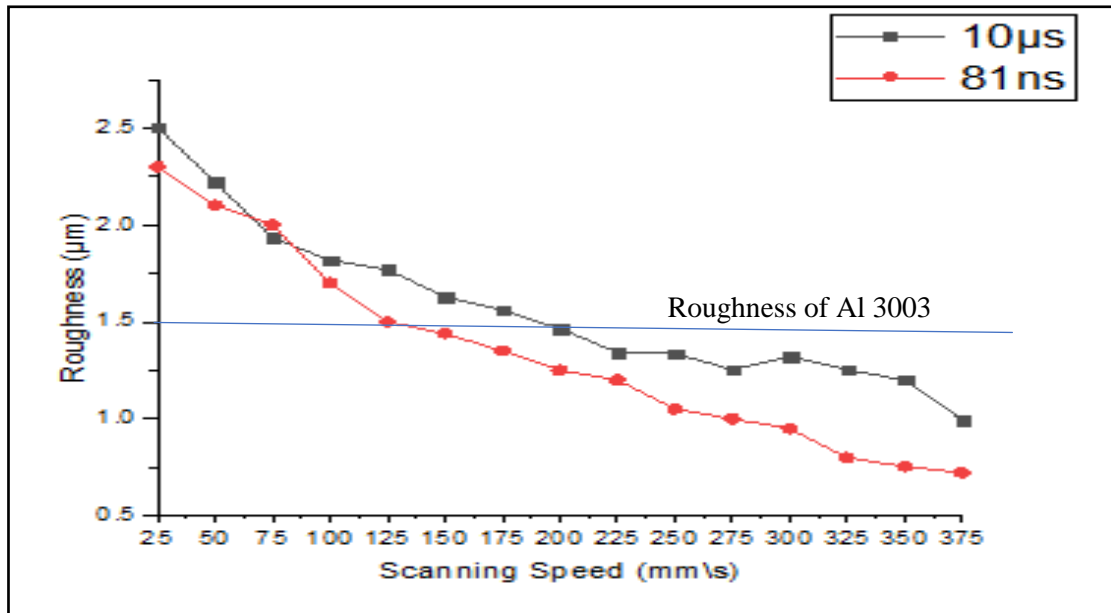


**Figure (3-30):** Comparison roughness of Al 3003 results between microsecond and nanosecond pulse width at power 6 W, hatch 0.001mm and scanning speed (25-375) mm/s

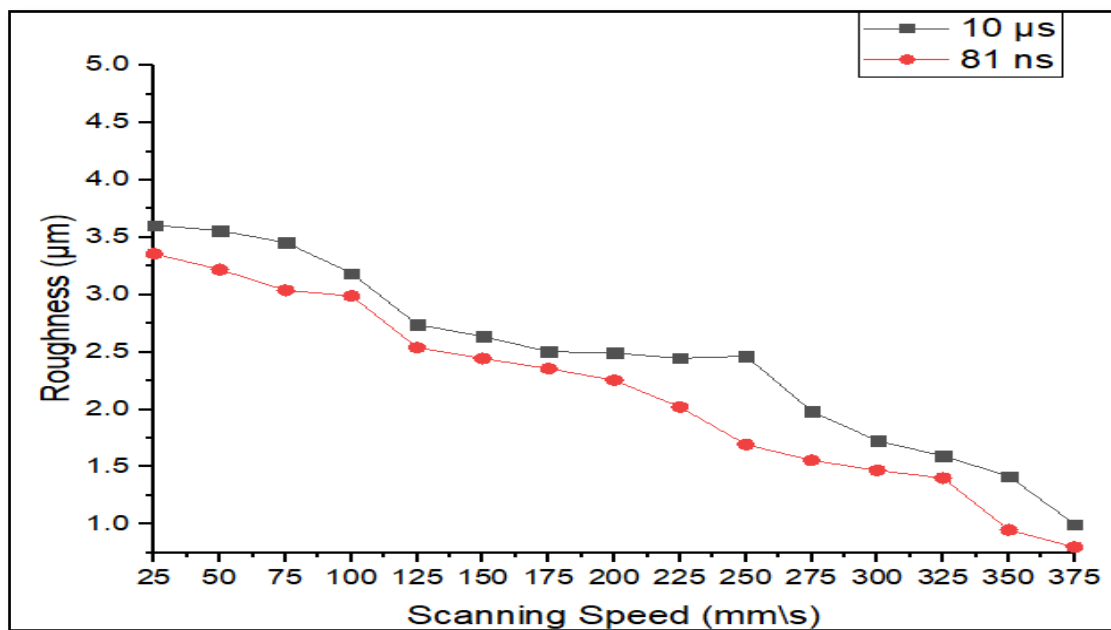


**Figure (3-31):** Comparison roughness of Al 3003 results between microsecond and nanosecond pulse width at power 6 W, hatch 0.005mm and scanning speed (25-375) mm/s.

### 3.3.8 Corrosion Results of Al 3003

The corrosion current density ( $I_{\text{corr}}$ ) for laser untreated Aluminum was high ( $6.55\mu\text{A}/\text{cm}^2$ ) compared with microsecond laser treated Aluminum which was ( $0.005\mu\text{A}/\text{cm}^2$ ) and ( $0.504\mu\text{A}/\text{cm}^2$ ) for the nanosecond laser treated one (Figure 3-32). The IE for microsecond, laser treated Aluminum was (99.75%) while for the nanosecond laser treated Aluminum was (92.3%), where both laser types coloring parameters of P (6W), h (0.005mm) and scanning speed (150 mm/s), at temperature range (298-328) K.

The corrosion resistance for microsecond treated aluminum was more than that of nanosecond treated samples due to more thicker oxide layer created over the colored surface.

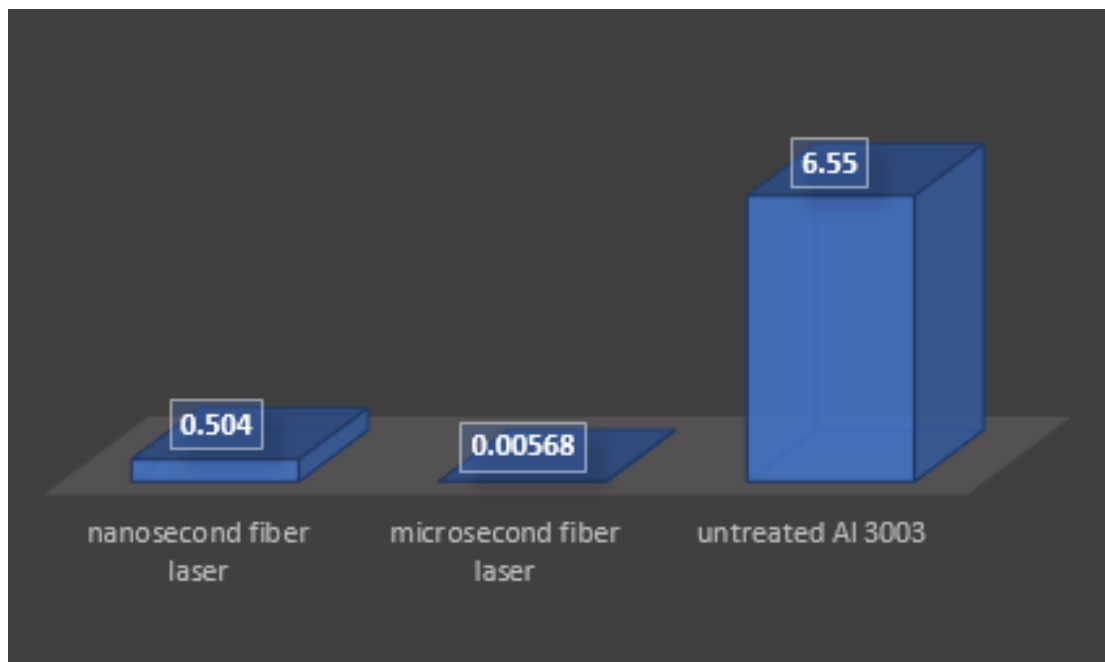


**Figure (3-32): Comparison corrosion result between base Al 3003, microsecond and nanosecond pulse width at power 6 W hatching 0.005mm with scanning speed 150mm/s and frequency 80 kHz.**

---

### 3.4 Conclusions

The primary effect of laser treatment is an energy source that is distributed as heat and results in material surface changes. The quantity of energy absorbed varies depending on the laser beam power, scanning speed and laser pulse frequency. Laser-induced oxidation produced a thin oxide -film colored on stainless steel 304 and Aluminum 3003, when using nanosecond and microsecond pulse width. The following remarks are drawn from the experimental results.

#### **A - For stainless steel 304: -**

- 1- Twenty colors were obtained and the color change from dark to light with increasing the scanning speed.
- 2- There was more oxygen content on surface of sample after laser treatment due to oxidation process and element changes.
- 3- The roughness is inversely proportional to the scanning speed. Colored surfaces by nanosecond laser are less rough than microsecond laser-colored surfaces, also less roughness obtained with smaller hatch value.
- 4- Nanosecond pulse width laser treatment give more protection against corrosive environment than microsecond pulse width treatment, due to present Nickel in the oxide layer.

#### **B – For Aluminum 3003: -**

- 1- Laser coloring of aluminum resulting in white and gray color only for both lasers (nano and micro second).
- 2- The thickness of Aluminum oxide layer produced when Aluminum treated with microsecond laser was thicker than nanosecond laser.
- 3- Higher roughness result when reducing both hatch (line space) and scanning speed.

- 4- Corrosion resistance was higher for microsecond pulse width laser treatment than that of nanosecond pulse width, due to the higher thickness of oxide layer for microsecond fiber laser.

### **3.5 Future projects suggested**

To improve the current research, several additional work measures are recommended for the future;

- 1- Using other pulse durations of the same laser form, such as picosecond and femtosecond pulse durations.
- 2- Using assist gases in coloring process.
- 3- Use of other metals for more evaluation of coloring surfaces such as copper, silver and so on because the corrosion properties of these metals may be modified.
- 4- Studying the effect of pre-heating the workpiece before laser treatment.

# References

- [1] Dywel, P., Szczesny, R., Domanowski, P., & Skowronski, L. (2020). "Structural and Micromechanical Properties of Nd: YAG Laser Marking Stainless Steel (AISI 304 and AISI 316)". *Materials*, 13(9), 2168.
- [2] Zhang, W., & Yao, Y. L. (2002). "Laser materials processing," in General Electric Global Research Center Schenectady, New York Columbia University New York, New York, vol. 11, no. 2–3, p. ch 34.
- [3] Dahotre, N. B., & Harimkar, S. (2008). "Laser fabrication and machining of materials". Springer Science & Business Media.
- [4] Baufay, L., Houle, F. A., & Wilson, R. J. (1987). "Optical self-regulation during laser-induced oxidation of copper". *Journal of applied physics*, 61(9), 4640-4651.
- [5] Antończak, A. J., Stępak, B., Koziol, P. E., & Abramski, K. M. (2014). "The influence of process parameters on the laser-induced coloring of titanium." *Applied Physics A*, 115(3), 1003-1013.
- [6] Ion, J. (2005). "Laser processing of engineering materials: principles, procedure and industrial application". Elsevier.
- [7] ŠVANTNER, M., KUČERA, M., HOUDKOVÁ, Š., & Riha, J. (2011). "Influence of laser ablation on stainless steel corrosion behavior". In Proceedings of 20th International Conference on Metallurgy and Materials METAL.
- [8] Leontyev, A. (2011). "Laser decontamination and cleaning of metal surfaces: modelling and experimental" studies (Doctoral dissertation, Université Paris Sud-Paris XI).
- [9] Issa, A., & Brabazon, D. (2021). Laser Micro-and Nano-Scale Processing; Fundamentals and applications. Laser Micro-and Nano-Scale Processing.
- [10] Ready, J. F. (1982). Material processing—An overview. *Proceedings of the IEEE*, 70(6), 533-544.
- [11] Garbacz, H., Fortuna, E., Marczak, J., Strzelec, M., Rycyk, A., Koss, A., ... & Kurzydłowski, K. J. (2010). "Laser cleaning of copper roofing sheets subjected to long-lasting environmental corrosion". *Applied Physics A*, 100(3), 693-701.

- [12] **J. F. Ready**, "Industrial Application of Lasers". Academic Press, San Diego, (1997).
- [13] **Mishra, S., & Yadava, V. (2015)**. "*Laser beam micromachining (LBMM)—a review*". Optics and lasers in engineering, 73, 89-122.
- [14] **Schaaf, P. (Ed.). (2010)**. "*Laser processing of materials: fundamentals, applications and developments*" (Vol. 139). Springer Science & Business Media.
- [15] **Majumdar, J. D., & Manna, I. (2003)**. "*Laser processing of materials*". Sadhana, 28(3), 495-562.
- [16] **Dutta, M. J., & Manna, I. (2011)**. "*Laser material processing*". International Materials Reviews, 56(5-6), 341-388.
- [17] **Steen, W. M., & Mazumder, J. (2010)**. "*Laser material processing*". springer science & business media.
- [18] **Williams, S., & Suder, W. (2011)**. "*Use of fundamental laser material interaction parameters in laser welding*". In CLEO: 2011-Laser Science to Photonic Applications (pp. 1-2).
- [19] **Amara, E. H., Haid, F., & Noukaz, A. (2015)**. "*Experimental investigations on fiber laser color marking of steels*". Applied Surface Science, 351, 1-12.
- [20] **Burgan, B. A., Baddoo, N. R., & Gilsenan, K. A. (2000)**. "*Structural design of stainless steel members—comparison between Eurocode 3, Part 1.4 and test results*". Journal of Constructional Steel Research, 54(1), 51-73.
- [21] **Fraser, A., Maltais, J., & Godmaire, X. P. (2018, March)**. "*Analysis of laser marking performance on various non-ferrous metals*". In TMS Annual Meeting & Exhibition (pp. 937-941). Springer, Cham.
- [22] **Fedorycheva, I., & Hammer, M. (2015)**. "*A Description of Safety Triad Models of Safety Culture as a tool in Human Performance Research*". MM Science Journal, 4, 768-771
- [23] **Klimt, B. H. (1988)**. "*Review of laser marking and engraving*". Lasers Optronics, 7(9), 61-62.
- [24] **Bosman, J. (2007)**. "Processes and strategies for solid state Q-switch laser marking of polymers.

- [25] Lazov, L., Deneva, H., & Narica, P. (2015, June). " *Laser marking methods. In ENVIRONMENT. TECHNOLOGIES. RESOURCES*". Proceedings of the International Scientific and Practical Conference (Vol. 1, pp. 108-115).
- [26] Czerwińska, K., & Pacana, A. (2019). " *Analysis of the implementation of the identification system for directly marked parts-DataMatrix code*". Production Engineering Archives, 23.
- [27] Li, C. L. (2018, June). " *Nanosecond laser direct-part marking of data matrix symbols on titanium alloy substrates*". In IOP Conference Series: Materials Science and Engineering (Vol. 380, No. 1, p. 012022). IOP Publishing.
- [28] Sobotova, L., & Badida, M. (2017). " *Laser marking as environment technology*". Open Engineering, 7(1), 303-316.
- [29] Liu, H., Lin, W., & Hong, M. (2019). " *Surface coloring by laser irradiation of solid substrates*". Apl Photonics, 4(5), 051101.
- [30] Dusser, B., Sagan, Z., Soder, H., Faure, N., Colombier, J. P., Jurlin, M., & Audouard, E. (2010). " *Controlled nanostructures formation by ultra-fast laser pulses for color marking*". Optics express, 18(3), 2913-2924.
- [31] Khare, P. K. G. Rajeev.(2012). " *Laser Physics and Technology*". Springer Proceedings in Physics. P,141-149.
- [32] Han, A., & Gubencu, D. (2008). " *Analysis of the laser marking technologies*". Nonconventional Technologies Review, 4, 17-22.
- [33] Lu, J., Ueda, K. I., Yagi, H., Yanagitani, T., Akiyama, Y., & Kaminskii, A. A. (2002). " *Neodymium doped yttrium aluminum garnet (Y3Al5O12) nanocrystalline ceramics—a new generation of solid state laser and optical materials*". Journal of alloys and compounds, 341(1-2), 220-225.
- [34] Kratky, A., Schuöcker, D., & Liedl, G. (2009, April). " *Processing with kW fiber lasers: advantages and limits*". In XVII International Symposium on Gas Flow, Chemical Lasers, and High-Power Lasers (Vol. 7131, p. 71311X). International Society for Optics and Photonics.

- [35] Narica, P., Teilans, A., Lazov, L., Cacivkins, P., & Teirumnieks, E. (2018, December). "Mathematical Model of Forecasting Laser Marking Experiment Results". In Proceedings of The 9th EUROSIM Congress on Modelling and Simulation, EUROSIM 2016, The 57th SIMS Conference on Simulation and Modelling SIMS 2016 (No. 142, pp. 800-804). Linköping University Electronic Press.
- [36] Fraser, A., Brochu, V., Gingras, D., & Godmaire, X. P. (2016). "Important considerations for laser marking an identifier on aluminum". In Light Metals 2016 (pp. 261-264). Springer, Cham.
- [37] Maltais, J., Brochu, V., Frayssinous, C., Vallée, R., Godmaire, X., & Fraser, A. (2016). "Surface analysis study of laser marking of aluminum". Proceedings of ICSOBA.
- [38] Chang, C. L., Wu, J. W., & Lee, C. Y. (2012). "Coloration of Stainless Steel Utilizing Fiber Laser Oxidation". In Applied Mechanics and Materials (Vol. 121, pp. 70-74). Trans Tech Publications Ltd.
- [39] Li, C. L., & Lu, C. H. (2017). "Influence of nanosecond laser processing parameters on the titanium alloy surfaces colorization". In Key Engineering Materials (Vol. 744, pp. 223-227). Trans Tech Publications Ltd.
- [40] Ma, X., Nie, X., Zhao, J., Shrotriya, P., Zhang, Y., Cui, Y., & Wang, J. (2020). "Effect of nanosecond pulsed laser parameters on the color making of 304 stainless steel". Optics & Laser Technology, 126, 106104.
- [41] Ma, X., Nie, X., Zhao, J., Han, Y., Shrotriya, P., Wang, Y., & Guo, J. (2020). "Coloring stability analysis of nanosecond pulsed laser induced surface coloring on stainless steel". Optics & Laser Technology, 123, 105936.
- [42] Faucon, M., Laffitte, A., Lopez, J., & Kling, R. (2014, March). "Surface blackening by laser texturing with high repetition rate femtosecond laser up to 1MHz". In Frontiers in Ultrafast Optics: Biomedical, Scientific, and Industrial Applications XIV (Vol. 8972, p. 89721M). International Society for Optics and Photonics.
- [43] Huang, H., Yang, L. M., Bai, S., & Liu, J. (2015). "Blackening of metals using femtosecond fiber laser". Applied optics, 54(2), 324-333.

- [44] Vorobyev, A. Y., & Guo, C. (2008). "Colorizing metals with femtosecond laser pulses". Applied Physics Letters, 92(4), 041914.
- [45] Ahsan, M. S., Ahmed, F., Kim, Y. G., Lee, M. S., & Jun, M. B. (2011). "Colorizing stainless steel surface by femtosecond laser induced micro/nano-structures". Applied surface science, 257(17), 7771-7777.
- [46] Suebka, C. (2019). "Laser cleaning of aluminium alloys". The University of Manchester (United Kingdom).
- [47] OIV.( 2006 ). "COMPENDIUM OF INTERNATIONAL ANALYSIS OF METHODS -OIV Chromatic Characteristics Method OIV-MA-AS2-11 Determination of chromatic characteristics according to CIELab," Available: <http://www.oiv.int/oiv/files/6 - Domaines scientifiques/6 - 4 Methodes d analyses/6-4-1/EN/OIV-MA-AS2-11.pdf>.
- [48] Mirjalili, F., Luo, M. R., Cui, G., & Morovic, J. (2019). "Color-difference formula for evaluating color pairs with no separation:  $\Delta E_{NS}$ ". JOSA A, 36(5), 789-799.
- [49] Chen, Y., Zhang, M., Fan, D., Fan, K., & Wang, X. (2018). "Linear regression between CIE-lab color parameters and organic matter in soils of tea plantations". Eurasian soil science, 51(2), 199-203.
- [50] Mokrzycki, W., & Tatol, M. (2014). "Color difference Delta EA survey Color difference  $\Delta EA$  survey". Machine Vision and Applications, 1, 14-18.
- [51] Hunter Lab, (1996). "CIE L\*a\*b\* Color Scale Background," Insight Color, vol. 8, no. 7, pp. 1-4, Available: [Online]. Available: <http://cobra.rdsor.ro/cursuri/cielab.pdf>
- [52] Phatare, P. B., Opara, U. L., & Al-Said, F. A. (2012). "Color measurement and analysis in fresh and processed food: A review". Food Bioprocess Technol, 6, 36-60.
- [53] McLaren, K. (1976). "XIII—The development of the CIE 1976 ( $L^* a^* b^*$ ) uniform color space and color-difference formula". Journal of the Society of Dyers and Colorists, 92(9), 338-341.

- [54] Lazov, L., Deneva, H., & Narica, P. (2015, June). "Factors influencing the color laser marking. In ENVIRONMENT. TECHNOLOGIES". RESOURCES. Proceedings of the International Scientific and Practical Conference (Vol. 1, pp. 102-107).
- [55] Liu, M., Zhang, B. M., Shum, P. P., & Cheng, X. (2016). "Nanosecond pulse fiber laser blackening of aluminum alloy with alumina surface". IEEE Photonics Technology Letters, 28(23), 2701-2704.
- [56] Odintsova, G., Andreeva, Y., Salminen, A., Roozbahani, H., Van Cuong, L., Yatsuk, R., ... & Veiko, V. (2019). "Investigation of production related impact on the optical properties of color laser marking". Journal of Materials Processing Technology, 274, 116263.
- [57] Ready, J. F., & Farson, D. F. (2001). "LIA Handbook of Laser Materials Processing, Laser Institute of America Magnolia Publishing". Inc, United State of America.
- [58] Peckner, D., Bernstein, I. M., & Peckner, D. (1977). "Handbook of stainless steels". (pp. 19-3). New York: McGraw-Hill.
- [59] Saeidi, K. (2016). "Stainless steels fabricated by laser melting: Scaled-down structural hierarchies and microstructural heterogeneities" (Doctoral dissertation, Department of Materials and Environmental Chemistry (MMK), Stockholm University).
- [60] Askeland, D. R., Fulay, P. P., & Wright, W. J. (2010). "The science and engineering of materials 6th edition". Cengage Learning Inc, 889.
- [61] Plaut, R. L., Herrera, C., Escriba, D. M., Rios, P. R., & Padilha, A. F. (2007). "A short review on wrought austenitic stainless steels at high temperatures: processing, microstructure, properties and performance". Materials Research, 10(4), 453-460.
- [62] Outokumpu,(2013) "Handbook of Stainless Steel," pp. 1–89, [Online]. Available: <http://www.outokumpu.com/sitecollectiondocuments/outokumpu-stainless-steel-handbook.pdf>.

- [63] Santos, M. C., Machado, A. R., Sales, W. F., Barrozo, M. A., & Ezugwu, E. O. (2016). *"Machining of aluminum alloys: a review"*. The International Journal of Advanced Manufacturing Technology, 86(9), 3067-3080.
- [64] Budd, G. (1999). *"Resources and production of aluminium"*. European Aluminium Association, Birmingham.
- [65] Hamade, R. F., & Ismail, F. (2005). *"A case for aggressive drilling of aluminum"*. Journal of materials processing technology, 166(1), 86-97.
- [66] Davis, J. R. (2001). *"Aluminum and aluminum alloys"*. ASM international.
- [67] Callister, W. D., Rethwisch, D. G., Blicblau, A., Bruggeman, K., Cortie, M., Long, J., ... & Orwa, J. (2021). *"Materials science and engineering: an introduction"*. Wiley.
- [68] Aluminum Association, Inc. (1990). *"Rolling aluminum: from the mine through the mill"*. Aluminum Association.
- [69] Reddy, A. C. (2017). *"Low and High Temperature Micromechanical Behavior of BN/3003 Aluminum Alloy Nanocomposites"*. International Journal of Mechanical Engineering and Technology 6.4 (2017): 27, 34.
- [70] Murty, K. L., & Charit, I. (2008). *"Structural materials for Gen-IV nuclear reactors: Challenges and opportunities"*. Journal of Nuclear Materials, 383(1-2), 189-195.
- [71] Akasaka, N., Yamashita, S., Yoshitake, T., Ukai, S., & Kimura, A. (2004). *"Microstructural changes of neutron irradiated ODS ferritic and martensitic steels"*. Journal of nuclear materials, 329, 1053-1056.
- [72] Wharry, J. P., Swenson, M. J., & Yano, K. H. (2017). *"A review of the irradiation evolution of dispersed oxide nanoparticles in the bcc Fe-Cr system: Current understanding and future directions"*. Journal of Nuclear Materials, 486, 11-20.
- [73] Miller, M. K., Hoelzer, D. T., Kenik, E. A., & Russell, K. F. (2005). *"Stability of ferritic MA/ODS alloys at high temperatures"*. Intermetallics, 13(3-4), 387-392.
- [74] Gaskell. (1973). *"Introduction Metallurgical Thermodynamics"* .

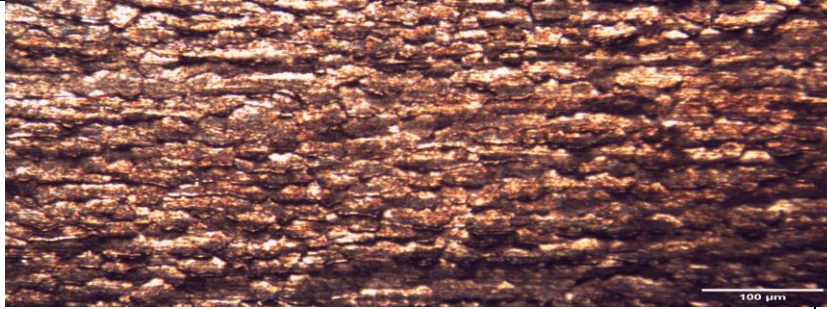
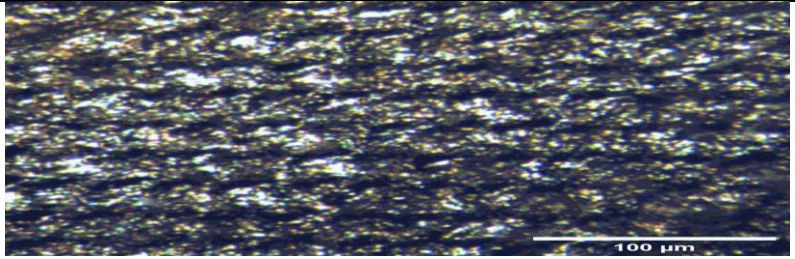
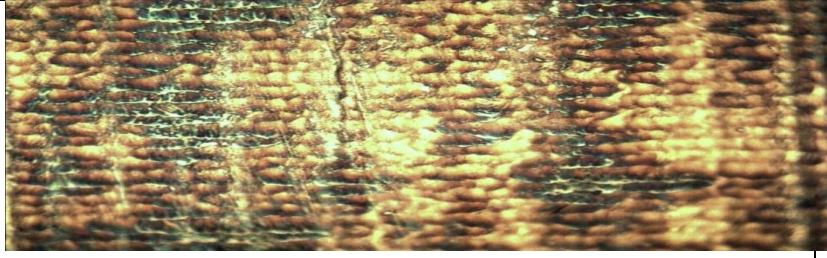
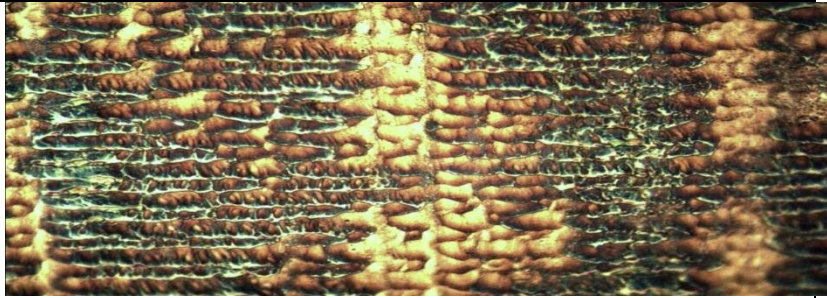
- [75] Cramer, S. D., & Covino Jr, B. S. (2003). *"Corrosion: Fundamentals, Testing, and Protection, Volume 13A, ASM Handbook"*. Journal of Thermal Spray Technology, 12(4), 459.
- [76] Cui, C., Hu, J., Liu, Y., Gao, K., & Guo, Z. (2008). *"Morphological and structural characterizations of different oxides formed on the stainless steel by Nd: YAG pulsed laser irradiation"*. Applied Surface Science, 254(20), 6537-6542.
- [77] Rechner, R., Jansen, I., & Beyer, E. (2012). *"Optimization of the aluminum oxide properties for adhesive bonding by laser surface pretreatment"*. Journal of Laser Applications, 24(3), 032002.
- [78] Zhu, H., Ehrhardt, M., Lorenz, P., Zajadacz, J., Lu, J., & Zimmer, K. (2019). *"Combined effects of nanosecond laser-induced surface oxidation and nanostructure formation for selective colorization of nickel surfaces"*. Applied Physics A, 125(10), 1-10.
- [79] Andreeva, Y. M., Luong, V. C., Lutoshina, D. S., Medvedev, O. S., Mikhailovskii, V. Y., Moskvina, M. K., ... & Veiko, V. P. (2019). *"Laser coloration of metals in visual art and design"*. Optical Materials Express, 9(3), 1310-1319.
- [80] Del Pino, A. P., Serra, P., & Morenza, J. L. (2002). *"Oxidation of titanium through Nd: YAG laser irradiation"*. Applied surface science, 197, 887-890.
- [81] Lavisse, L., Jouvard, J. M., Imhoff, L., Heintz, O., Korntheuer, J., Langlade, C., ... & de Lucas, M. M. (2007). *"Pulsed laser growth and characterization of thin films on titanium substrates"*. Applied surface science, 253(19), 8226-8230.
- [82] Lin, C. J., Wang, Y. C., Lin, L. D., Chiou, C. R., Wang, Y. N., & Tsai, M. J. (2008). *"Effects of feed speed ratio and laser power on engraved depth and color difference of Moso bamboo lamina"*. Journal of materials processing technology, 198(1-3), 419-425.
- [83] Zheng, H. Y., Li, Z. L., Teh, K. M., Liu, Y. C., Lim, G. C., Seng, H. L., & Yakovlev, N. L. (2009). *"Analysis of oxide formation induced by UV laser coloration of stainless steel"*. Applied Surface Science, 256(5), 1582-1588.

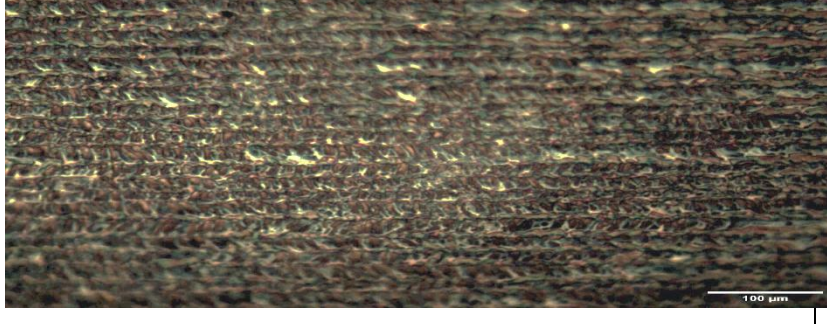
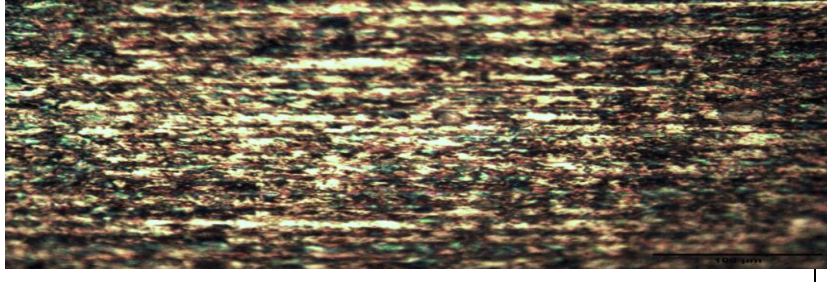
- [84] Lehmuskero, A., Kontturi, V., Hiltunen, J., & Kuittinen, M. (2010). "Modeling of laser-colored stainless steel surfaces by color pixels". Applied Physics B, 98(2), 497-500.
- [85] Leone, C., Genna, S., Caprino, G., & De Iorio, I. (2010). "AISI 304 stainless steel marking by a Q-switched diode pumped Nd: YAG laser". Journal of Materials Processing Technology, 210(10), 1297-1303.
- [87] Adams, D. P., Hodges, V. C., Hirschfeld, D. A., Rodriguez, M. A., McDonald, J. P., & Kotula, P. G. (2013). "Nanosecond pulsed laser irradiation of stainless steel 304L: Oxide growth and effects on underlying metal". Surface and coatings technology, 222, 1-8.
- [88] Li, X. S., He, W. P., Lei, L., Wang, J., Guo, G. F., Zhang, T. Y., & Yue, T. (2016). "Laser direct marking applied to rasterizing miniature Data Matrix Code on aluminum alloy". Optics & Laser Technology, 77, 31-39.
- [89] Lu, Y., Shi, X., Huang, Z., Li, T., Zhang, M., Czajkowski, J., ... & Cao, W. (2017). "Nanosecond laser coloration on stainless steel surface". Scientific reports, 7(1), 1-8.
- [90] Linggamm, R., Quazi, M. M., Ishak, M., Aiman, M. H., Zafiuddin, A. Q., & Qaban, A. (2021, February). "Formation of colors on SS304L stainless steel induced by laser coloring". In IOP Conference Series: Materials Science and Engineering (Vol. 1078, No. 1, p. 012015). IOP Publishing.
- [91] Lazov, L., Angelov, N., Draganov, I., Atanasov, A., Lengerov, A., Teirumnieks, E., & Balchev, I. (2021, March). "Finite element modeling of laser aluminum marking". In Journal of Physics: Conference Series (Vol. 1859, No. 1, p. 012017). IOP Publishing.
- [92] Wang, B., & Gallais, L. (2013). "A theoretical investigation of the laser damage threshold of metal multi-dielectric mirrors for high power ultrashort applications". Optics express, 21(12), 14698-14711.
- [93] Vilar, R. (Ed.). (2016). "Laser surface modification of biomaterials: techniques and applications".
- [94] Jassim, R. A., Farhan, A. M., & Ali, A. M. (2014). "Corrosion protection study of carbon steel and 316 stainless steel alloys coated by nanoparticles". Baghdad Science Journal, 11(1).

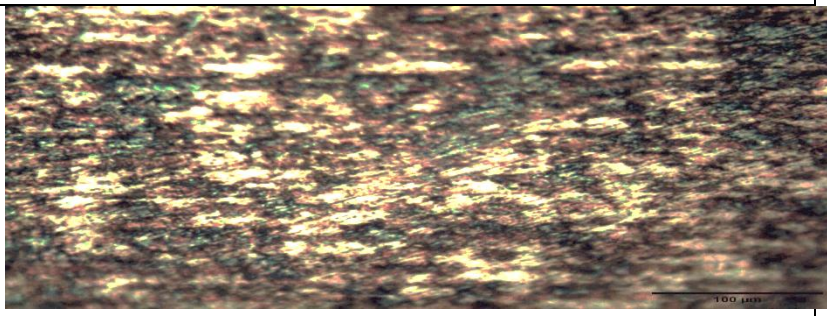
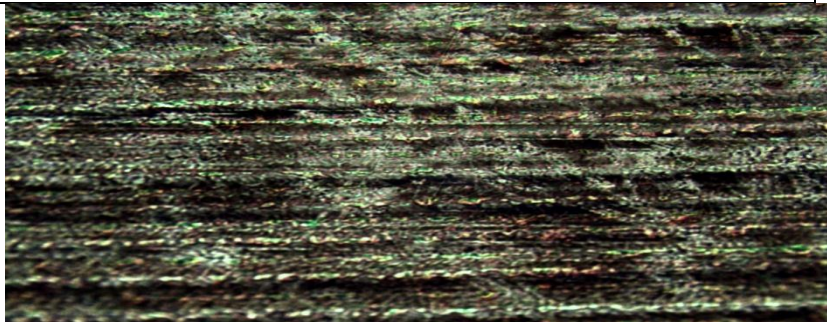
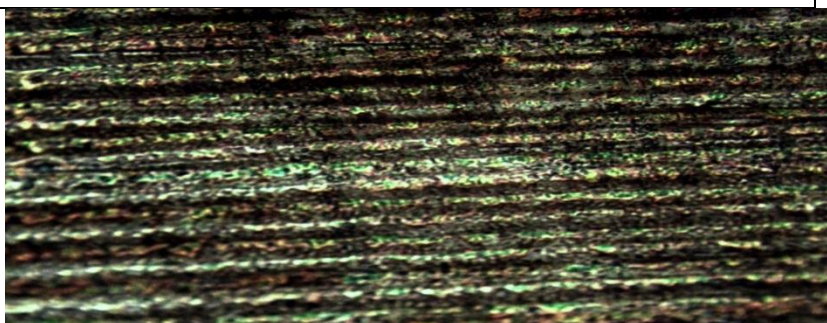
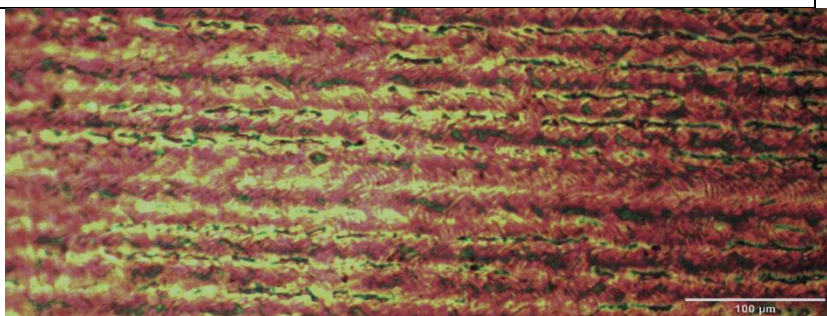
- [95] Brihmat-Hamadi, F., Amara, E. H., & Kellou, H. (2017). *"Characterization of titanium oxide layers' formation produced by nanosecond laser coloration"*. Metallurgical and Materials Transactions, 48(3), 1439.

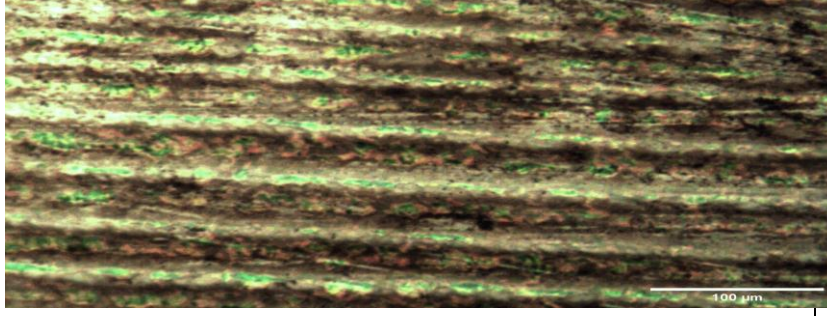
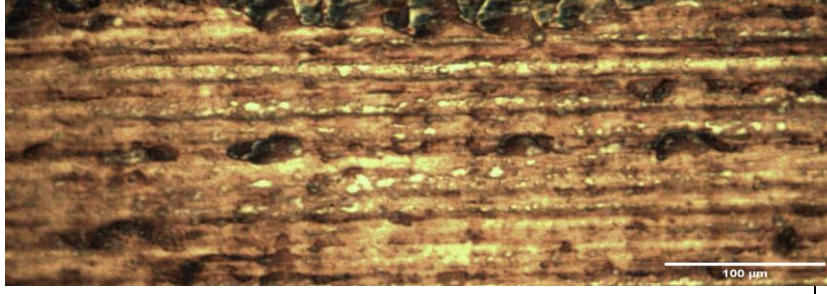
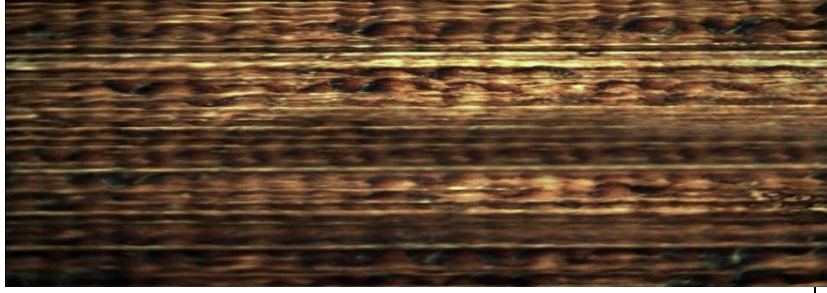
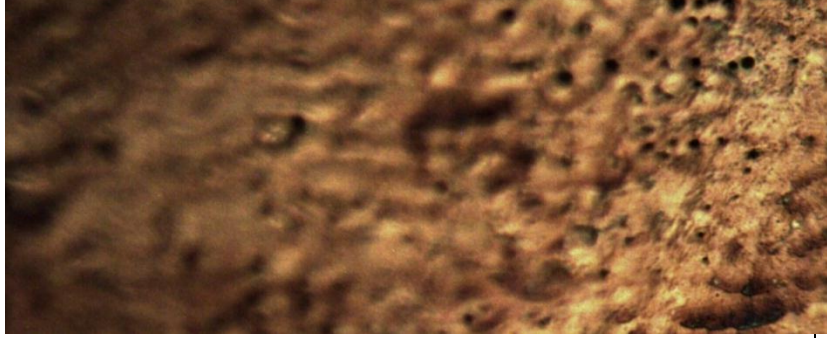
# **Appendix A**

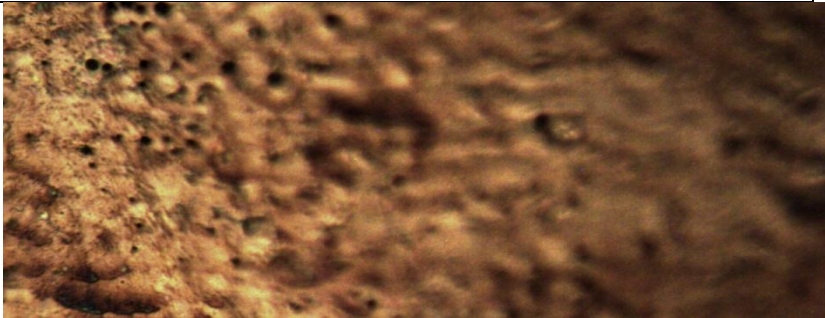
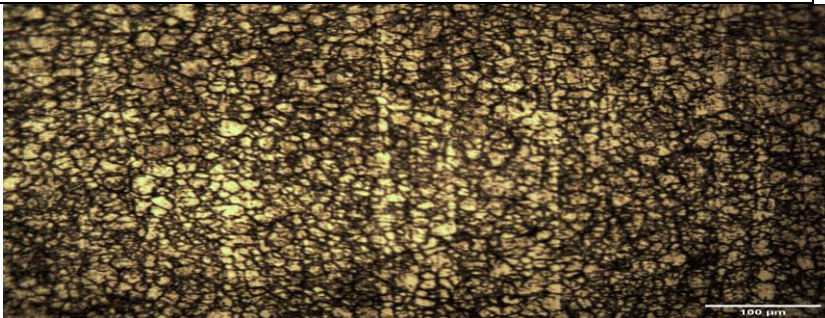
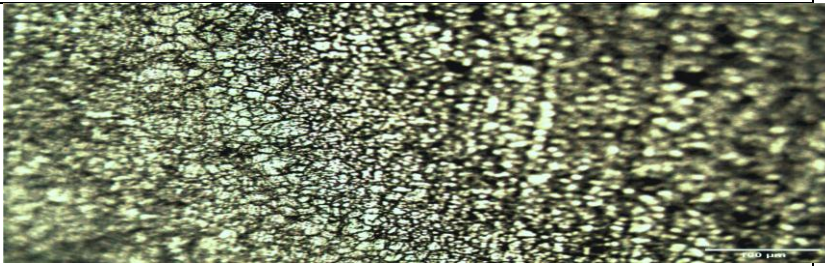
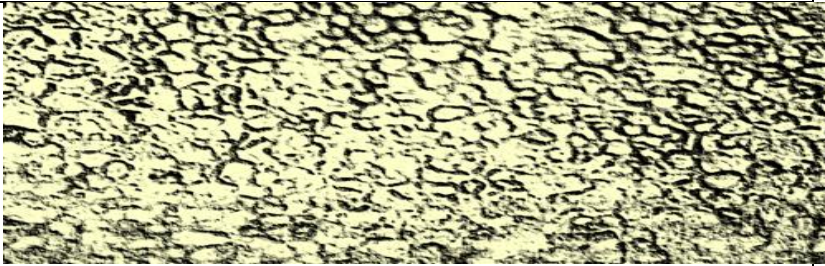
Microscopic images magnification 10 X of the colored samples : power (8 )W, frequency (80) KHz, hatch( 0.01)mm, pulse width (10)  $\mu$ s and scanning speed (50-650)mm/s , steep 25.

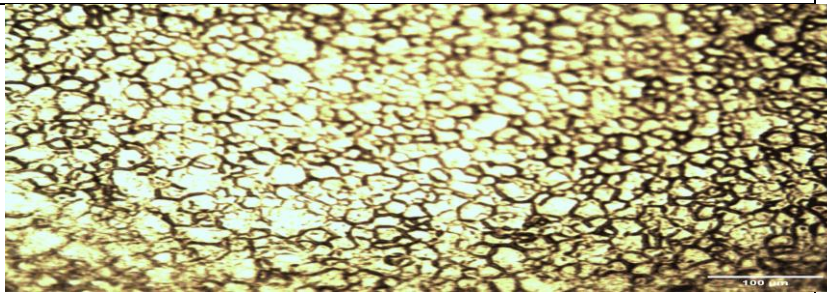
Scanning speed	optical image
50 mm/s	
75 mm/s	
100 mm/s	
125 mm/s	

Scanning speed	optical image
150 mm/s	
175 mm/s	
200mm/s	
225mm/s	
250mm/s	

Scanning speed	optical image
275 mm/s	
300mm/s	
325mm/s	
350mm/s	
375mm/s	

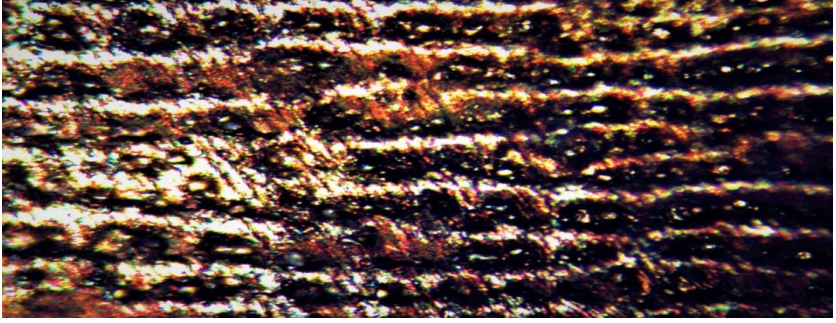
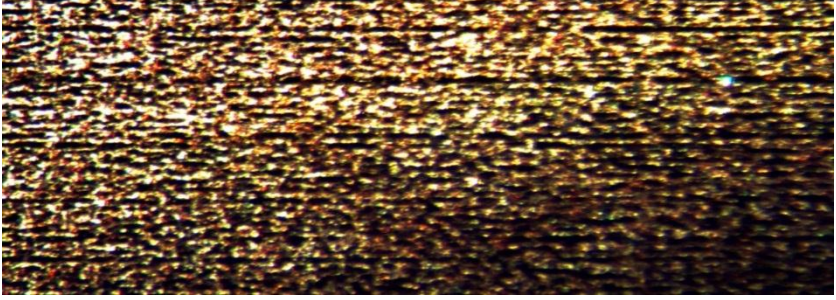
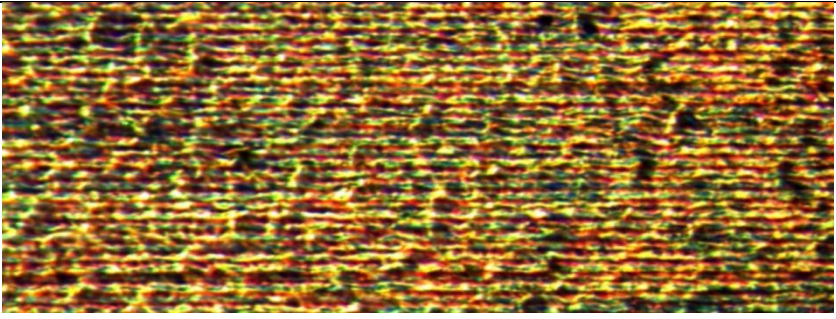
Scanning speed	optical image
400mm/s	 <p>Optical image at 400mm/s scanning speed. The surface shows a complex pattern of green and brown colors, likely representing different material properties or defects. A scale bar in the bottom right corner indicates 100 μm.</p>
425mm/s	 <p>Optical image at 425mm/s scanning speed. The surface shows a pattern of brown and yellow colors, indicating a different texture or composition compared to the 400mm/s scan. A scale bar in the bottom right corner indicates 100 μm.</p>
450mm/s	 <p>Optical image at 450mm/s scanning speed. The surface shows a pattern of brown and yellow colors, similar to the 425mm/s scan, but with a slightly different texture. A scale bar in the bottom right corner indicates 100 μm.</p>
475 mm/s	 <p>Optical image at 475 mm/s scanning speed. The surface shows a pattern of brown and yellow colors, with a more granular texture. A scale bar in the bottom right corner indicates 100 μm.</p>
500mm/s	 <p>Optical image at 500mm/s scanning speed. The surface shows a pattern of brown and yellow colors, with a highly granular and textured appearance. A scale bar in the bottom right corner indicates 100 μm.</p>

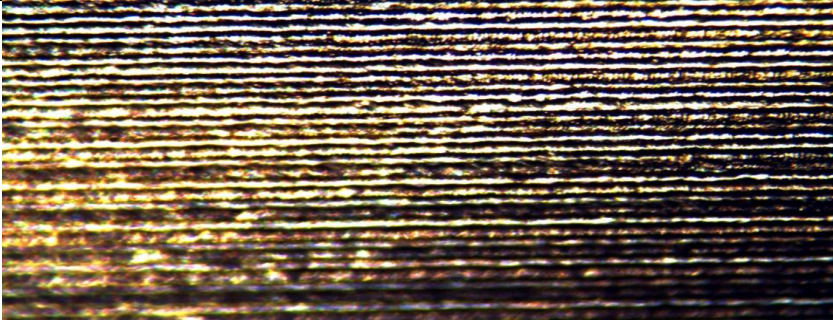
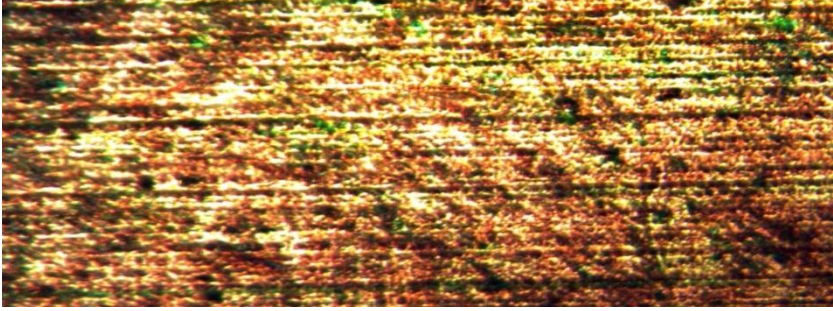
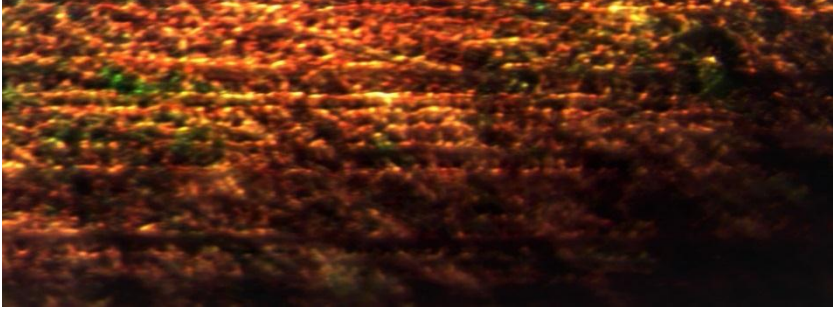
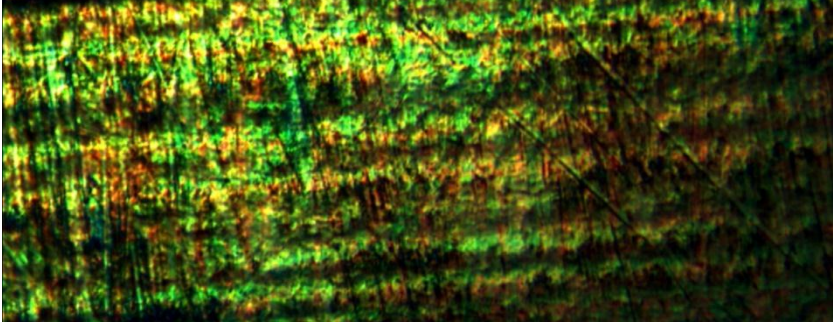
Scanning speed	optical image
525mm/s	
550mm/s	 100 μm
575mm/s	 100 μm
600mm/s	
625mm/s	

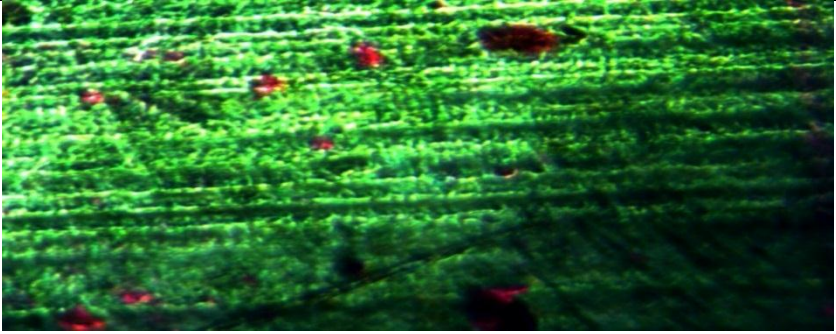
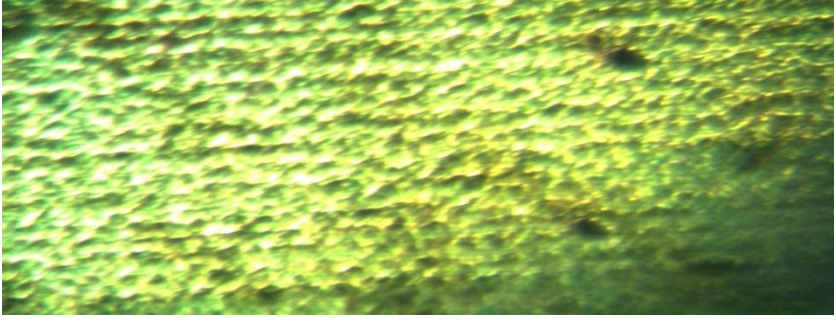
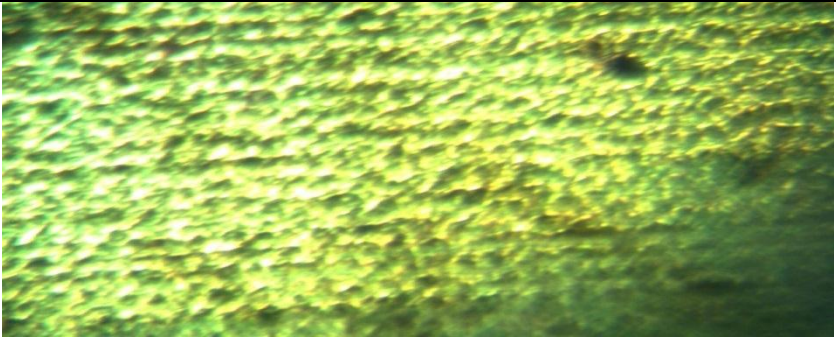
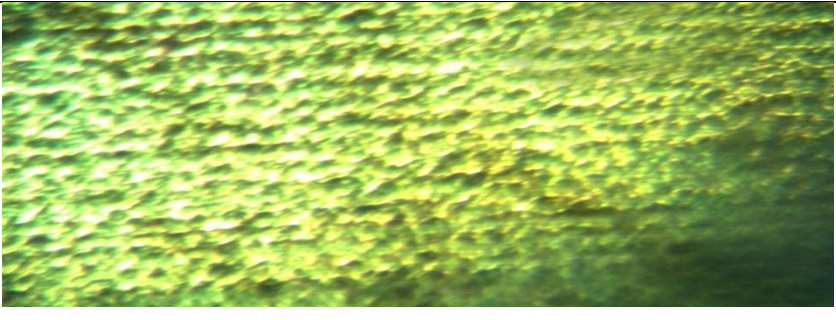
Scanning speed	optical image
650mm/s	 An optical micrograph showing a dense, interconnected network of bright, irregularly shaped particles or fibers. The structure appears porous and highly textured, with a yellowish-gold color palette. A small scale bar in the bottom right corner of the image indicates 100 μm.

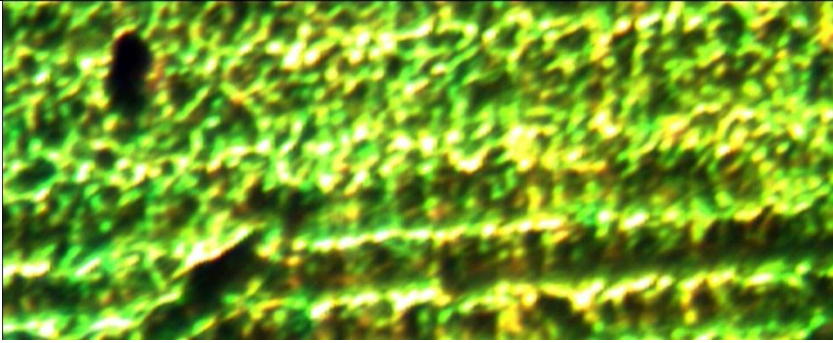
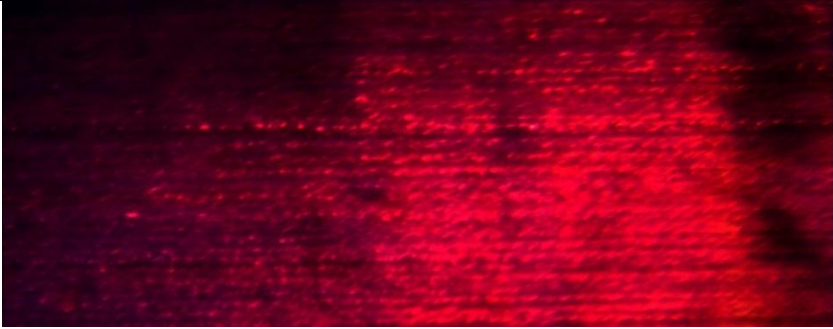
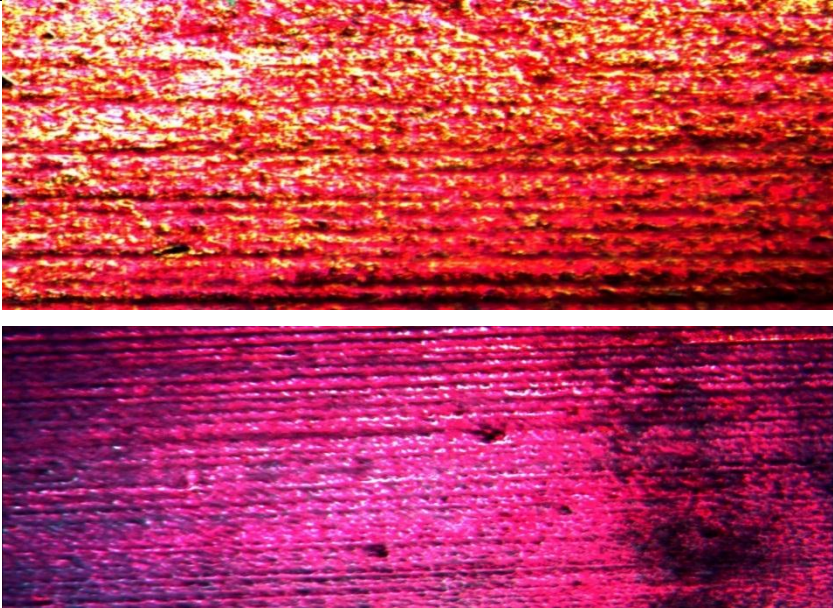
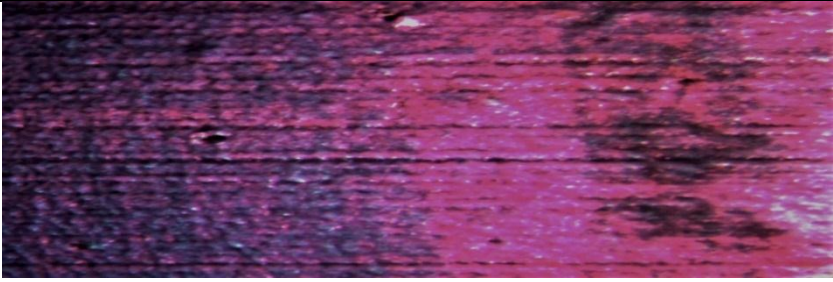
# **Appendix B**

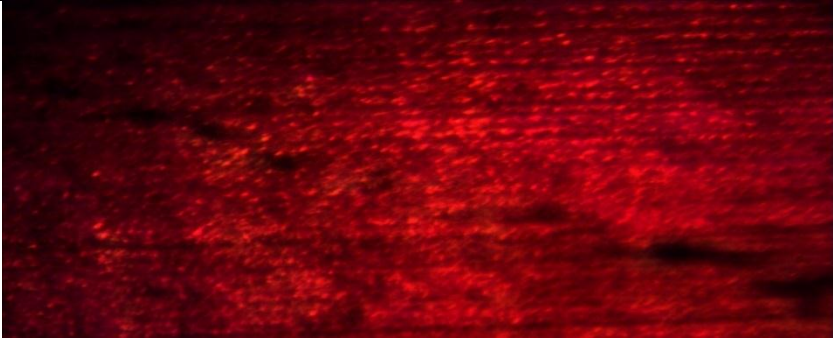
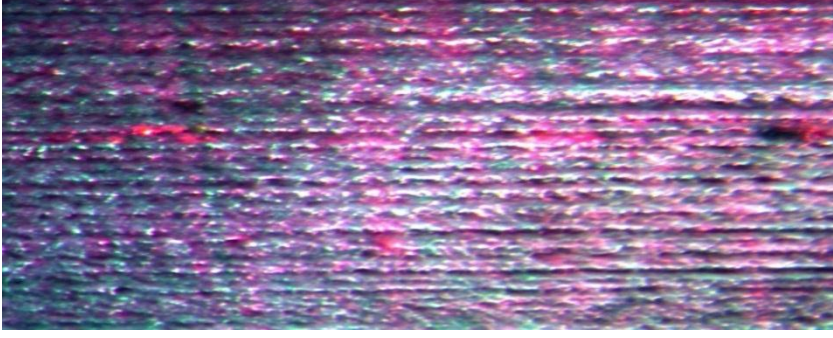
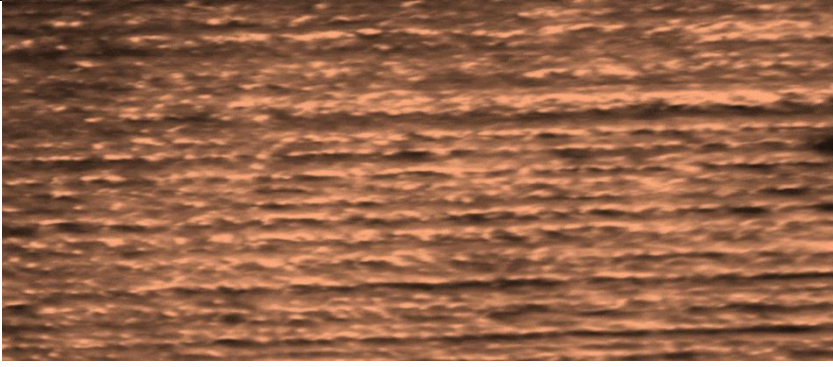
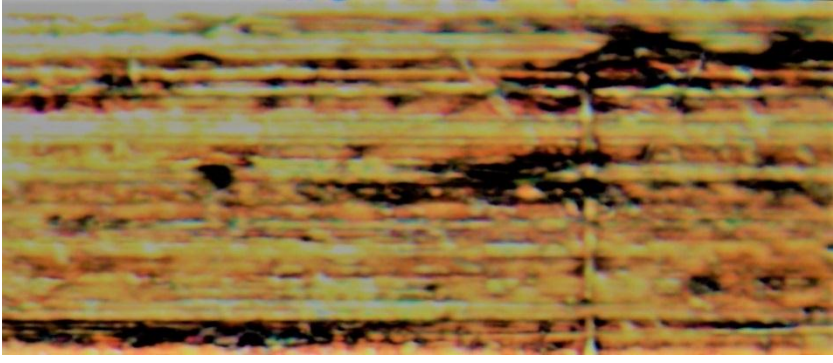
Microscopic images magnification 10 X of the colored sample: power (4) W, frequency( 80 )KHz, hatch( 0.001)mm, (10) $\mu$ s and scanning speed (50-650)steep 25.

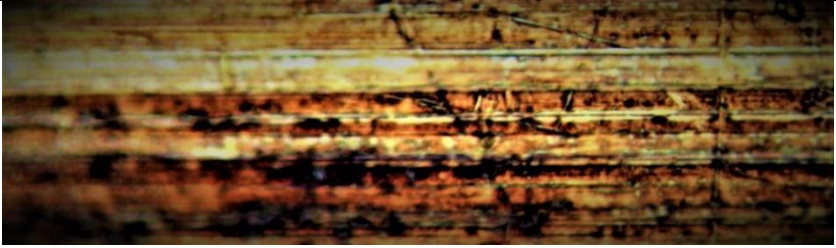
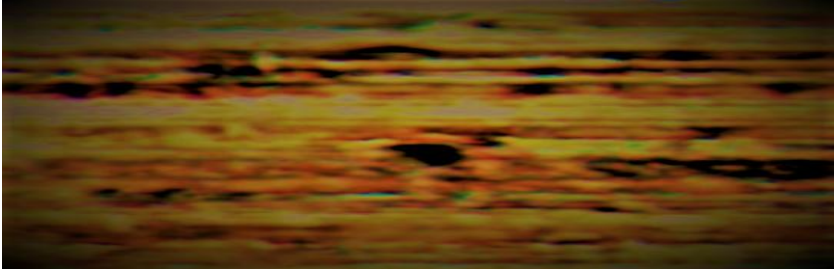
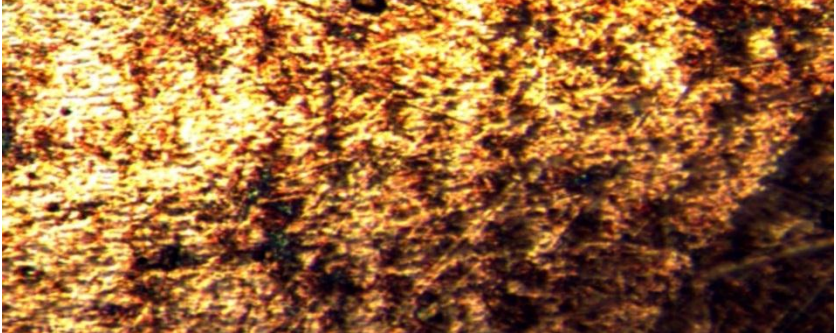
scanning speed mm/s	optical image
50mm/s	
75mm/s	
100mm/s	
125mm/s	

scanning speed mm/s	optical image
150mm/s	
175mm/s	
200mm/s	
225mm/s	
250mm/s	

scanning speed mm/s	optical image
275mm/s	 An optical image showing a surface with a complex, textured appearance. The surface is predominantly green and yellow, with several distinct red spots scattered across it. The texture appears somewhat fibrous or layered.
300mm/s	 An optical image showing a surface with a complex, textured appearance. The surface is predominantly green and yellow, with a more uniform texture than the 275mm/s image. There are some darker spots and a slight gradient of color.
325mm/s	 An optical image showing a surface with a complex, textured appearance. The surface is predominantly green and yellow, with a more uniform texture than the 300mm/s image. There are some darker spots and a slight gradient of color.
350mm/s	 An optical image showing a surface with a complex, textured appearance. The surface is predominantly green and yellow, with a more uniform texture than the 325mm/s image. There are some darker spots and a slight gradient of color.

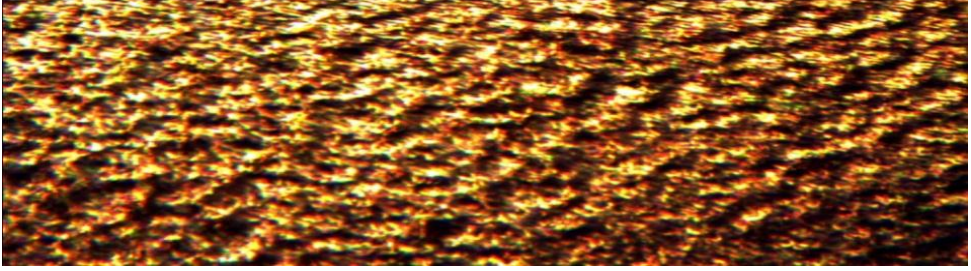
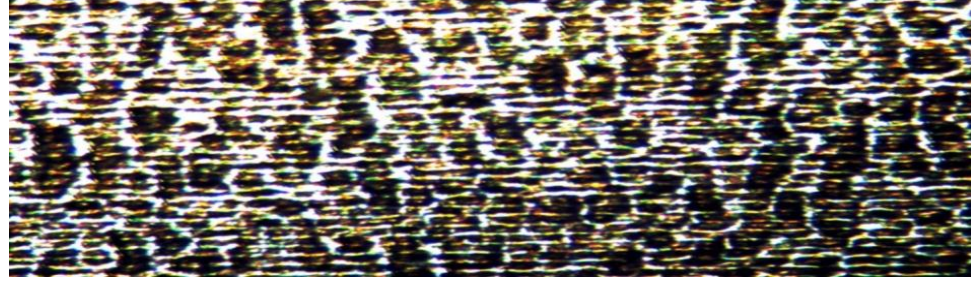
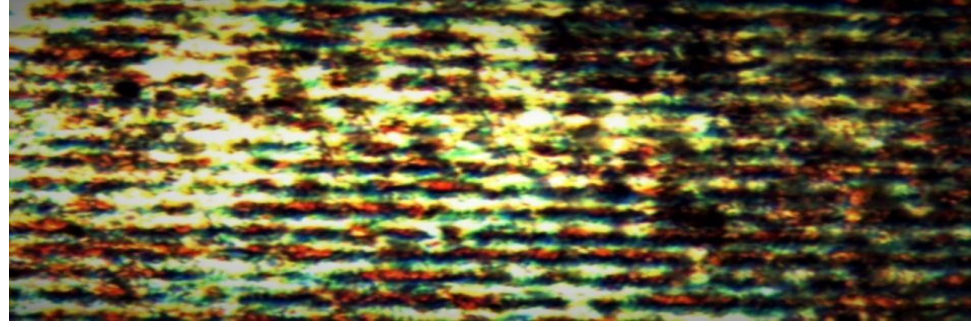
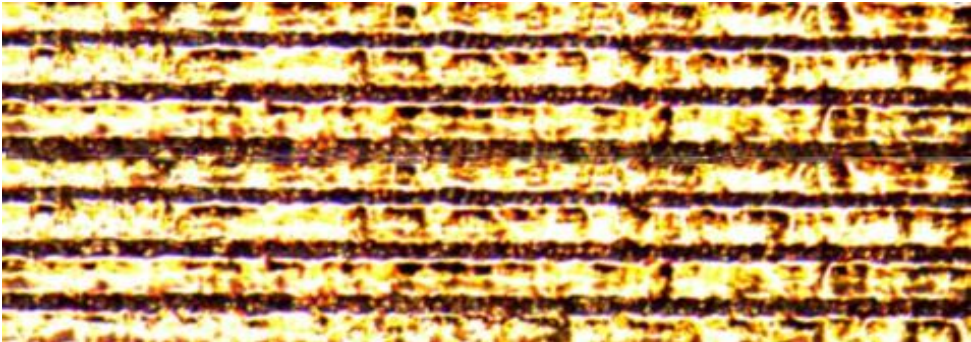
scanning speed mm/s	optical image
375mm/s	
400mm/s	
425mm/s	
450mm/s	

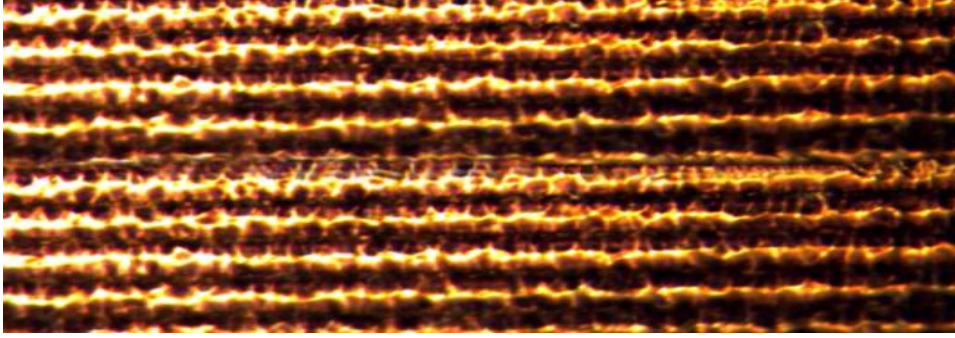
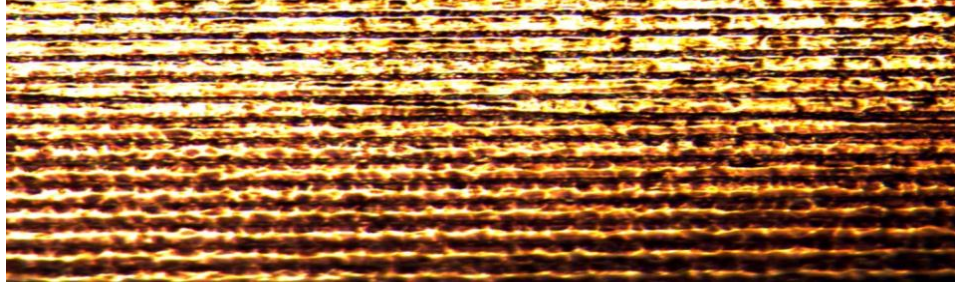
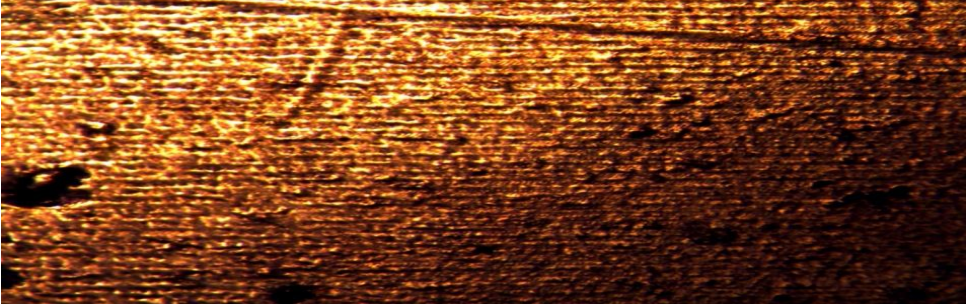
scanning speed mm/s	optical image
475mm/s	 The image shows a dense, granular surface with a strong red color. The texture is somewhat irregular and porous, with many small, interconnected particles or fibers.
500mm/s	 The image shows a surface with a complex, multi-colored appearance. The colors range from purple to blue, with some green and red highlights. The texture is fibrous and somewhat layered, suggesting a woven or layered structure.
525mm/s	 The image shows a smooth, brownish surface with a fine, wavy texture. The color is a mix of light and dark brown, giving it a mottled appearance. The surface appears relatively uniform in color and texture.
550mm/s	 The image shows a highly textured, yellowish-brown surface. The texture is very rough and irregular, with many small, dark spots and fibers. The overall appearance is that of a highly porous and fibrous material.

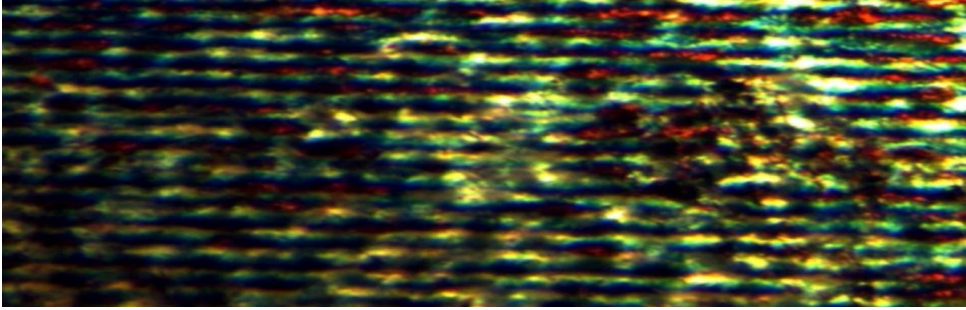
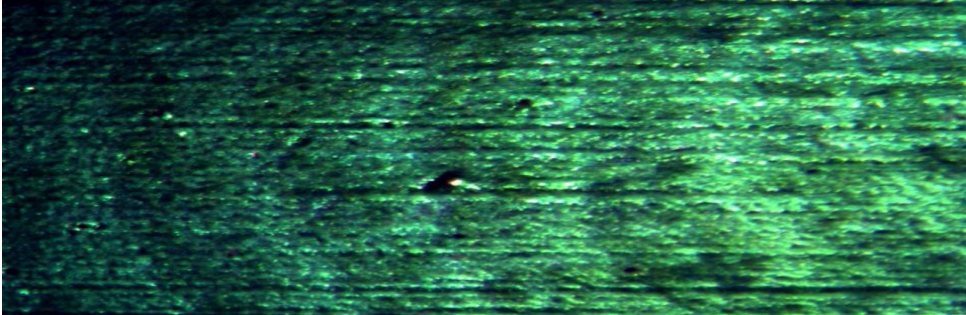
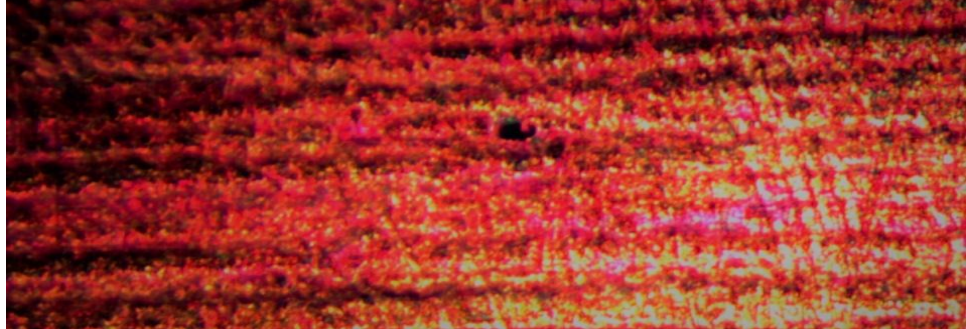
scanning speed mm/s	optical image
575mm/s	
600mm/s	
625mm/s	
650 mm/s	

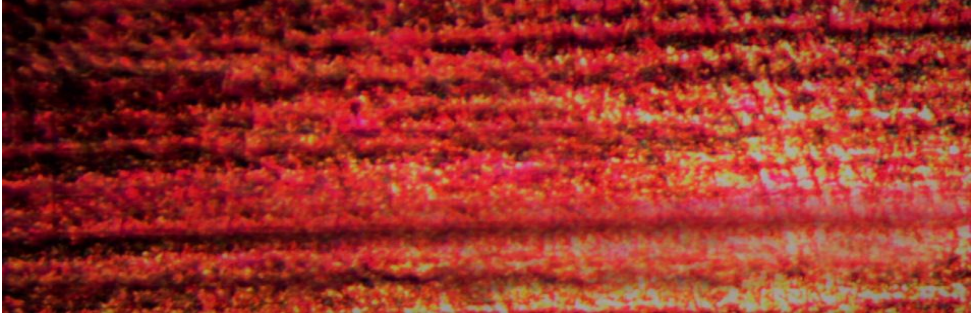
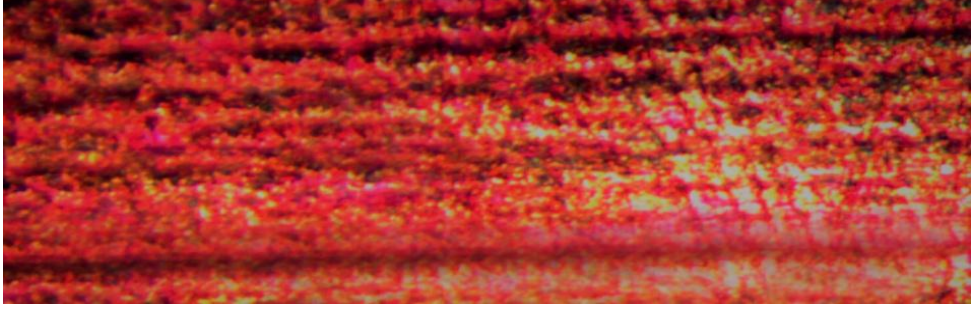
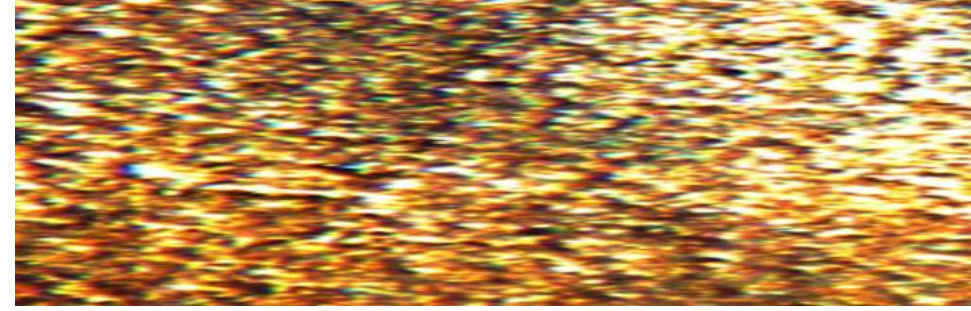
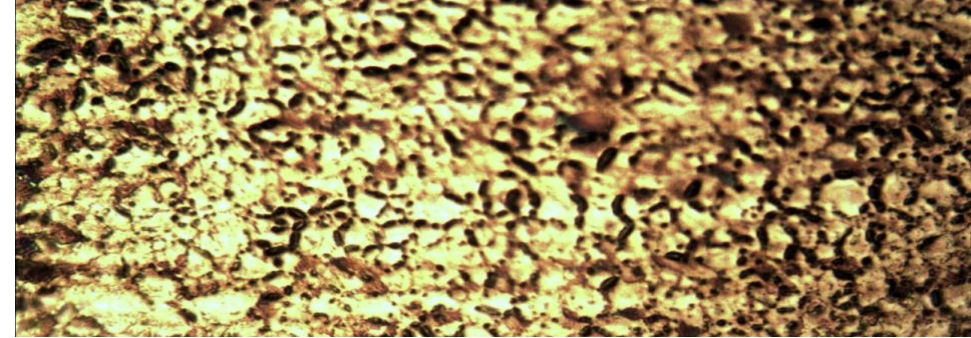
# **Appendix C**

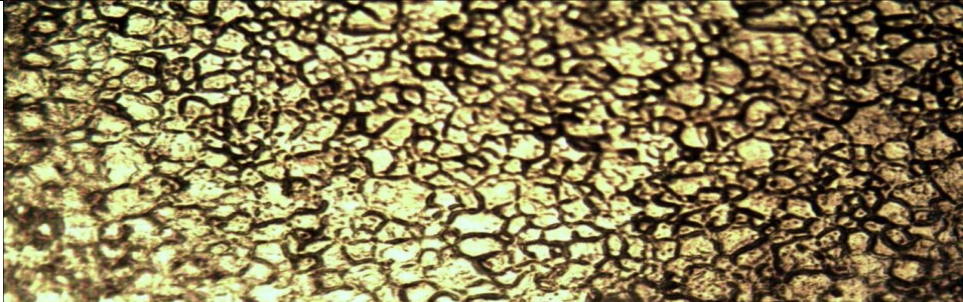
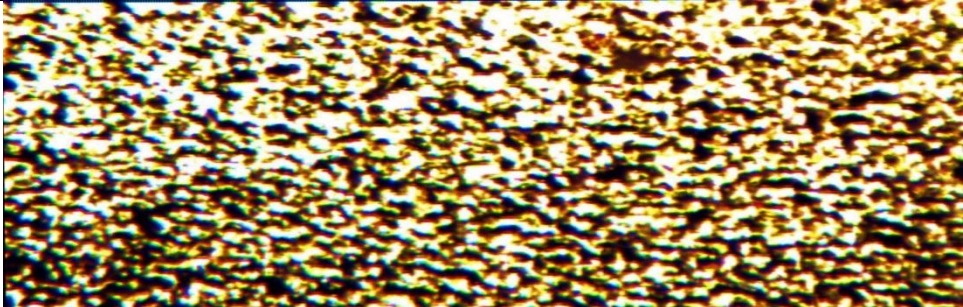
Microscopic images magnification 10 X of the colored samples power ( 8)W, frequency (80) KHZ, hatch( 0.01)mm ,(81)ns pulse width and scanning speed (50-650)mm/s.

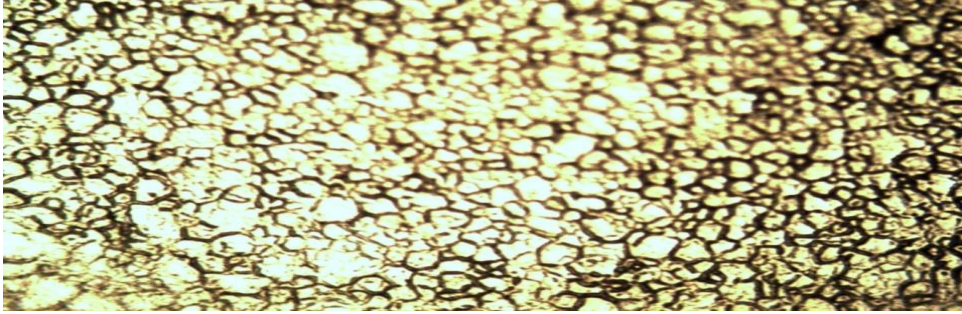
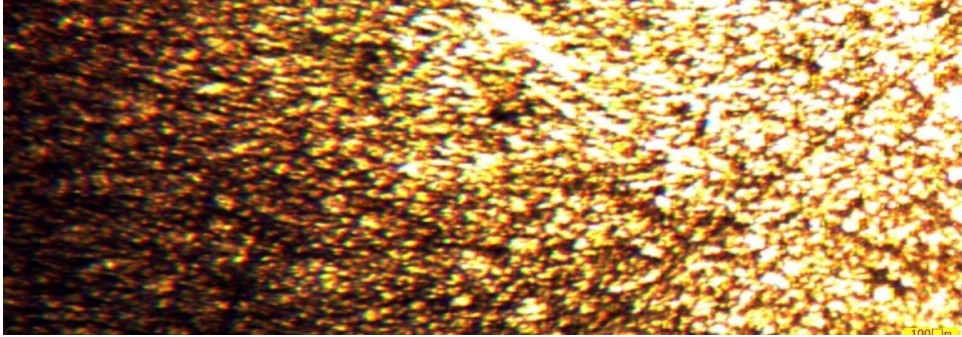
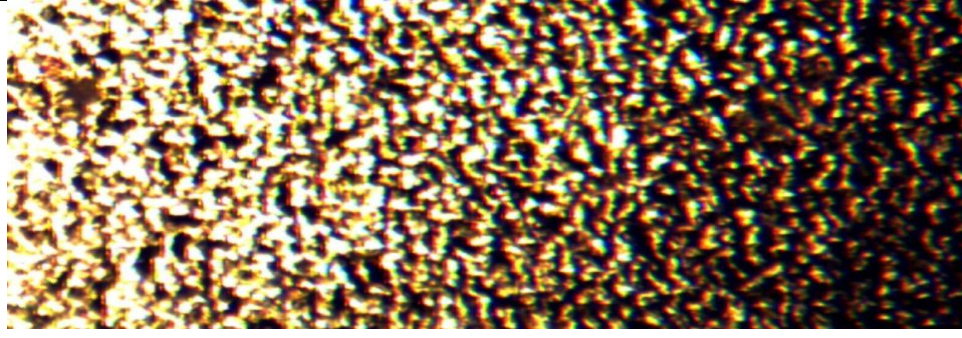
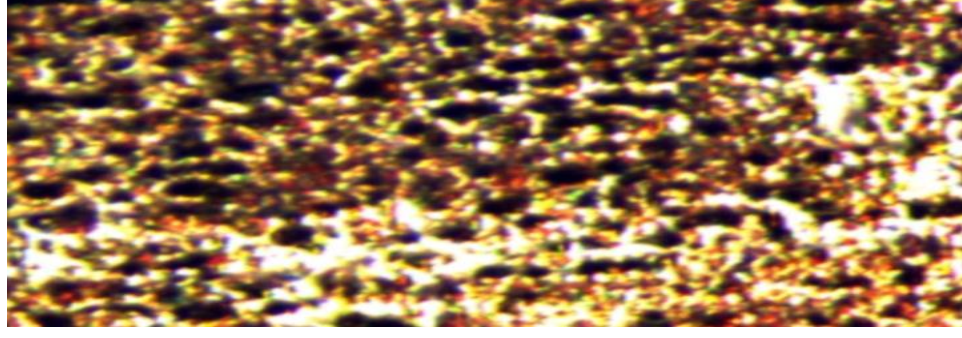
scanning speed mm/s	optical image
50mm/s	
75mm/s	
100mm/s	
125mm/s	

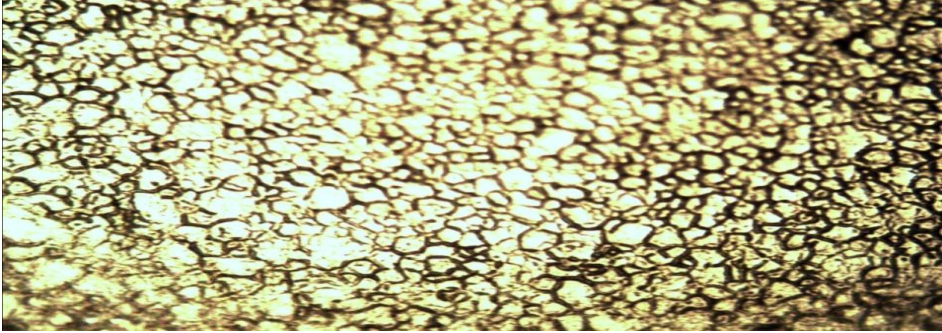
scanning speed mm/s	optical image
150mm/s	
175mm/s	
200mm/s	
225mm/s	

scanning speed mm/s	optical image
250mm/s	
275mm/s	
300mm/s	
325mm/s	

scanning speed mm/s	optical image
350mm/s	 An optical image showing a dense, granular surface with a color palette dominated by reds, oranges, and yellows. The texture appears somewhat uniform but with fine-scale variations.
375mm/s	 An optical image showing a dense, granular surface with a color palette dominated by reds, oranges, and yellows. The texture appears somewhat uniform but with fine-scale variations.
400mm/s	 An optical image showing a dense, granular surface with a color palette dominated by yellows, oranges, and browns. The texture appears somewhat uniform but with fine-scale variations.
425mm/s	 An optical image showing a dense, granular surface with a color palette dominated by yellows, oranges, and browns. The texture appears somewhat uniform but with fine-scale variations.

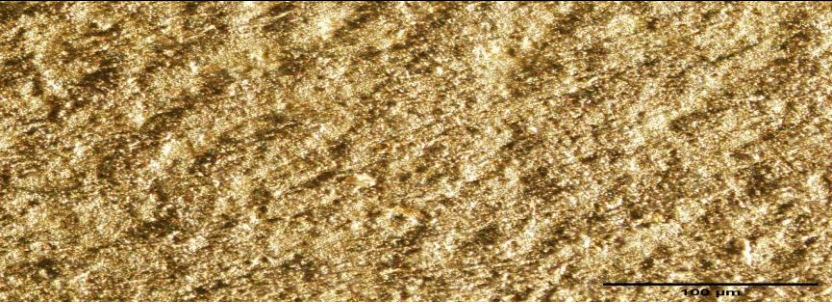
scanning speed mm/s	optical image
450mm/s	
475mm/s	
500mm/s	
525mm/s	

scanning speed mm/s	optical image
550mm/s	
575mm/s	
600 mm/s	
625mm/s	

scanning speed mm/s	optical image
650 mm/s	

# **Appendix D**

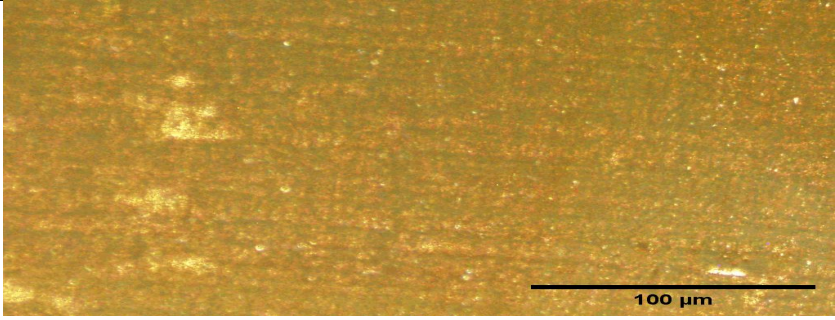
Microscopic images magnification 10 X of the colored samples : power (4)W,(80 )kHz, Hatch( 0.001) mm, pulse width( 81)ns and scanning speed (50-650).

scanning speed mm/s	optical image
50 mm/s	
75 mm/s	
100 mm/s	
125 mm/s	

scanning speed mm/s	optical image
150 mm/s	
175 mm/s	
200mm/s	
225mm/s	
250mm/s	

scanning speed mm/s	optical image
275mm/s	 Optical image showing a granular, textured surface with a yellowish-brown color. A scale bar in the bottom right corner indicates 100 μm.
300mm/s	 Optical image showing a granular, textured surface with a yellowish-brown color. A scale bar in the bottom right corner indicates 100 μm.
325mm/s	 Optical image showing a granular, textured surface with a yellowish-brown color. A scale bar in the bottom right corner indicates 100 μm.
350mm/s	 Optical image showing a granular, textured surface with a yellowish-brown color. A scale bar in the bottom right corner indicates 100 μm.
375mm/s	 Optical image showing a granular, textured surface with a yellowish-brown color. A scale bar in the bottom right corner indicates 100 μm.

scanning speed mm/s	optical image
400mm/s	 An optical micrograph showing a granular surface texture. The surface is composed of small, irregular particles. A scale bar in the bottom right corner indicates 100 μm.
425mm/s	 An optical micrograph showing a granular surface texture. The surface is composed of small, irregular particles. A scale bar in the bottom right corner indicates 100 μm.
450mm/s	 An optical micrograph showing a granular surface texture. The surface is composed of small, irregular particles. A scale bar in the bottom right corner indicates 100 μm.
475mm/s	 An optical micrograph showing a granular surface texture. The surface is composed of small, irregular particles. A scale bar in the bottom right corner indicates 100 μm.

scanning speed mm/s	optical image
500mm/s	 Optical image showing a granular surface texture. A scale bar in the bottom right corner indicates 100 μm.
525mm/s	 Optical image showing a granular surface texture. A scale bar in the bottom right corner indicates 100 μm.
550mm/s	 Optical image showing a granular surface texture. A scale bar in the bottom right corner indicates 100 μm.
575mm/s	 Optical image showing a granular surface texture. A scale bar in the bottom right corner indicates 100 μm.
600mm/s	 Optical image showing a granular surface texture. A scale bar in the bottom right corner indicates 100 μm.

scanning speed mm/s	optical image
625mm/s	
650mm/s	

## الخلاصة

تلوين سطح المعادن الحديدية وغير الحديدية بمعالجتها بالليزر العديد من التطبيقات المثيرة للاهتمام في مجالات مختلفة مثل تعليم على المنتجات و التجميل والفنون. بالمقارنة مع عمليات التلوين التقليدية، الميزة الرئيسية للتلوين بالليزر هي ان منتجاته خالية من السمية.

نظرًا لقلة الدراسات المتعلقة بالنقش بالألوان باستخدام ليزر المايكروثانية ، قمنا بتقديم الدراسة الحالية باستخدام نوعين من ليزر الألياف الإيتربيوم (Ytterbium fiber) ذو الطول موجي 1064 nm. الأول هو ليزر الألياف المايكروثانية ذو عرض النبضة 10 μs والثاني عبارة هو ليزر الألياف النانو ثانية ذو عرض النبضة 81 ns ، لتلوين نوعين من المعادن الفولاذ المقاوم للصدأ 304 والألومنيوم 3003.

تتم عملية التلوين عن طريق أكسدة السطح نتيجة تسخين سطح المعدن بشعاع الليزر في ظل الظروف الجوية الاعتيادية وبالتزامن مع توظيف معلمات مختلفة من قدرة الليزر و سرعة المسح و تباعد خطوط المسح. بسبب التأثيرات الحرارية الناتجة من امتصاص و تفاعلات الليزر مع السطوح المعدنية تنتج العملية الوانا مختلفة على الفولاذ المقاوم للصدأ بتغير القدرة من 4 W الى 8 W ، وسرعة المسح من 50 إلى 650 mm/s ، بمعدل تكرار النبضات 80 kHz و تباعد خطوط المسح 0.001 mm و 0.01 mm. انتج ليزر المايكروثانية اللون البني الداكن عند سرعة 125 mm/s والبني عند سرعة 275 mm/s والرمادي عند 450 mm/s والأصفر عند 650 mm/s. وانتج ليزر النانو ثانية الألوان الرمادي الفاتح عند سرعة 50 mm/s ، والأخضر الداكن عند سرعة 275 mm/s ، والأزرق البحري عند سرعة 475 mm/s والأصفر الباهت عند سرعة 600 mm/s.

باستخدام الليزر النبضي النانو ثانية اظهرت النتائج خشونة أقل من الليزر النبضي بالمايكروثانية وأكثر حماية ضد التآكل بسبب احتواء طبقة الأوكسيد على النيكل. اظهر الألومنيوم سلوكًا مختلفًا حيث انتج اللون أبيض حصرا عند سرعة 200 mm/s وقدرة ليزر 6 W و تباعد خطوط 0.005 mm. كذلك تم انتاج اللون الرمادي عند سرعة 25 mm/s ، و تباعد خطوط 0.005 mm. ابدت العينات المعالجة بنبضات الليزر بالمايكروثانية مقاومة أعلى للتآكل بالمقارنة مع الليزر الاخر.

تم اجراء العديد من الفحوصات لتقييم التغييرات اللونية ، لهذا الغرض تم استخدام العديد من الأدوات ، مثل المجهر الضوئي لتقييم التعديلات التي حصلت على حالة السطح. تم الفحص

بالمجهر الالكتروني FESEM و EDS لدراسة التشكل السطحي والتكوين الأولي . تم اجراء تحليل XRD لتحديد الاطوار المتكونة على السطح. تم اجراء اختبار خشونة الاسطح المختلفة و فحوصات قياس الطول الموجي ومقياس الألوان اليدوي لطيف الانعكاس وتحديد قياسات استقطاب اللون والتآكل لفحص ثبات اللون مقابل الظروف البيئية.



جمهورية العراق

وزارة التعليم العالي والبحث العلمي

جامعة بغداد

معهد الليزر للدراسات العليا

# تأثير معلمات التشغيل لليزري الألياف المايكروثانية والنانوثانية على تلوين المعادن SS 304 و AI 3003

رسالة مقدمة الى

معهد الليزر للدراسات العليا / جامعة بغداد / لاستكمال متطلبات نيل شهادة

ماجستير

علوم في الليزر / هندسة ميكانيك

من قبل

آيات خلف رحمه

بكالوريوس هندسة عمليات تصنيع - 2008

بإشراف

الأستاذ المساعد الدكتور زياد اياد طه